Measuring Reliable Elastic Modulus on Brittle Materials by Indentation

by

Jiahui Xu

A dissertation submitted to the Graduate Faculty of
Auburn University
in partial fulfillment of the
requirements for the Degree of
Doctor of Philosophy

Auburn, AL
December 14, 2019

Keywords: thin films, nanoindentation, sputter,
brittle material, elastic modulus

Committees:

Dr. Barton C. Prorok, Chair, Professor of Materials Engineering
Dr. Pengyu Chen, Professor of Materials Engineering
Dr. Dong-Joo Kim, Professor of Materials Engineering
Dr. Jeff Suhling, Professor of Mechanical Engineering

Abstract

Mechanical properties such as elastic modulus can be tested and acquired by using various methods for materials. Nanoindentation is a reliable and robust tool to extract material properties in recent years. It is challenging to obtain brittle material's elastic modulus traditionally because of cracks and defects generation. In this research, an indirect indentation method called the Chen-Prorok model, which is based on the Zhou-Prorok model can predict the brittle material's elastic modulus by depositing a thin layer of film on it and indenting into the film without penetrating brittle material. This indirect method prevents damages on brittle material with a protective coating. Within this research, the film thickness was characterized by several ranges and tested to optimize the application of the Chen-Prorok model. The possible reasons were explained by analyzing the deposition and indentation processes. A different sputter method was chosen to coat film on the substrate that works better than previous methods in a few hundred nanometers range. The test results from nanoindentation are comparable to previous research within the nanoscale. The new sputter method enables the deposition process economically and efficiently compared with conventional methods.

Next, the key factors of elastic properties like Poisson's ratio were discussed and decoupled in the indirect indentation method. This research confirmed that the indirect indentation method was barely affected by these factors.

Furthermore, different thickness film and substrates combinations were examined to prove the model accuracy of extracted elastic modulus from brittle materials. Overall, this work improves the extraction of unknown brittle material's elastic behavior conveniently and accurately in the nanoindentation field. Additionally, the deposition process was simplified and suggested by introducing a new method within hundred nanometers range for nanoindentation tests.

Acknowledgments

I would like to thank first, most sincerely, my advisor Dr. Bart Prorok. I feel so lucky he could guide me and lead me in the right way. He is not only a dedicated professor but also help me as a father. I am really appreciated he picked me to join his group. I will keep working hard in the future. Next, I would like to thank my committee members Dr. Chen for his suggestions and improvement, Dr. Kim for his kind guide on my course and dissertation, and my outside reader, Dr. Thompson, for committee help and dissertation advice. Furthermore, I would like to thank Cheryl Rhodes and Steven Moore for their kind assistance. They try their best to support me in finishing my graduation process.

Next, I would like to thank my lab mates: Marianne Sullivan, who helps me go over the whole process and continue to work on the field of nanoindentation. Hossein Talebinezhad, Rong Zhao,Anna Kate, and Hayden Price read through my proposal and dissertation. Ralf Fisher shares his idea about the presentation. Pu Deng and give some suggestions about the research. Xingxing Zhang, Lang Zhou, and Hossein Talebinezhad help me with my qualify exam. Zhan Xu, Anqi Zhang, Yan Chen, Jiawei Zheng help me during my five-year career.

Finally, I would like to thank my family and my friends' help, including Jian Xu, Jihong Chen and my friends Zhiji Lu, Mingyuan Chang. Without their support, I might get a hard time to continue my research.

Table of Contents

Abstract 2

Acknowledgments 3

1.0 Introduction 11

2.0 Motivation and Goals 12

2.1 Film Thickness Effects on the Indirect Indentation Method 12

2.2 Investigate Simple Gold Coater for Widespread Use of Indirect Indentation Method 12

2.3 Parameters Effects on the Indirect Indentation Method 12

3.0 Literature Review 14

3.1 Nanoindentation 14

3.1.1 Continuous Stiffness Measurement 16

3.2 Approach 17

4.0 Experimental Procedure 29

4.1 Material Selection 29

4.2 Film Deposition 30

4.3 Thickness Measurement 33

4.4 Nanoindentation 35

4.5 Scanning Electron Microscopy 36

4.6 Heat Treatment 37

5.0 Results 39

5.1 Film Thickness's Effects on the Indirect Indentation Method 39

5.1.1 Fitting the Indirect Indentation Method to Gold films on Silicon by Denton 46

5.2 Investigate Simple Gold Coater for Widespread Use of the Indirect Indentation Method 57

5.2.1 Fitting the Indirect Indentation Method on Pelco Sputtered Gold film on Silicon 57

5.2.2 Results Comparisons between Denton Sputtered Films and Pelco Sputtered Films 62

5.2.3 Different Substrates' Effects 71

5.2.4 Various Substrates with Different Gold Film Thickness 75

5.3 Approach to Analyze Parameters that may Affect the Indirect Indentation Method 86

5.3.1 Different Thickness's Effects 86

5.3.2 Different Poisson's ratios' Effects 89

6.0 Conclusions 94

7.0 Future Work 95

8.0 Reference 100

List of Tables

Table 1. Elastic properties of the direct and indirect indentation methods as compared with literature values

Table 2. Material Properties of Chosen Films and Substrates

Table 3. Sputter coating conditions for gold films by using Denton sputtering systems.

Table 4. Sputtering conditions for gold films by using Denton sputtering systems without Ti

Table 5. Sputtering conditions for gold films by using Pelco SC-6 sputter coater

Table 6. Gold Thickness and deposition time by Denton

Table 7. Slopes and indirect modulus with different thickness (Denton)

Table 8. Gold Thickness and deposition time by Pelco

Table 9. Average Indentation Modulus from direct and indirect indentation

Table 10. Slopes and indirect modulus with different thickness (Pelco)

Table 11. Slopes and indirect modulus with 76nm gold on different substrates

Table 12. Comparison between direct modulus and indirect of gold film on different substrates

Table 13. Slopes and indirect modulus with 76nm,96nm,154nm gold on fused silica

Table 14. Slopes and indirect modulus with 76nm,96nm,154nm gold on CaCO3

Table 15. Slopes and indirect modulus with 76nm,96nm,154nm gold on MgO

Table 16. Slopes and indirect modulus with different modified thickness

Table 17. Slopes and indirect modulus with different Poisson's ratio

Table 18. literature values of film and substrates

List of Figures

Figure 1. Load-displacement curve during nanoindentation test

Figure 2. An illustration of indentation during the loading and unloading process

Figure 3. Schematic of the dynamic indentation model

Figure 4. Plot of modulus versus displacement into the surface for indenting Al2O3 directly

Figure 5. Plot of hardness versus displacement into the surface for indenting Al2O3 directly

Figure 6. Indentation mark of Aluminum Oxide.

Figure 7. Scanning electron micrograph and focused-ion-beam cross-section of a residual indentation on the Au/Al2O3 composite.

Figure 8. Gold on Aluminum oxide following by Zhou-Prorok model

Figure 9. The relationship between hyperbolic function and linear function

Figure 10. An illustration of linear approximation.

Figure 11. Experimental indentation results of the Cr/Al2O3 film/substrate composite and calculated reduced modulus.

Figure 12. Scanning electron micrograph and focused-ion-beam cross-section of a residual indentation on the Cr/Al2O3 composite.

Figure 13. Indirect substrate modulus for the Cr/Al2O3 composites

Figure 14. Indirect substrate modulus for the chromium film on 4 different substrates

Figure 15. Harmonic Displacement after h'>0.8

Figure 16. Denton Sputter Coating system

Figure 17. Pelco Sputter Coating system

Figure 18. Thickness reference chart

Figure 19. Thickness measurement under Secondary Electron Mode

Figure 20. Thickness measurement under Backscattered Electron Mode

Figure 21. MTS Nanoindenter XP

Figure 22. JEOL 7000F Scanning Electron Microscope

Figure 23. VWR Gravity Convention Oven

Figure 24. Direct indentation modulus on silicon substrate modulus (solid markers) with literature value (solid line)

Figure 25. Indents on silicon substrate with 500nm depth(left) and 1000nm depth(right)

Figure 26. 598nm deposition thickness measurement under SEI and COMPO mode

Figure 27. Composite modulus of 598nm gold on silicon

Figure 28. Reduced modulus of 598nm gold on silicon

Figure 29. 598nm gold on silicon indirect modulus

Figure 30. Composite modulus of different thickness gold on silicon

Figure31. Reduced modulus of different thickness gold on silicon

Figure 32. Indirect modulus of different thickness gold on silicon

Figure 33. Average indirect modulus of different thickness gold on silicon

Figure 34. 107nm deposition thickness measurement under SEI and COMPO mode

Figure 35. Composite modulus of 107nm Au on silicon without Ti

Figure 36. Reduced modulus of 107nm Au on silicon without Ti

Figure 37. Indirect modulus of 107nm Au on silicon without Ti

Figure 38. Deposition thickness measurement under SEI and COMPO mode

Figure 39. Composite modulus of 76nm gold on silicon

Figure 40. Reduced modulus of 76nm gold on silicon

Figure 41. Indirect modulus by applying Chen-Prorok model (solid markers) of gold film of 76nm thicknesses on silicon with literature value (solid line)

Figure 42. Indirect modulus by applying Chen-Prorok model (solid markers) on 76nm thicknesses gold on silicon and direct indentation modulus on silicon substrate (void markers)

Figure 43. Experimental modulus for all thicknesses of gold film on silicon substrate

Figure 44. Reduced modulus for all thicknesses of gold film on silicon substrate

Figure 45. Indirect modulus for all thicknesses of gold film on silicon substrate

Figure 46. Average indentation results from Chen-Prorok model with different thickness gold on silicon substrates deposited by Pelco sputter coater

Figure 47. 27nm Gold film surface (left) and 50nm Gold film surface (right)

Figure 48. 27nm (left) and 50nm gold film surface with heat treatment(right)

Figure 49. Comparisons between Denton and Pelco sputter film

Figure 50. Composite modulus of 76nm gold on ceramic substrates

Figure 51. Reduced modulus of 76nm gold on ceramic substrates

Figure 52. Indirect modulus of 76nm gold on ceramic substrates

Figure 53. Composite modulus of 76nm,96nm,154nm gold on fused silica

Figure 54. Reduced modulus of 76nm,96nm,154nm gold on fused silica

Figure 55. Indirect modulus of 76nm,96nm,154nm gold on fused silica

Figure 56. Composite modulus of 76nm,96nm,154nm gold on CaCO3

Figure 57. Reduced modulus of 76nm,96nm,154nm gold on CaCO3

Figure 58. Indirect modulus of 76nm,96nm,154nm gold on CaCO3

Figure 59. Composite modulus of 76nm,96nm,154nm gold on MgO

Figure 60. Reduced modulus of 76nm,96nm,154nm gold on MgO

Figure 61. Indirect modulus of 76nm,96nm,154nm gold on MgO

Figure 62. Average modulus versus thickness error ratio

Figure 63. Reduced modulus of 107nm gold on silicon with changed thickness

Figure 64. Average modulus versus different Poisson's ratio

Figure 65. Reduced modulus of 107nm gold on silicon with changed Poisson's ratio

Figure 66. Indirect modulus for all thicknesses of chromium film on silicon substrate by applying Chen-Prorok model

Figure 67. Average indirect indentation results from Chen-Prorok model with different thickness chromium on silicon substrates

1.0 Introduction

Various thin films on substrates have been widely used in a range of fields. Reliably measuring the mechanical properties of thin films and substrates is crucial for preventing failure and continuing to operate in certain periods. Nanoindentation is an excellent tool used to detect and analyze the properties of thin films and substrates. This technique could cause minor damage to the sample's surface and get decent amount of data points in very small scales even in nanoscale which large scale test methods don't work. Additionally, the sample preparation for nanoindentation is convenient compared with other tests. It doesn't require samples need to have a regular shape or size as long as mounting properly. This research was to make improvements on film on ceramic substrates by using nanoindentation as an important tool to extract ceramic substrates' elastic modulus. Ceramic material's elastic modulus is hard to be acquired since most of them are brittle with low Poisson's ratios. Film works as a protective layer to minimize cracks generated and propagated in substrates when the tip indents into film and substrate combinations. There is also a challenge to find methods to counteract film's effects in order to get real substrate's mechanical property. Models and equations are applied and improved in this research based on nanoindentation theories.

Furthermore, there are a lot of depositing film methods in nanoindentation. It is vital to provide an easy and common deposit technique for most applications. This is a direction that most of research haven't fully covered. Deposition are limited by costs, equipment, environment and other factors. Some techniques take few hours to deposit a layer and other require very high vacuum state chamber to get a uniform layer. It is difficult to provide reference and guides for common use. Sometimes, collapsed film or unprofessional deposition may affect the indentation result and stick to tip. In order to solve this issue, novel techniques were suggested and compared with traditional sputter system. Parameters which may affect deposition process and final result are discussed and analyzed.

This dissertation goal is to predict and improve the extraction of ceramic material's elastic modulus without piercing into them based on models our group developed and to introduce a new way to deposit film for most researchers conveniently and economically.

2.0 Motivation and Goals

Nanoindentation techniques have been applied in broad areas like micro-electrical mechanical systems and micro-electronic system to test and characterize mechanical properties. In our previous group work, the Zhou-Prorok equation fits the elastic property outstandingly with a different combination of thin films and substrates. Chen revised the model into a new equation to extract the substrate's elastic property without punching into it. To take it further, we want to focus on various thin films on substrates to characterize the elastic property in a reasonable thickness range. By using Chen's and Zhou-Prorok's equations, we try to propose a new method to deposit film easily and a guide to help researchers to obtain elastic properties from their samples reliably and efficiently. These will be discussed in the next following sections.

2.1 Film Thickness Effects on the Indirect Indentation Method

Zhou-Prorok' and the indirect indentation method fit most of the film thicknesses on substrates from several hundred nanometers to micron meters. It is vital to give a suggestion about the film thickness because this will help researchers coat substrates in a standard method. In this part, various thickness deposition on substrates were investigated if we could find a way to regulate the deposition process.

2.2 Investigate Simple Gold Coater for Widespread Use of Indirect Indentation Method

The Chen-Prorok model could extract the substrate's modulus in a small deviation range by using Pelco sputter system compared with Denton sputter system. Even though the films are not finely formed, the model still predicts the substrates' modulus. It is crucial to find the principle and mechanism to explain why the model has a good fit for film and substrate combination. In this research, it is necessary to compare these two systems and analyze them. Different film thickness and substrates combinations were analyzed. the effects from unique ceramic material structure were minimized and it is valuable to provide general suggestions for most ceramic material. Furthermore, we try to give a reference for people who are using our equations and reduce the cost while dealing with their samples since coating and sputtering are not cheap.

2.3 Parameters Effects on the Indirect Indentation Method

The indirect indentation method fits certain film thickness on substrates. It is vital to give a suggestion about parameters that affect the results because this will help researchers coat substrates

in a standard method. In this work, thickness and Poisson's ratio were discussed and studied in details. Each of these parameters plays a role in the equations and needs to be decoupled individually. Additionally, if these parameters can be explained and counteracted, it may be possible to predict the brittle material's modulus exactly.

3.0 Literature Review

3.1 Nanoindentation

Nanoindentation is one of the simplest methods to determine the modulus and hardness of thin film on substrates. This technique is widely used because it is able to obtain the mechanical properties without breaking the films or substrates [1]. Nanoindentation uses a probe called the indenter tip to indent numerous points on a surface. Then, the mechanical properties, such as hardness and modulus, are determined from a load-displacement curve similar to the curve shown in Figure 1. In our studies, the Berkovich tip was used as the indenter tip. This tip is a three-sided pyramid and geometrically self-similar to determine the samples' properties.

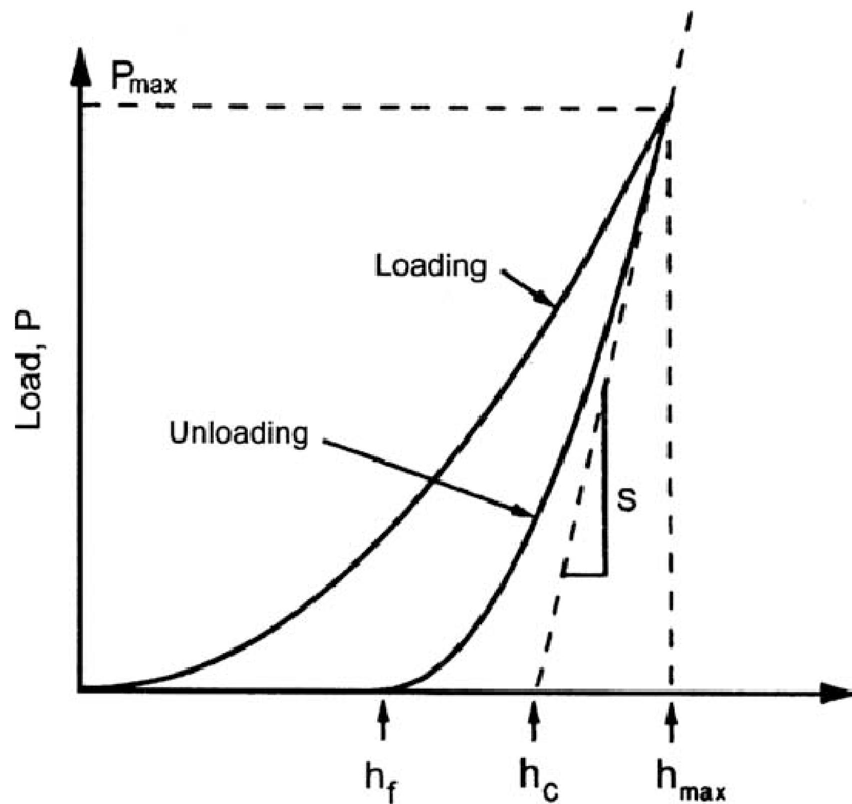

Figure 1. Load-displacement curve during nanoindentation test [2]

h_f is the final displacement after unloading, h_{max} is the displacement at maximum load, h_c is the contact depth, S is stiffness which could be calculated from the unloading slope.

After we got the load-displacement curve from the nanoindentation test, we could calculate the stiffness S from Equation 1:

$$S = \frac{dP}{dh} = \frac{2}{\sqrt{\pi}} E_r \sqrt{A} \quad (1)$$

P is the load, h is the displacement, E_r is the reduced modulus, A is the contact area which could be calculated from the contact depth h_c shown in Figure 2.

Hardness H is determined by Equation 2

$$H = \frac{P_{max}}{A} \quad (2)$$

P_{max} is the maximum load, A is the projected area which could be obtained from contact depth [5].

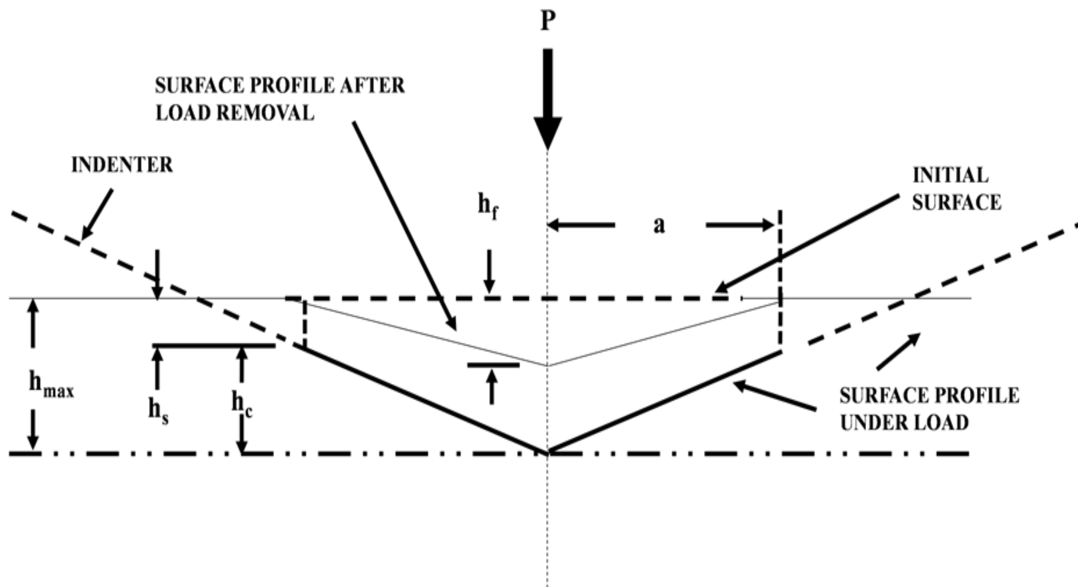

Figure 2. An illustration of indentation during the loading and unloading process [3]

P is the indentation load, h_{max} is the displacement at maximum load, h_c is the contact depth, a is the radius of the contact area

Reduced modulus E_r could be obtained from Equation 3

$$\frac{1}{E_r} = \frac{(1-\nu^2)}{E} + \frac{(1-\nu_i^2)}{E_i} \quad (3)$$

Where E and E_i are sample's elastic modulus and indenter tip's elastic modulus, and ν and ν_i are Poisson's ratio of sample and indenter tip. The parameters of the Berkovich tip in our group are E_i=1140Gpa, ν_i=0.07.

3.1.1 Continuous Stiffness Measurement

The continuous stiffness measurement technique is regarded as one of the important enhancements in the nanoindentation field. The traditional way to measure the stiffness is called static measurement, while the stiffness is calculated from the unloading slope. Static measurement usually takes long holding time and more sensitive to thermal drifts compared with CSM. Since the stiffness is obtained from the unloading cycle, limited data points are acquired.

However, stiffness can be measured dynamically under the loading process by CSM. There is less requirement for minimum indentation depth to retrieve the data as well. This method is achieved by applying a harmonic damping spring in the indenter column which oscillates at a certain frequency as Figure 3 shows. The indenter involves variable stiffness and displacement based on loading. The oscillating frequency for the indenter column is optimized to prevent interference with test samples. This improvement makes the indenter monitor and obtains stiffness at any time during the indentation process which is useful for the ultra-thin film within the nanometer range.

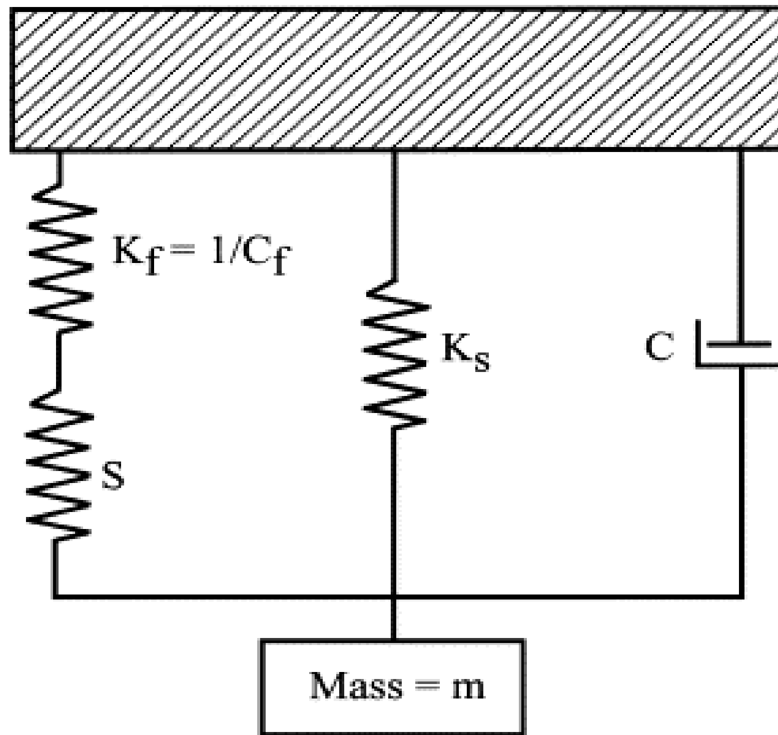

Figure 3 Schematic of the dynamic indentation model [3]

3.2 Approach

Although the Oliver-Pharr method improves a lot, there are still a lot of limitations and deficiencies. For example, as our research continues, more problems have been indicated while indenting the brittle material directly. From Figure 4 and 5, the aluminum oxide's modulus and hardness decrease as the indentation depth increases. It is hard to identify the elastic modulus and hardness of aluminum oxide. This is due to cracks forming along with other defects while indenting, which is shown in Figure 6. This Figure shows that the cracks formed at the corner of the indentation marks. With forming and propagating along the direction, the stored elastic energy was reduced. Hence, the consistent elastic modulus cannot be acquired and leads to lower values than expected. The hardness value decreases with the indent depth because hardness is a combination of elastic and plastic behaviors.

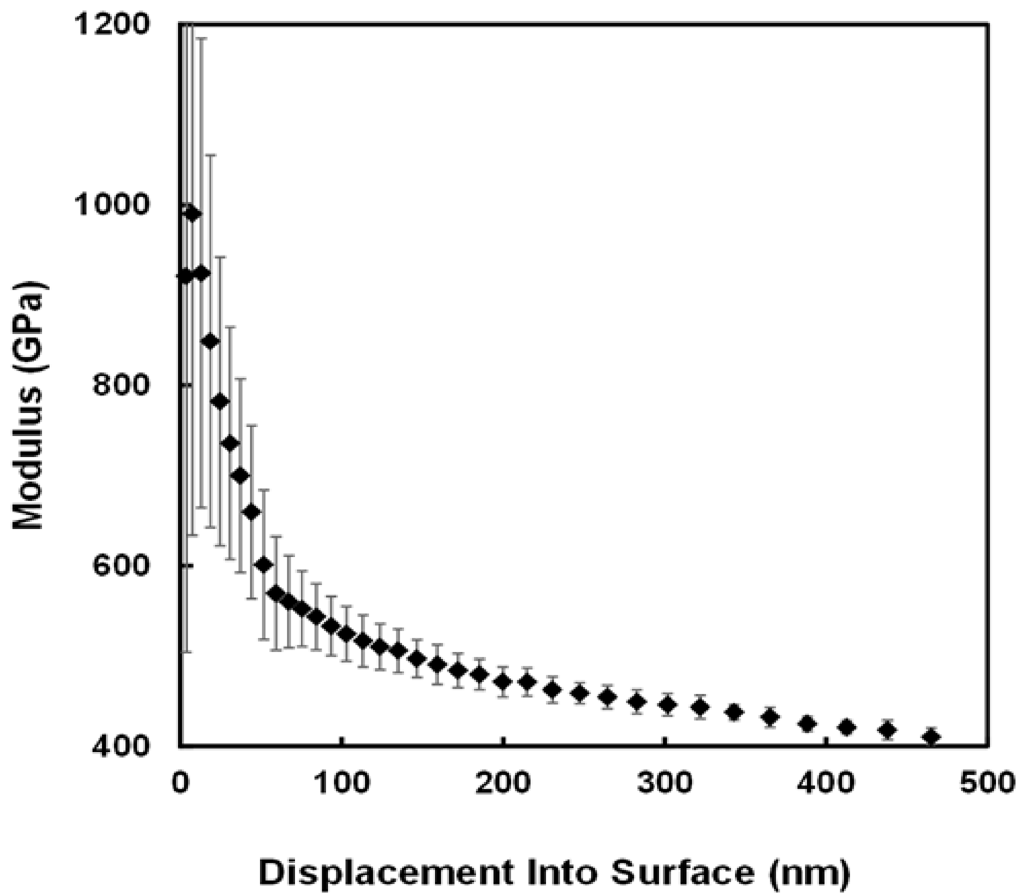

Figure 4 Plot of modulus versus displacement into the surface for indenting Al2O3 directly

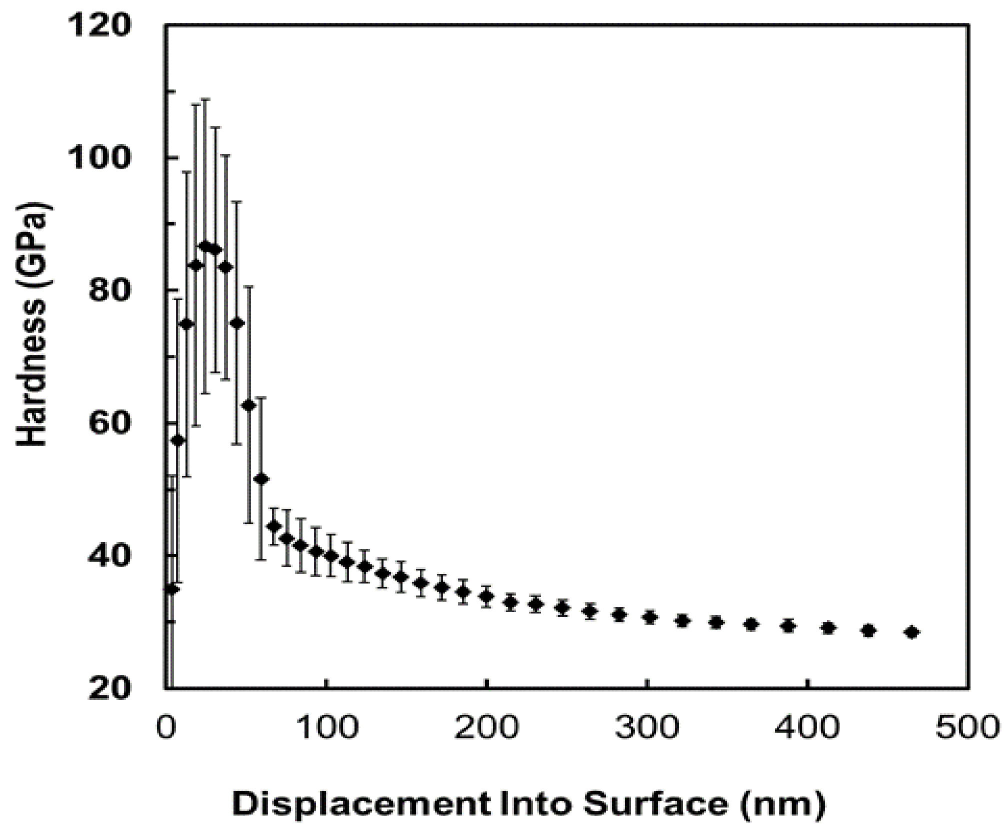

Figure 5 Plot of hardness versus displacement into the surface for indenting Al2O3 directly

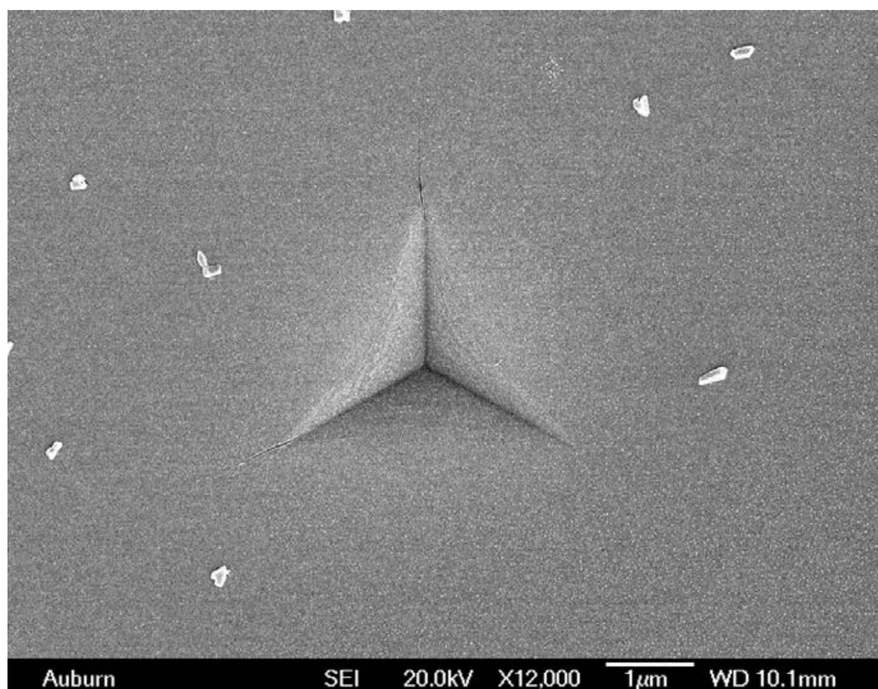

Figure 6 Indentation mark of Aluminum Oxide

In order to solve the problem, our group coated the brittle substrates with thin gold film as Figure 7 shows. The thin film will absorb the inelastic energy and protect the substrate from cracking or failure. From the sight of the focus ion beam, there is no crack between the film and substrate interface.

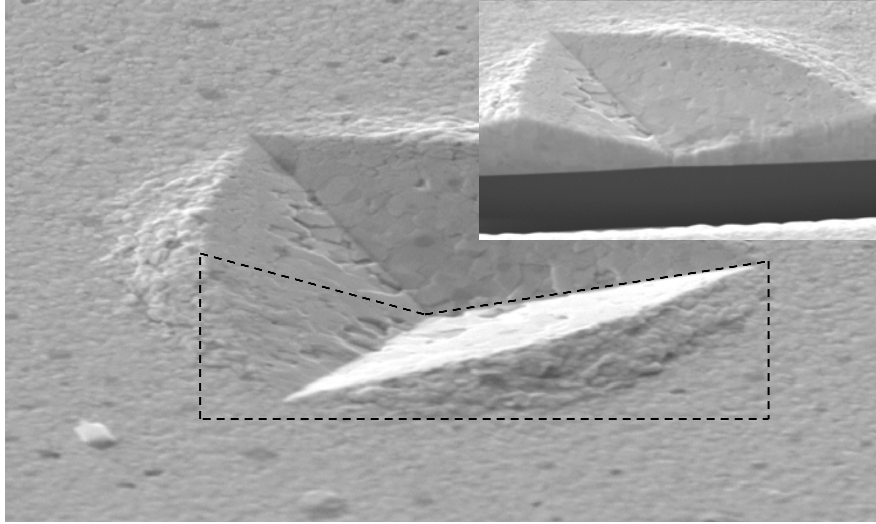

Figure 7 Scanning electron micrograph and focused-ion-beam cross-section of a residual indentation on the Au/Al2O3 composite.

Moreover, our group created a model, which significantly improved the equation based on the previous research. [5-7] The Zhou- Prorok model is defined as

$$\frac{1}{E'} = \frac{1}{E'_f}(1 - \Phi_s) \cdot \left(\frac{E'_f}{E'_s}\right)^{0.1} + \frac{1}{E'_s}\Phi_f \tag{4}$$

where $\Phi_s = e^{-\alpha_s\left(\frac{t}{h}\right)}$,and $\Phi_f = e^{-\alpha_f\left(\frac{t}{h}\right)}$,[9,10]

Where E' is the reduced modulus of the composite material, E'_f is reduced film modulus, E'_s is reduced substrate modulus, α_s and α_f are Poisson's ratio of substrate and film, t is the film thickness and h is, the indentation depth. [8-11]

The Zhou-Prorok model for thin film indentation can be leveraged with deposition of a metallic film to probe the properties of the substrate without indentation generated defects. A 475 nm thick gold film was deposited on the single crystal (0001) aluminum oxide substrate used above and indented to a depth of 900 nm, approximately two times the film thickness. The measured composite modulus is shown as a function of the depth/thickness ratio (h/t), closed circles ●, in Fig. 8. The modulus begins at approximately 100 GPa and continually increases as the substrate is progressively engaged with penetration into the composite. The solid gray line is the result of the Zhou-Prorok model using fitted values of Ef = 80 GPa, ν_f = 0.42, Es = 475 and ν_s = 0.226. These values are very similar to literature values for both materials

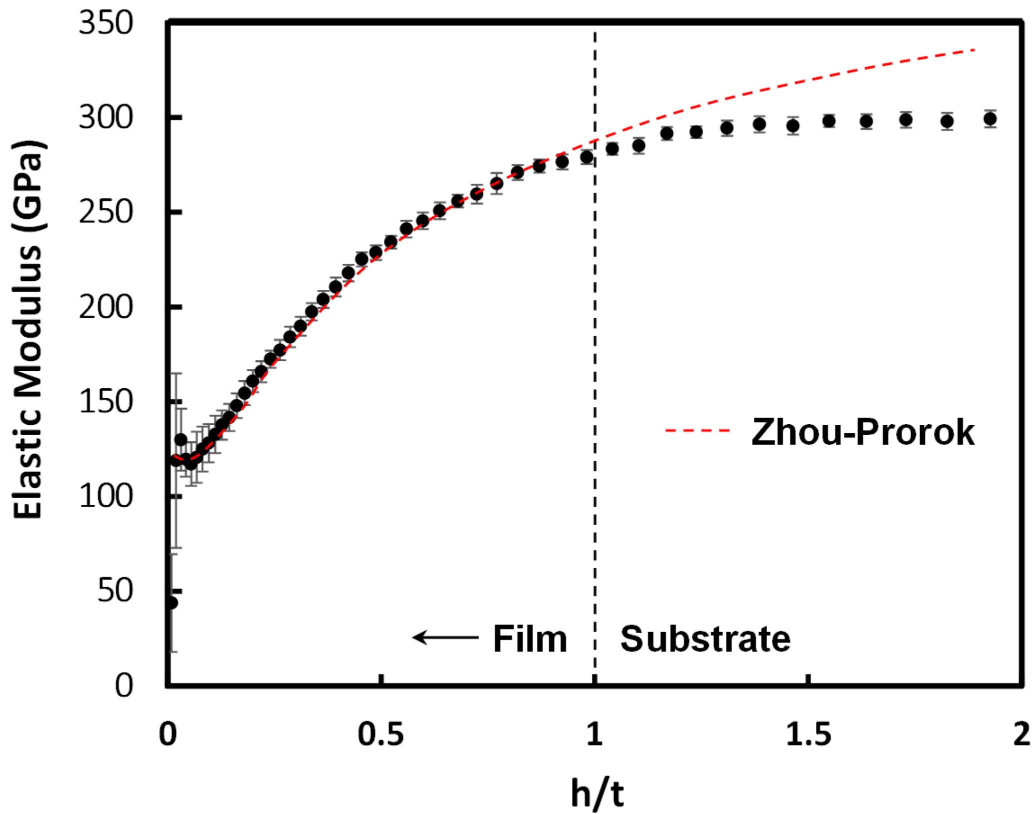

Figure 8 Gold on Aluminum oxide following by Zhou-Prorok model

To take it a step further, Chen revised the Zhou-Prorok model into a new form of the equation to more directly extract the substrate modulus from the composite systems. [16-18] He coated the aluminium oxide with chromium film. Chen's model is derived by following steps

$$\frac{1}{E_t} = \frac{1}{E'_f}\left(1 - exp\left(-\frac{\nu_s}{h'}\right)\right) + \frac{1}{E_s} exp\left(-\frac{\nu_f}{h'}\right)$$

$$L(h') = \frac{1}{E_t}\frac{1}{\left(1 - \exp\left(-\frac{\nu_s}{h'}\right)\right)} = \frac{1}{E'_f} + \frac{1}{E_s}\frac{\exp\left(-\frac{\nu_f}{h'}\right)}{\left(1 - \exp\left(-\frac{\nu_s}{h'}\right)\right)}$$

(5)

Where $\frac{1}{E'_f} = \frac{1}{E_f}\left(\frac{E'_f}{E'_s}\right)^{0.1}$

Equation 5 is a rearrangement of the Zhou-Prorok. The weighting factor on the film side is a from the hyperbolic function $\mathrm{F(x)} = 1/(1 + \exp(-1/x)$ which could be approximated by a linear function $\mathrm{f(x)} = 0.5 + x$ as equation 7 shows. There is also a mathematical Figure 9 to show that all hyperbolic functions approach an asymptote than can be approximated by a linear function. As shown in Figure 10. Then we could have Equation 8

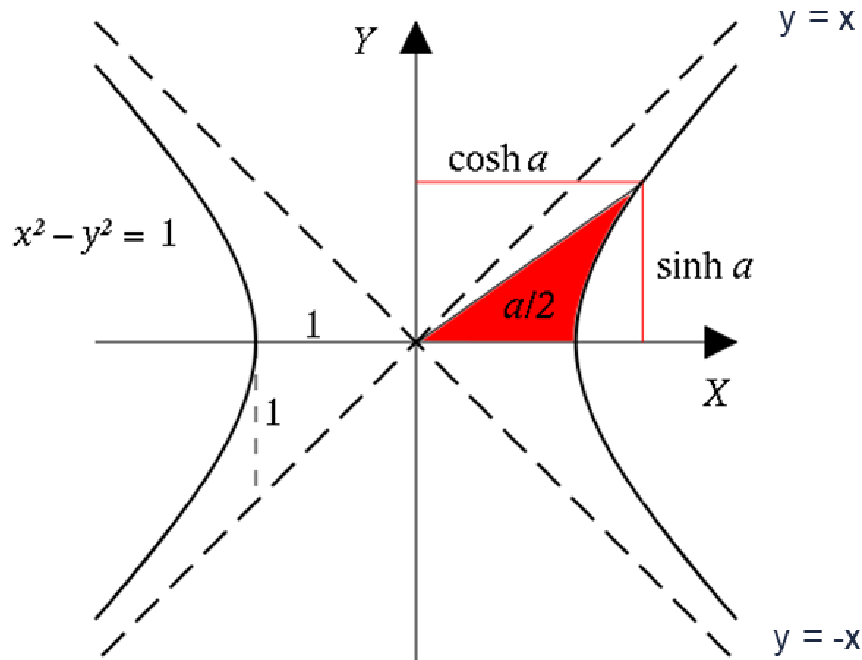

Figure 9 The relationship between hyperbolic function and linear function

$$F(\mathrm{x}) = \frac{1}{2}\left(1\text{-}coth\left(-\frac{1}{2\mathrm{x}}\right)\right) = \frac{1}{1-e^{-(1/x))}}$$

(6)

$$I(h') = \frac{\exp\left(-\frac{\nu_f}{h'}\right)}{\left(1-\exp\left(-\frac{\nu_s}{h'}\right)\right)} \qquad I'(h') = \frac{\nu_s - \nu_f}{\nu_s} - 0.5 + \frac{h'}{\nu_s}$$

(7)

$$L(h') \sim \frac{1}{E'_f} + \frac{1}{E_s}\left(\frac{\nu_s - \nu_f}{\nu_s} - 0.5 + \frac{h'}{\nu_s}\right)$$

(8)

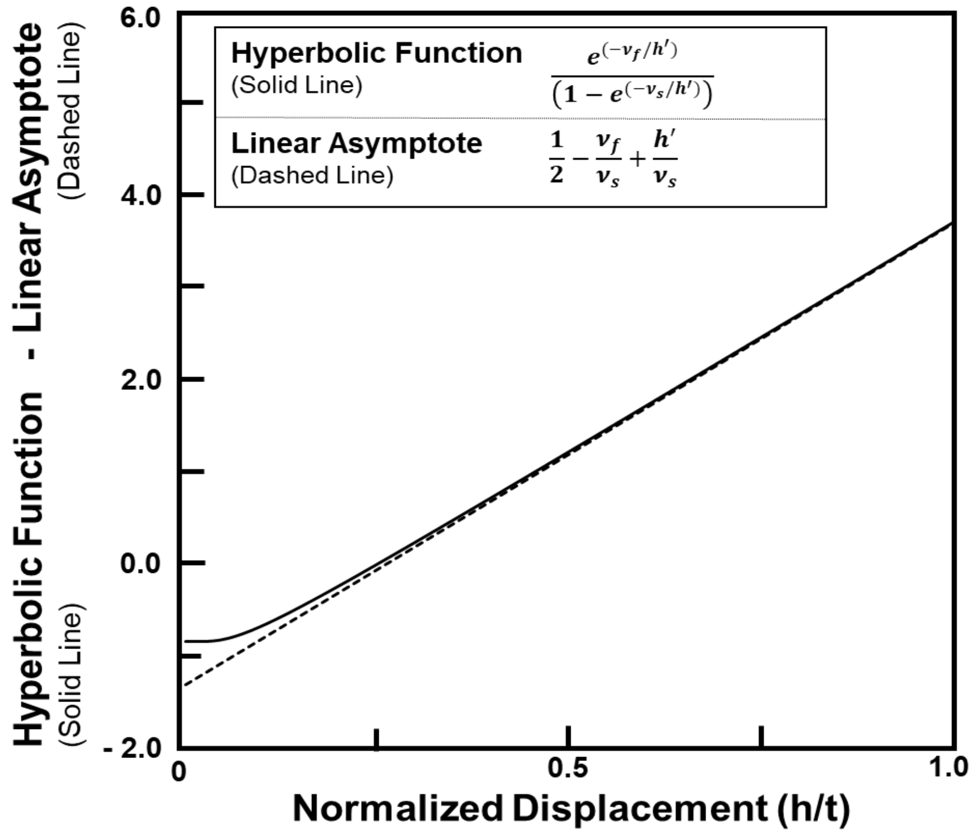

Figure 10 An illustration of linear approximation

The whole equation is regarded as the function of h'. The slope of L(h') is $\frac{1}{E_s\nu_s}$, hence the experiment data can convert into the linear function and, the substrate modulus could be extracted from the slope [19-23]. This is called the Chen-Prorok model, and it does not rely on the film's

Poisson's ratio. This model only requires an estimate of the film thickness. As Figure 11 shows, the Zhou-Prorok model was applied and fit the data rather well, solid gray line, with determined material parameters of; E_f = 190 GPa, E_s = 470 GPa, v_f = 0.210 and v_s = 0. 229.These fit the literature values rather well. In the Figure 12, there is no crack or defect on the substrate. The substrate modulus was extracted from the slope calculated in the Figure 13. It is nearly linear after h'>0.4 and the extracted value is 458GPa which is closer to the literature value compared with direct indentation data in the Table 1. Chen also confirmed that a few other ceramic substrates work for his method and the modulus could be accurately captured, which is shown in Table 1 and Figure 14. [23]

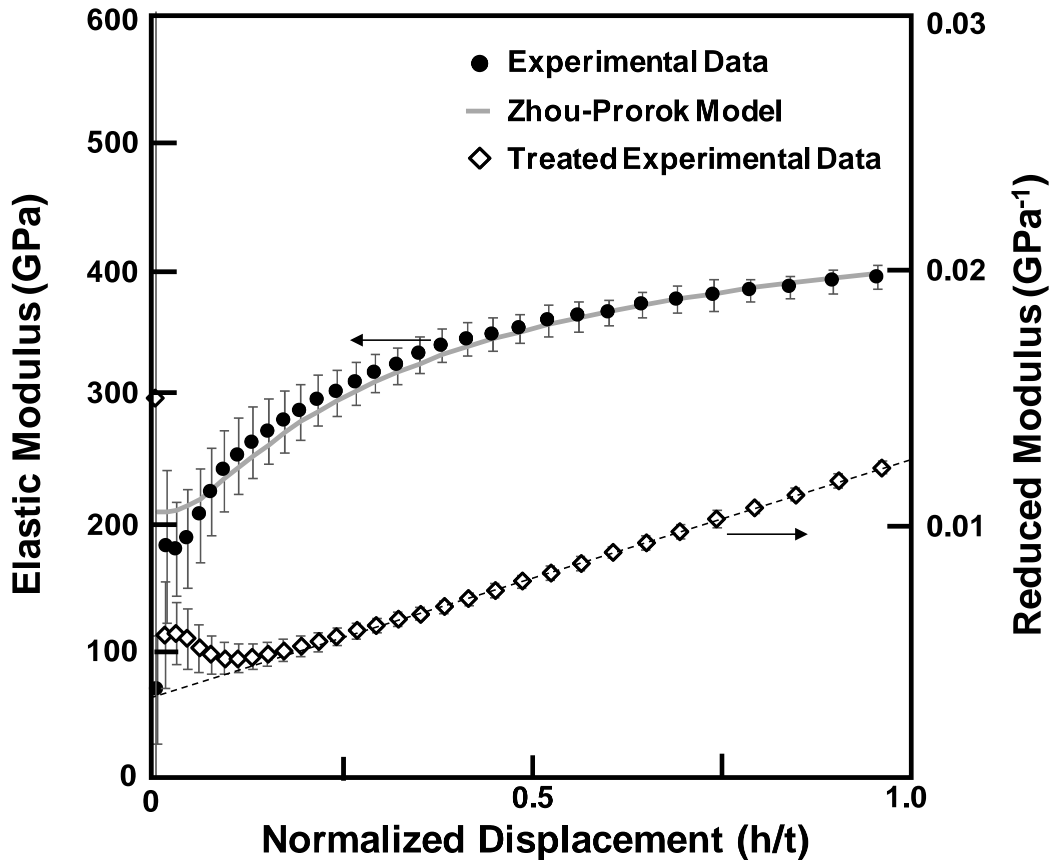

Figure 11 Experimental indentation results of the Cr/Al2O3 film/substrate composite and calculated reduced modulus.

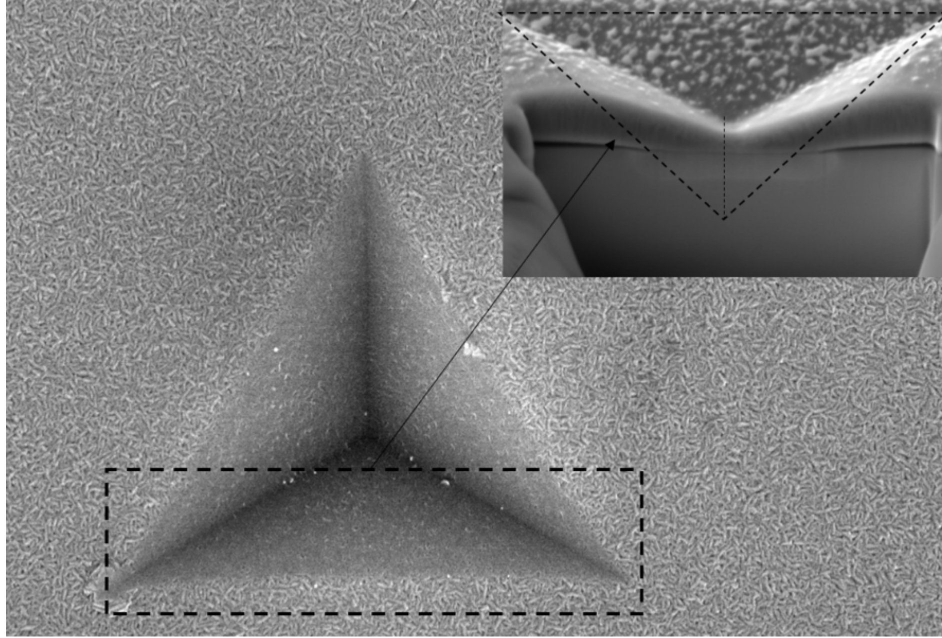

Figure 12 Scanning electron micrograph and focused-ion-beam cross-section of a residual indentation on the Cr/Al2O3 composite.

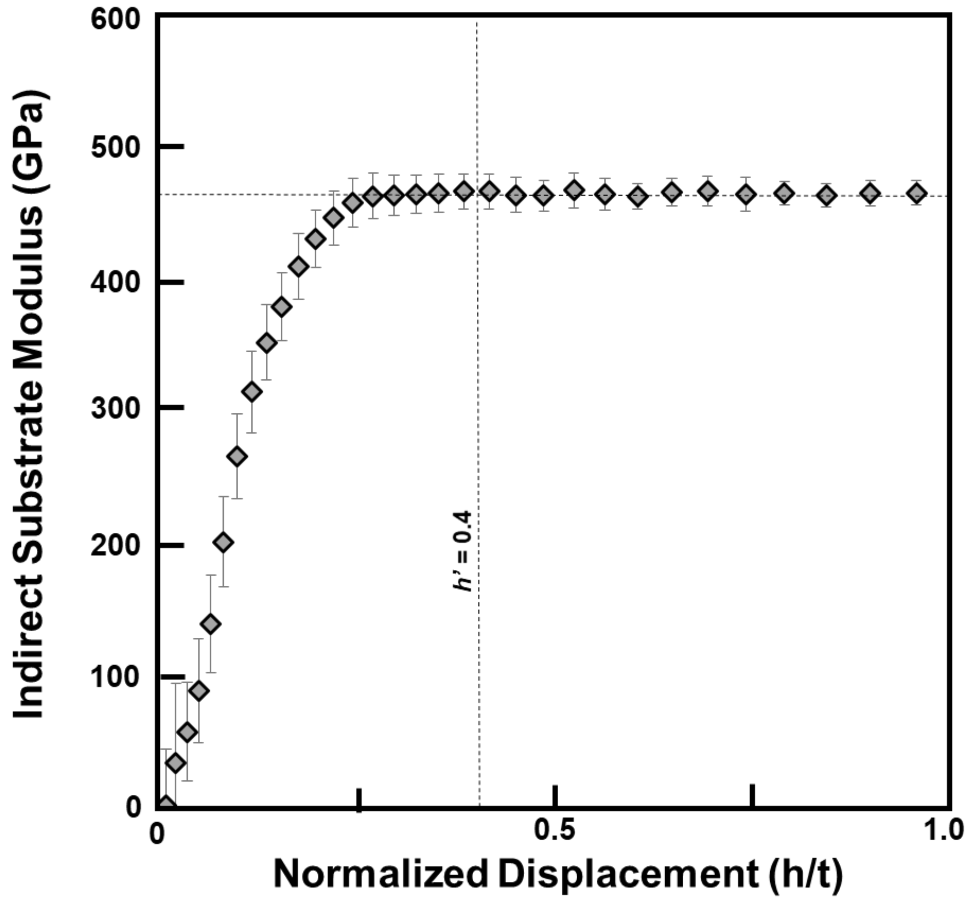

Figure 13 Indirect substrate modulus for the Cr/Al_2O_3 composites

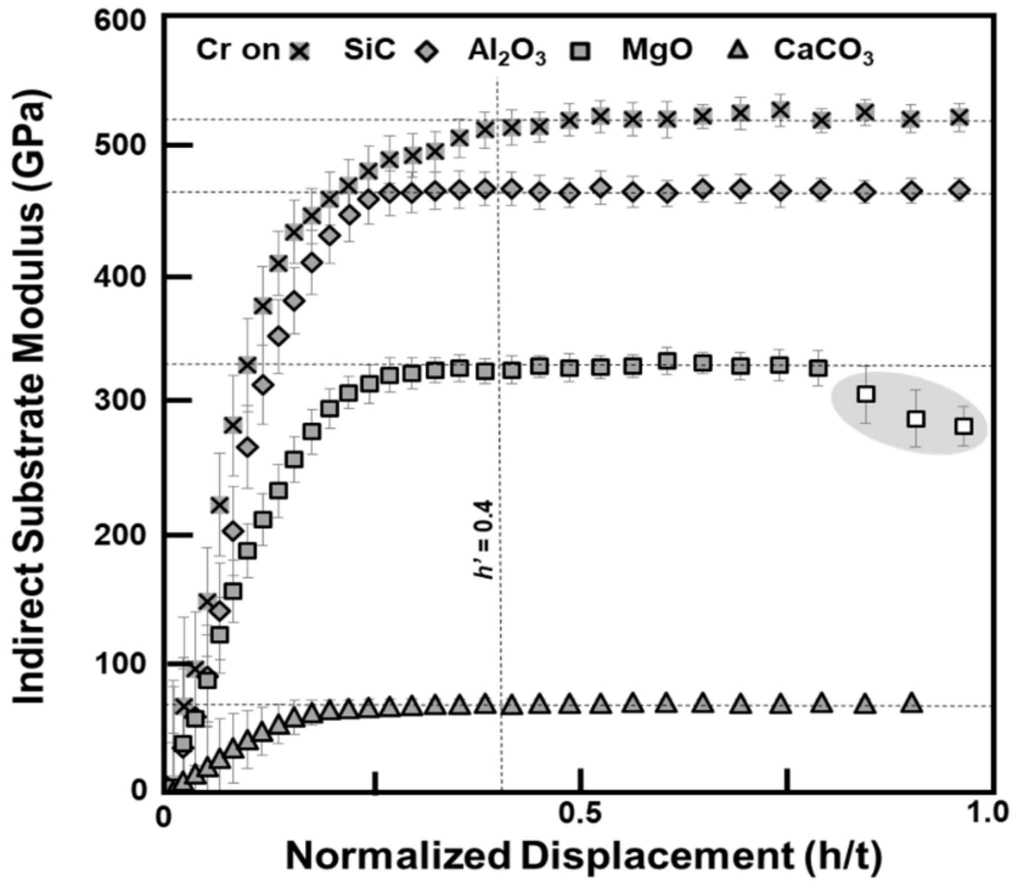

Figure 14 Indirect substrate modulus for the chromium film on 4 different substrates

Table 1 Elastic properties of the direct and indirect indentation methods as compared with literature values.

Material	**E (literature) (GPa)**	**v**	**Direct E (GPa)**	**Indirect E (GPa)**
MgO (100)	**330**	**0.239**	**290 (±5)**	**330 (±5)**
Al2O3 (0001)	**465**	**0.226**	**396 (±9)**	**458 (±10)**
SiC (0001)	**516**	**0.175**	**495 (±10)**	**522 (±11)**
CaCO3 (100)	**70**	**0.310**	**74 (±3)**	**70 (±3)**
Fused Silica	**74**	**0.180**	**70 (±5)**	**76 (±2)**

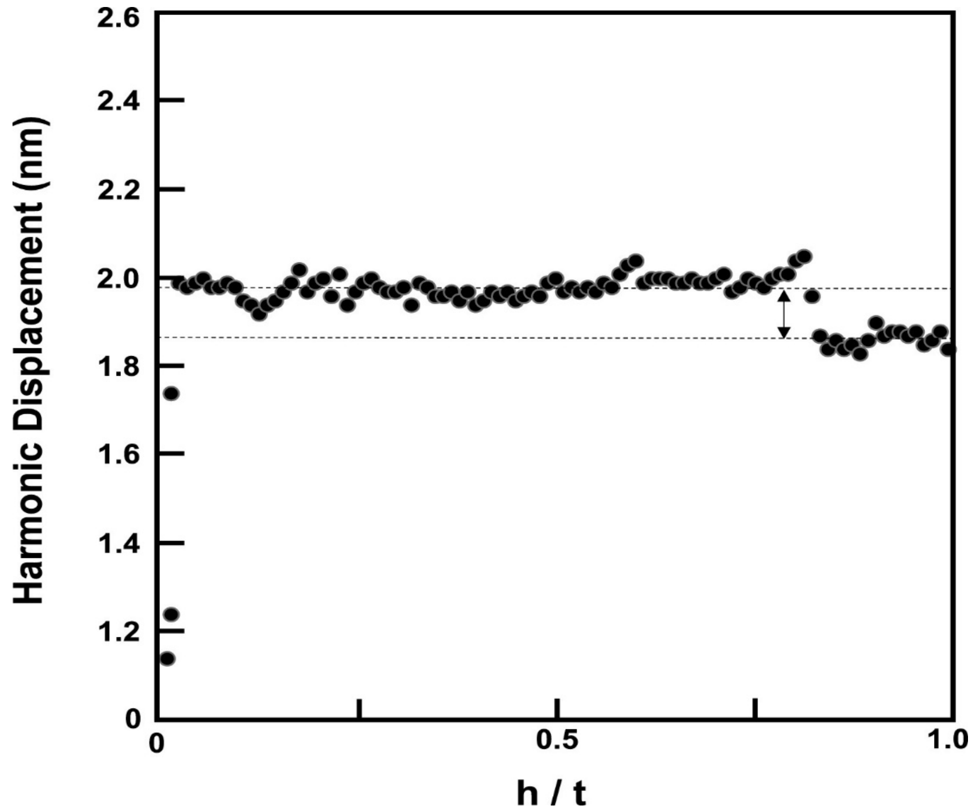

Figure 15 Harmonic Displacement after h’>0.8

4.0 Experimental Procedure

4.1 Material Selection

To keep the same quality, all the substrates are purchased from MTI Corp. Gold was chosen by common use and the stability of their mechanical properties. They are also easy to be sputtered on a wide range of substrates. Next, the substrates used were mainly ceramic materials listed in Table 2. All the substrates are plastically deformed to eliminate the difference between films and substrates during elastic deformation. The silicon was mainly chosen to be investigated due to its good wet ability and conductivity. A lot of reliable data from the literature was collected on this material. The other materials were fused silica (SiO2), calcium carbonate (CaCO3) and magnesium oxide (MgO) listed in Table 2. The films’ and substrates’ literature values (modulus and Poisson’ s ratio) are in Table 2.

Table 2 Material Properties of Chosen Films and Substrates.

	Elastic Modulus, E (GPa)	Poisson's Ratio, ν
Au	79	0.42
Si	179 ± 3	0.28
Fused Silica	74	0.17
$CaCO_3$	70	0.31
MgO	318 ± 7	0.23

4.2 Film Deposition

Two different sputtering units deposited the films. These were a Denton sputtering system using DC and RF power, and a Pelco SC-6 sputter coater. Table 3 and Table 4 show the sputtering parameters such as power(W), time(s), gas flow rate(sccm) and temperature(K) for the Denton Sputtering system. During the gold coating process, ~10nm Titanium was deposited on the substrate first aiming to help wet the substrate to get better gold films. Table 5 displays the typical conditions for using the Pelco SC-6 sputter coater as Figure 15 and 16 shows, vacuum chamber pressure and current, sputtering time are three main factors. Temperature are consistently controlled. Figure 17 provides some reference for thickness deposition.

Table 3 Sputter coating conditions for gold films by using Denton sputtering systems.

	DC	RF
Target	Au	Ti
Presputter Power	100 W	100W
Presputter Time	60sec	60sec
Sputter Power	100 W	100W
Sputter Time	Varies based on the thickness	20sec
Gas (Ar) flow rate	25 sccm	25sccm
Temperature	Room temperature	Room temperature

Table 4 Sputtering conditions for gold films by using Denton sputtering systems without Ti

Sputter Current	0.3mA
Sputter Time	Varies base on thickness
Temperature	Room temperature
Working Distance	30mm
Pressure	0.08mbar

Table 5 Sputtering conditions for gold films by using Pelco SC-6 sputter coater

	DC
Target	Au
Presputter Power	200W
Presputter Time	60sec
Sputter Power	200W
Sputter Time	Varies based on the thickness
Gas (Ar) flow	25sccm

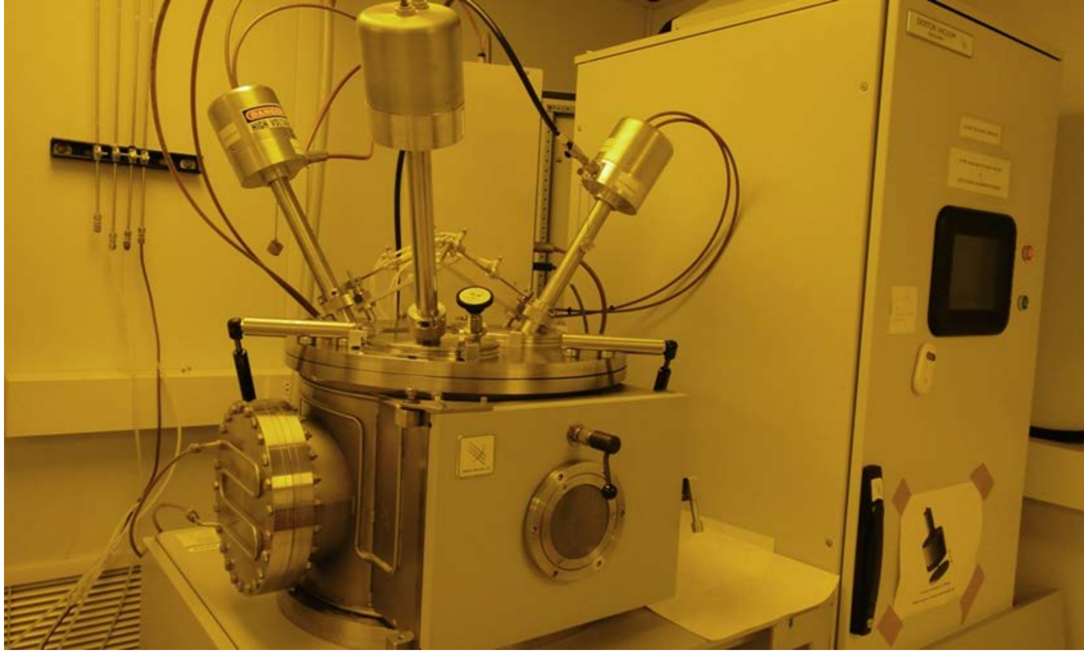

Figure 16 Denton Sputter Coating system

Figure 17 Pelco Sputter Coating system

Thickness Reference Chart

Results were compiled using a Gold target with Argon gas.
Working distance measured from sample table to target.
MTM Monitor settings: Density = 19.3, Tooling Factor = 1.4
All thickness values are approximate and are intended for reference only. Actual results may vary.

30 mm WORKING DISTANCE									
	0.02 mbar			0.05 mbar			0.08 mbar		
	20 sec	40 sec	60 sec	20 sec	40 sec	60 sec	20 sec	40 sec	60 sec
20 mA	12 nm	24 nm	36 nm	10 nm	21 nm	31 nm	7 nm	14 nm	21 nm
30 mA	17 nm	35 nm	53 nm	16 nm	33 nm	50 nm	13 nm	25 nm	38 nm
40 mA	22 nm	48 nm	67 nm	25 nm	51 nm	77 nm	19 nm	39 nm	57 nm

50 mm WORKING DISTANCE									
	0.02 mbar			0.05 mbar			0.08 mbar		
	20 sec	40 sec	60 sec	20 sec	40 sec	60 sec	20 sec	40 sec	60 sec
20 mA	7 nm	13 nm	20 nm	4 nm	9 nm	14 nm	3 nm	5 nm	7 nm
30 mA	9 nm	20 nm	30 nm	8 nm	16 nm	24 nm	5 nm	10 nm	14 nm
40 mA	17 nm	33 nm	50 nm	11 nm	22 nm	34 nm	8 nm	15 nm	23 nm

70 mm WORKING DISTANCE									
	0.02 mbar			0.05 mbar			0.08 mbar		
	20 sec	40 sec	60 sec	20 sec	40 sec	60 sec	20 sec	40 sec	60 sec
20 mA	4 nm	7 nm	11 nm	1.3 nm	2.7 nm	4.2 nm	0.9 nm	1.9 nm	2.8 nm
30 mA	6 nm	12 nm	18 nm	2.9 nm	5.8 nm	8.7 nm	1.7 nm	3.5 nm	5.3 nm
40 mA	7 nm	15 nm	23 nm	4.6 nm	9.4 nm	14 nm	2.6 nm	5.3 nm	8 nm

Figure 18 Thickness reference chart

4.3 Thickness Measurement

The films' thicknesses are measured by using a JEOL 7000F Scanning electron microscope (SEM). After sputtering the films on the substrates, the samples were fractured to get the cross-section areas. Each sample's thickness was evaluated by choosing five different areas' images to get the average thickness under two modes. The first mode is SEI (Secondary electron mode) Figure 18 and the second mode is COMPO (Back-scattered electron mode) Figure 19. The results are confirmed by two modes to minimize the deviation. This step was dragged across all four corners of the substrate and the thickness was estimated.

Additionally, film thickness from Scanning Electron Microscope was confirmed with focused ion beam (FIB) by TESCAN LYRA FIB-SEM from University of Alabama.

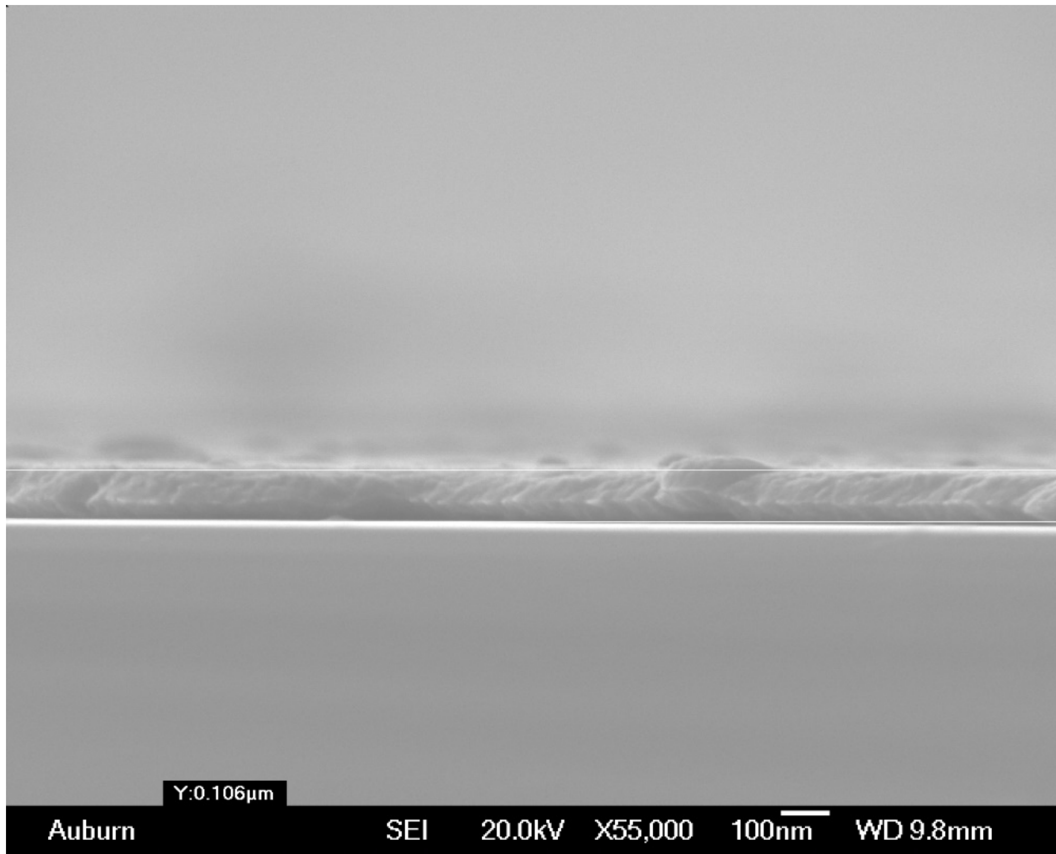

Figure 19 Thickness measurement under Secondary Electron Mode

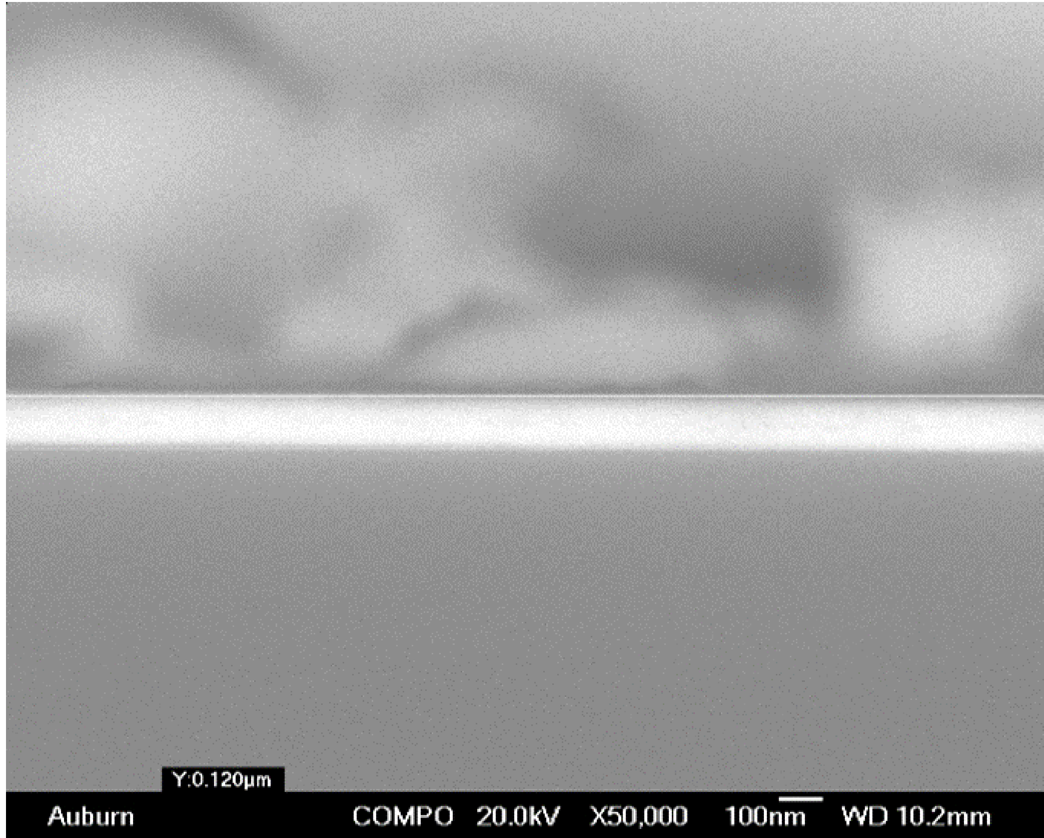

Figure 20 Thickness measurement under Backscattered Electron Mode

4.4 Nanoindentation

An MTS Nanoindenter XP as Figure 20 shows with a Berkovich diamond tip (three-sided pyramid) was utilized to do the indention tests. The tip radius is less than 50nm.The continuous stiffness method was applied to help get dynamic stiffness while indenting the samples. Each sample has 25 individual indent marks with a range of 50um*50um. Modulus and hardness data were chosen from the average data of 25 independent marks acquired from the equipment. The penetration depth was under film thicknesses referred to Chen-Prorok model that normally doesn't punch through the substrates. Thermal drift rate was controlled under 0.05nm/s to eliminate the surrounding effects. Test frequency was set to 45Hz, and the harmonic displacement was 2nm. [24-27]

Figure 21 MTS Nanoindenter XP

4.5 Scanning Electron Microscopy

The JEOL 7000F Scanning electron microscopy (SEM) as Figure 21 shows was used to capture the images of indentation marks and the thickness of the thin films' layers. All images were taken under the same magnification for comparing. The secondary electron and back-scattered electron modes are used to take images by different research purposes. The parameters were set to 20kV voltage and 10 mm working distance.

Figure 22 JEOL 7000F Scanning Electron Microscope

4.6 Heat Treatment

The VWR Gravity Convection Oven as Figure 23 shows was used for annealing different thickness gold on silicon. The temperature was set to 200 °C. The oven increases 5 °C every minute. All samples are placed in a seal glass holder in order to exclude other factors. The annealing time was one hour from room temperature to setting temperature, and all samples were air-cooled under room temperature.

Figure 23 VWR Gravity Convention Oven

5.0 Results

5.1 Film Thickness's Effects on the Indirect Indentation Method

To investigate if film thickness plays a role in the indirect indentation method, we started with gold on silicon. Gold is one of convenient material for sputtering. It is really stable without any oxidized layer to affect the coating and indentation result [36-41]. Next, silicon is easy to use and most common ceramic material as a substrate, much data has been collected on this material, so it was chosen to begin. Thus, gold on silicon substrate combination was chosen to study at first since our group have many reliable data to use as baseline to guide future research and in literature as well [42-46].

First, in order to confirm the limitation of nanoindentation without indirect indentation method, the raw silicon substrate without gold film was indented at first as Figure 24 shows. The solid marker denotes the experiment modulus from nano indenter and the solid straight line represents the literature value of silicon elastic modulus(79GPa). It is hard to get the real material modulus from the direct indentation. In the early stage of indentation, it seems that the indentation result is even higher than the literature value. This is because cracks are not generated yet and it is hard to get a SEM image under shallow depth. However, with the indenter tip punching through the film, cracks were generated which cause the stored elastic energy lost to generated to new surfaces. As Figure 24 shows, the direct indention modulus decreased continuously with deeper indentation depth. With deeper indentation depth, cracks appeared and propagated as Figure 25 shows. The cracks started to generate at the corner of indentation mark with 500nm indent depth and became even clearer in the indentation mark with 1000nm indent depth. It is difficult to acquire silicon elastic modulus according to the transition. In order to avoid the inelastic delegation by the indenter tip, the indirect indentation method uses a metallic film to absorb this damage so the substrate's properties can be accurately measured.

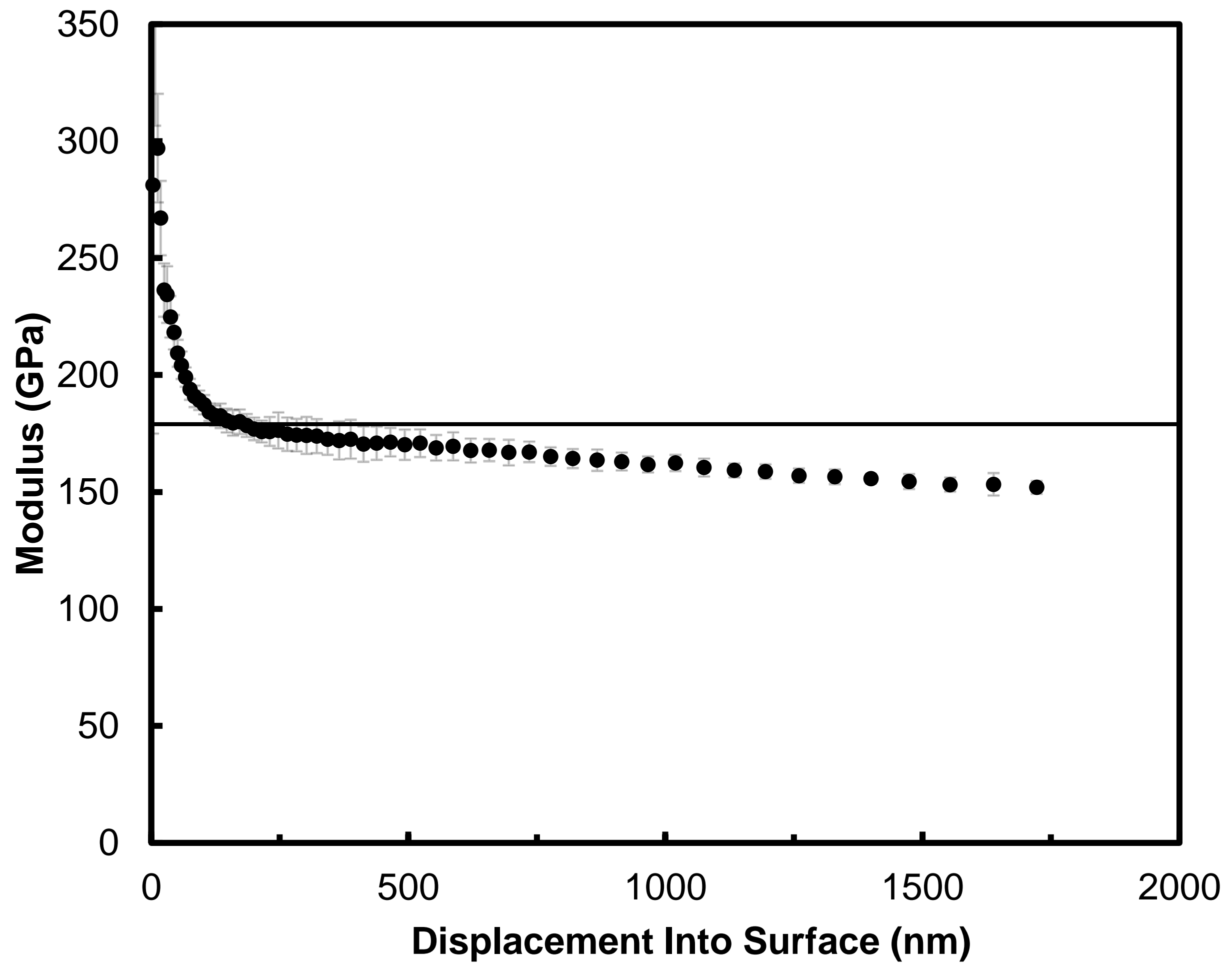

Figure 24 Direct indentation modulus on silicon substrate modulus (solid markers) with literature value (solid line)

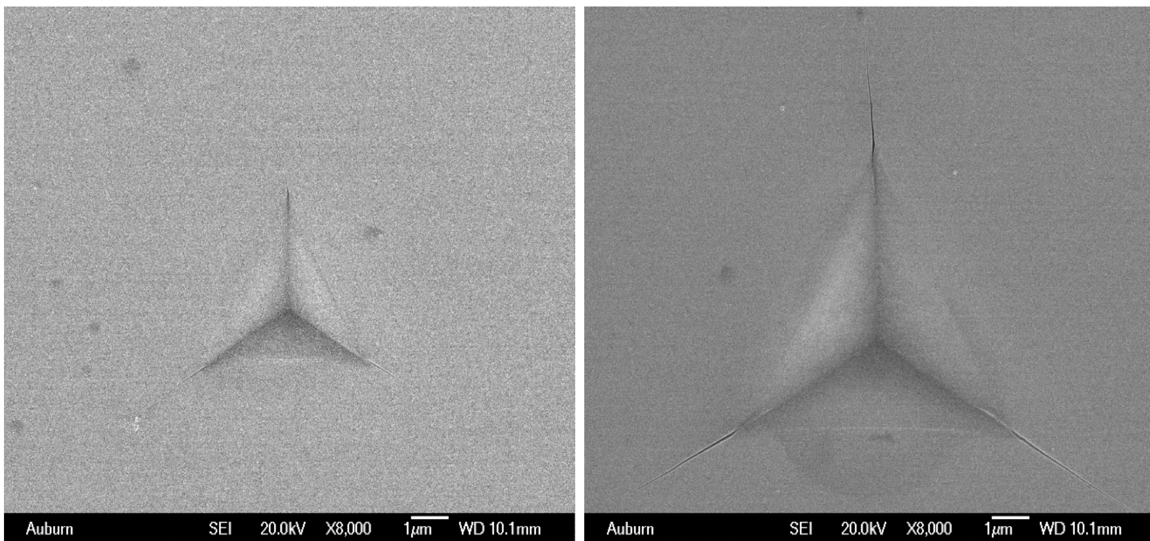

Figure 25 Indents on silicon substrate with 500nm depth(left) and 1000nm depth(right)

Then depositing gold films on the silicon substrate using Denton Sputter system can fill this role. Based on previous experience, the film thickness around half micro gets best performance and fitting result so we started to examine. The deposition time is Table 6 and the thickness was confirmed with SEI and COMPO mode under scanning electron microscope as Figure 26 shows. The area between two solid black line is gold film. These images indicate that uniform gold film was deposited on substrate. It was found that gold film appeared brighter in COMPO mode because the atomic number of gold is larger than silicon. The dark part under solid black line is silicon substrate.

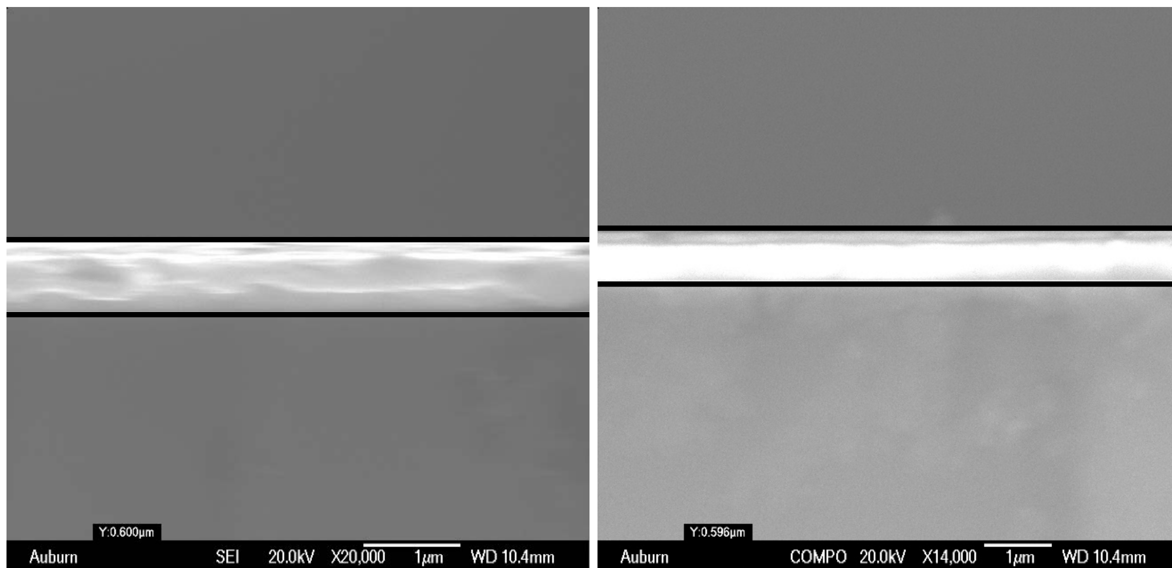

Figure 26 598nm deposition thickness measurement under SEI and COMPO mode

Table 6 Gold Thickness and deposition time by Denton

Denton Sputter System	**Thickness(nm)**	**Deposition Time(sec)**
	49	110
	118	216
	194	280
	298	430
	349	465
	447	650
	598	810
	946	1090

The Figure 27 gives the experiment result (composite modulus) of gold on silicon combination. In order to eliminate the thickness variations, the displacement into surface was divided by film thickness(598nm) which is called normalized displacement. It is obvious that the solid marks (composite modulus) is far off from the literature value(179GPa). It is clear that the lower modulus of the gold does not allow the composite modulus to reach the substrate value while the tip is still in the film. Even the indentation depth is approaching the maximum of the film thickness.

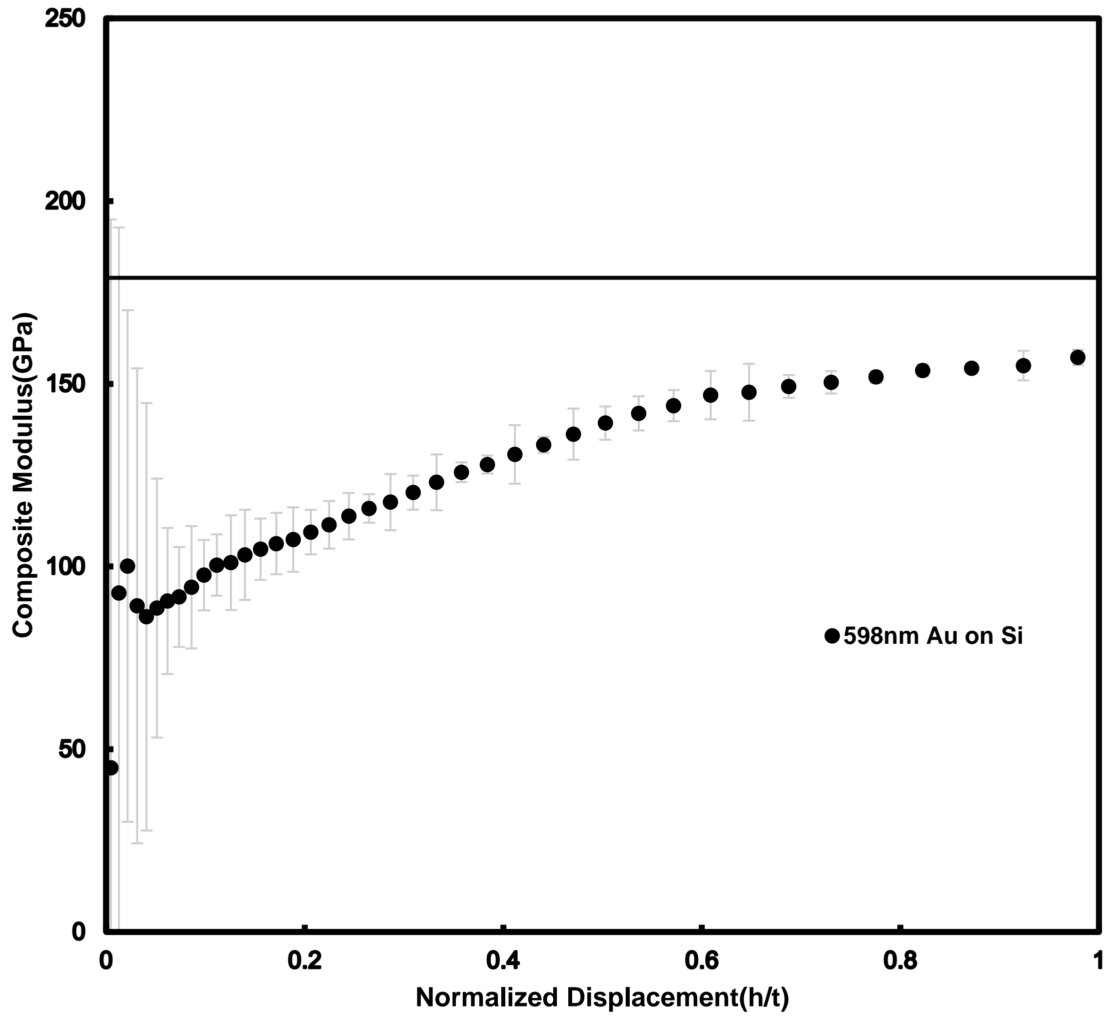

Figure 27 Composite modulus of 598nm gold on silicon

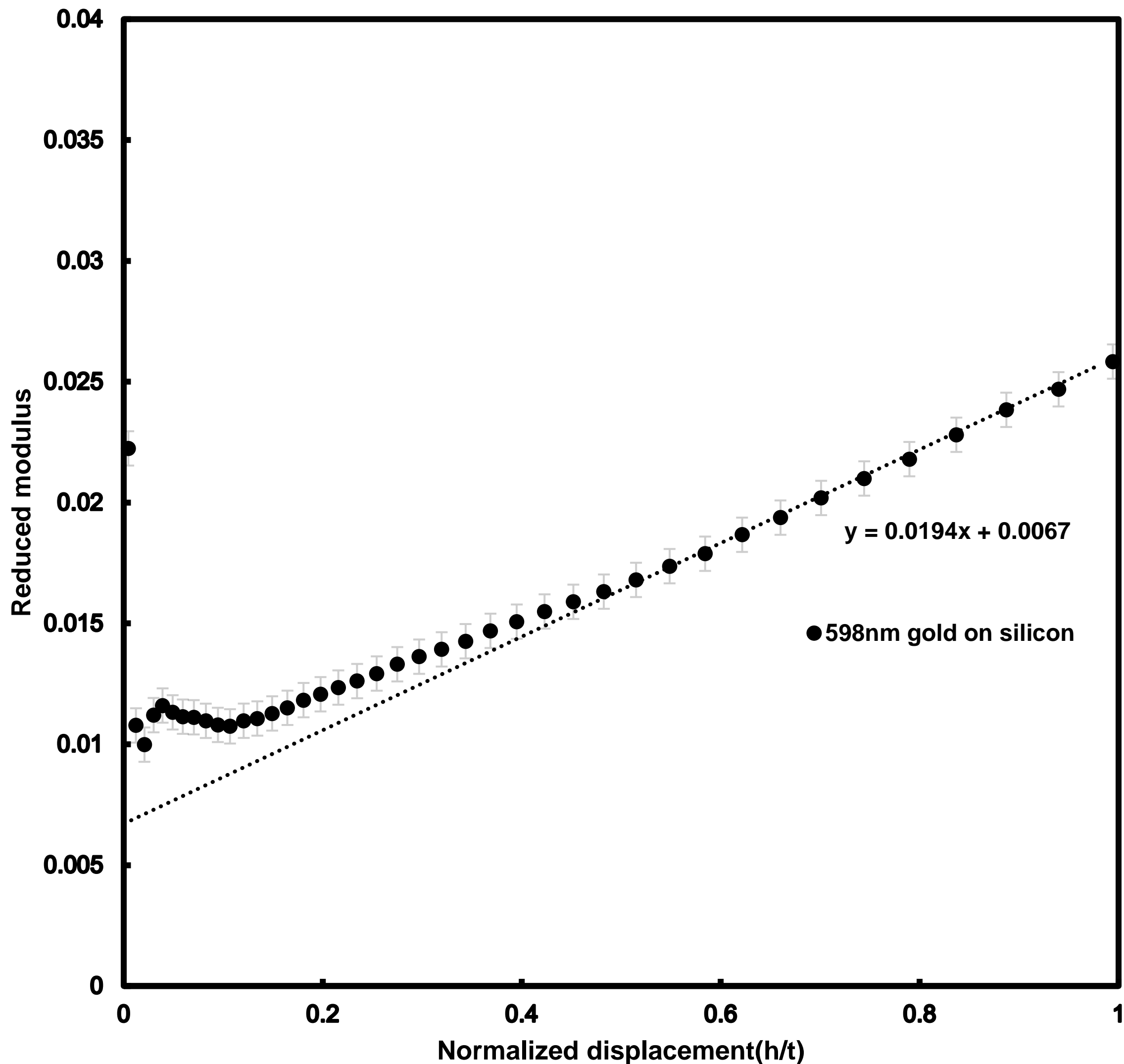

Figure 28 Reduced modulus of 598nm gold on silicon

Based on composite modulus given above, the reduced modulus was calculated by using the indirect indentation method as Figure 28 shows. This involves dividing the composite modulus by the film side weighting factor as described in approach section. The solid marks represent the reduced modulus. The dashed line represents the slope got from data points of h'=0.6~1.

Then we calculated the indirect modulus based on the reduced modulus's slope from h'=0.6~1, the slope equals one versus substrate modulus multiply substrate Poisson's ratio and then the substrate modulus was extracted from the composite modulus by one versus slope multiply substrate Poisson's ratio as shown in Figure 29.

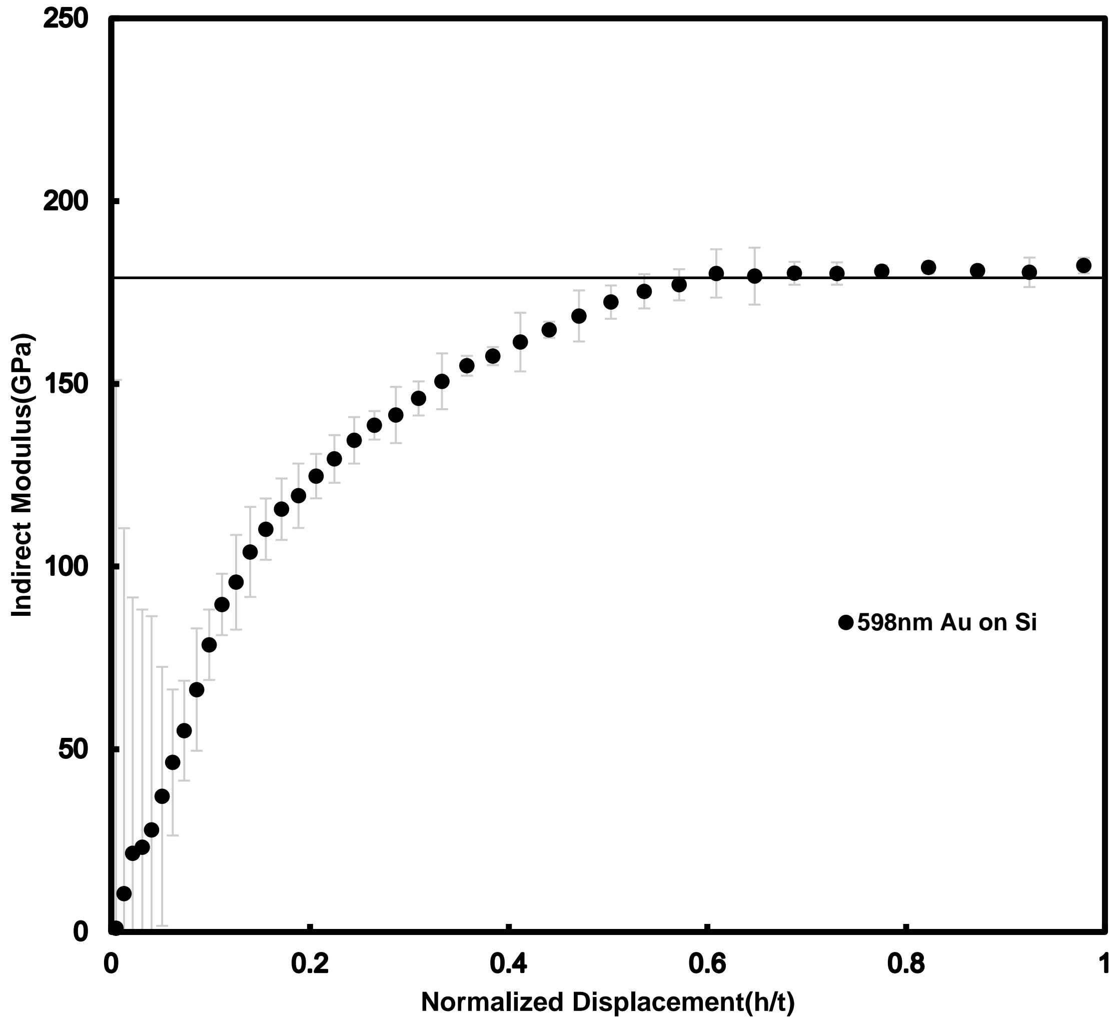

Figure 29 598nm gold on silicon indirect modulus

The silicon modulus was acquired in a small deviation range. At very initial range, the indenter tip might not fully contact with sample surface under certain frequency so there is a large error bar and deviation data. The black dotted marks show the indirect substrate modulus(182GPa), and the solid black line shows the literature substrate modulus (Si,179GPa). As h'>0.6, indirect indentation method (Chen-Prorok model) accurately predicted silicon's elastic modulus.

This shows the indirect indentation method works well with 598nm gold on silicon. It was curious to know whether the method fits different thickness gold on silicon substrate.

5.1.1 Fitting the Indirect Indentation Method to Gold films on Silicon by Denton

In order to prove the consistency of the indirect indentation method, seven more groups thickness (49nm,118nm,194nm,298nm,349nm,447nm,946nm) gold were deposited on silicon substrates and were indented by nano indenter. All the eight-group thickness on silicon substrates' indirect modulus data are shown on Figure 33 which are the average all datapoints from h'=0.6 to h'=1 based on Figure 31 and 32. The Figure 30 gives the composite modulus from indentation test and it is hard to tell the real elastic modulus of substrate. All data scattered in the Figure 30. For example, the composite modulus can be low to 140GPa from 946nm gold on silicon and high to 250GPa from 49nm gold on silicon. There is 110GPa difference. Although these substrates are the same manufactured from MTS, each may behave differently due to their microstructure and thickness. Then, the indirect indentation method was applied to all group. First, the reduced modulus was obtained from the composite modulus. It was clear that the reduced modulus of all groups was almost parallel to each other which means the slope are almost same. All the slopes' value is shown in Table 7. However, after applying indirect indentation method, the extracted modulus datapoints became straight line after h'>0.4 and parallel to each group. The extracted modulus of 49nm,118nm and 194nm gold on silicon substrate were relatively higher than literature value as figure 33 shows.

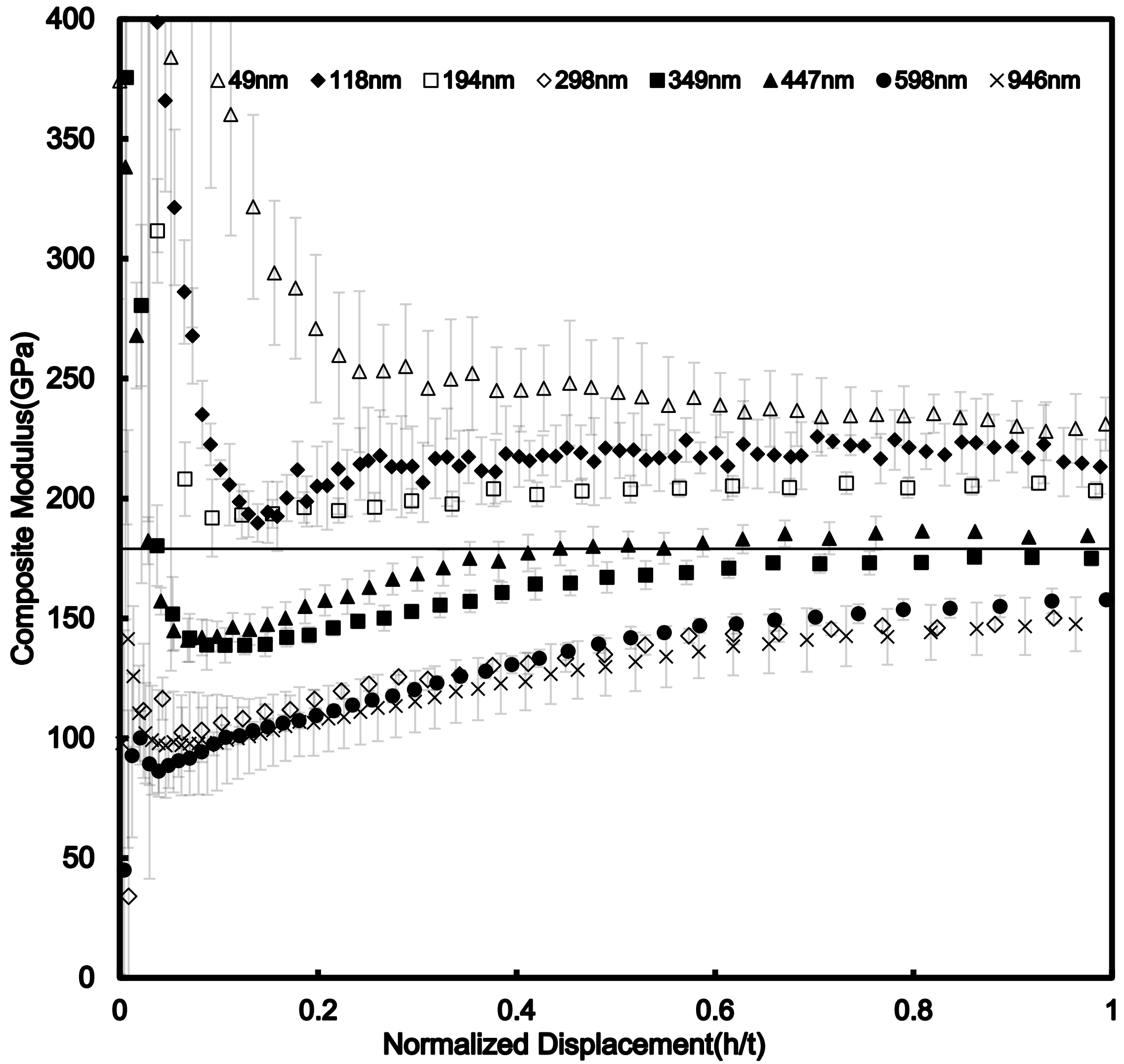

Figure 30 Composite modulus of different thickness gold on silicon

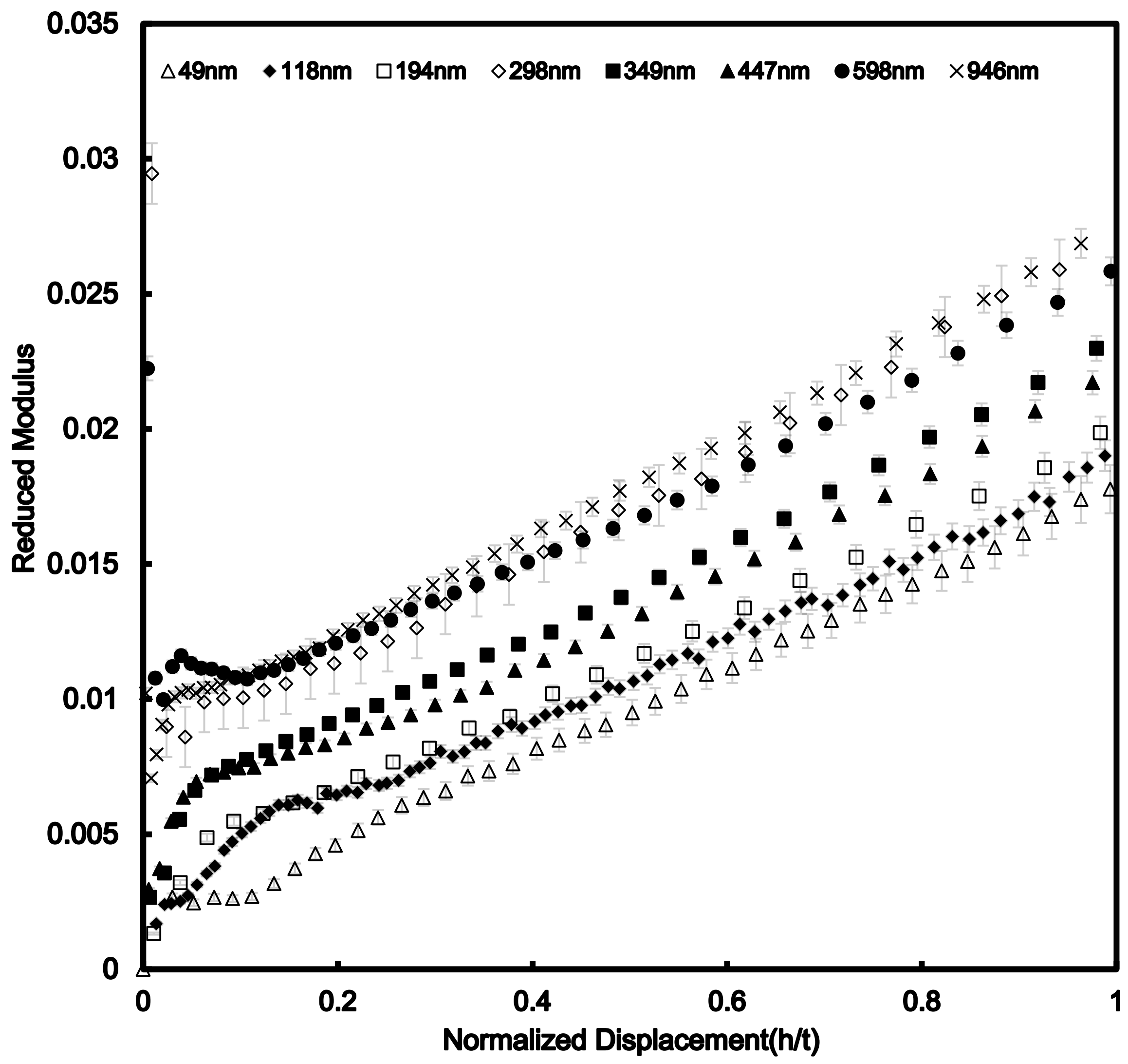

Figure 31 Reduced modulus of different thickness gold on silicon

Table 7 Slopes and indirect modulus with different thickness

Thickness(nm)	Slope	Indirect Modulus (GPa)
49	0.0167	214±4.7
118	0.0173	206±5.2
194	0.0174	205±4.6
298	0.0207	173±4.6
349	0.0192	187±4.4
447	0.0189	189±5.3
598	0.0194	182±4.5
946	0.0203	175±4.8

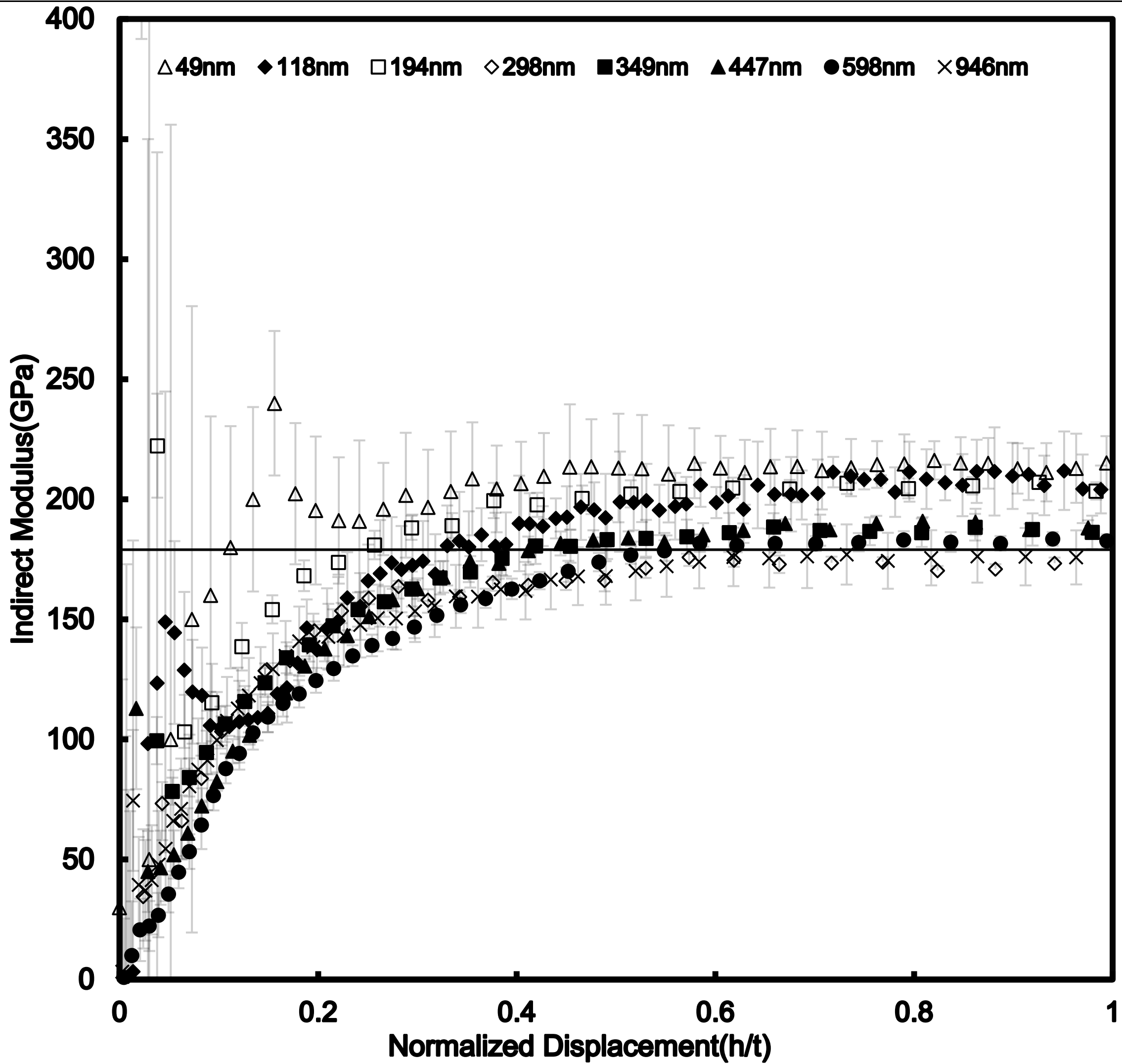

Figure 32 Indirect modulus of different thickness gold on silicon

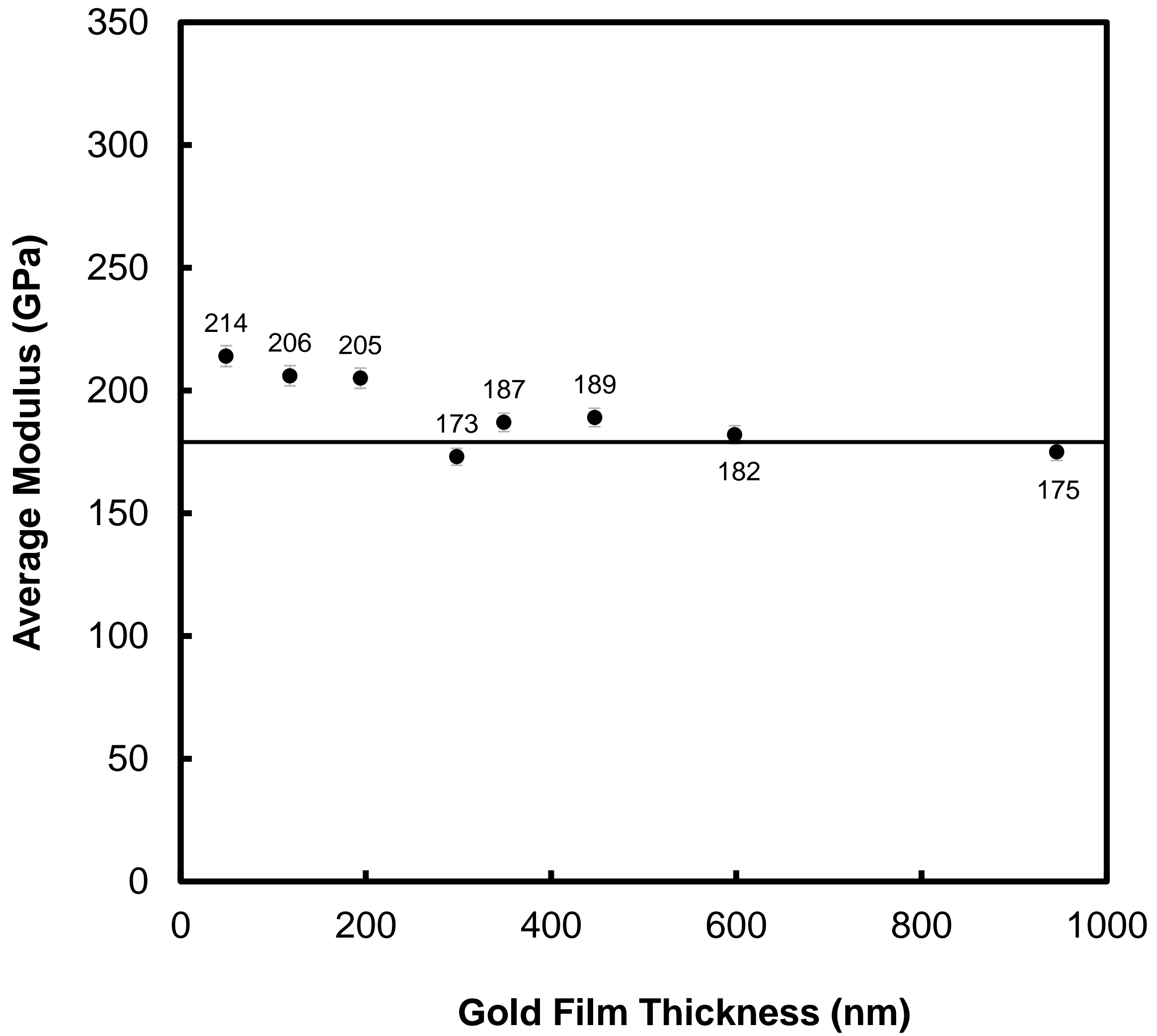

Figure 33 Average indirect modulus of different thickness gold on silicon

Each solid mark represents certain thickness gold on silicon. There is a clear trend that if thin film thickness passes 200nm, the extracted substrate modulus is pretty consistent within silicon literature value range.

Back to Denton sputter parameters, this phenomenon could be explained. Due to low surface adhesion of the metal, it is hard for gold to deposit on ceramic substrates directly. However, Ti is regarded as an interlayer between gold and ceramic substrates to improve coating ability. A titanium adhesion layer which was installed on RF side with an aim of 10~20nm film thickness was deposited initially before coating with gold. The literature value of titanium elastic modulus is 110Gpa and Poisson's ratio is 0.31 compared with 79Gpa and 0.42 of gold. This means titanium is stiffer and hard to be deformed when the indenter tip is punching through the film. The load will be most likely transferred to the substrate directly instead of spread out. As a result of titanium layer between silicon and gold, the stiffness changes during the unloading process which leads to higher substrate elastic modulus from extraction.

In order to confirm the assumption, 107nm gold film which is confirmed in Figure 34 was deposited on silicon substrate by Denton sputter system without titanium layer and indented. The bright layer indicated the gold film and the dark layer was silicon. From the compo image in Figure 34, there is no third layer contrast since there were only silicon and gold layers. The Figure 35 gave the composite modulus of 107nm gold film without titanium layer and compared with 118nm gold on silicon with titanium layer, the composite modulus dropped a lot which confirmed non-titanium layer in another direction. Based on Figure 35 and 36, the indirect modulus can be calculated. As Figure 37 shows, the solid straight line is silicon literature modulus and the dotted line is extracted silicon modulus by applying indirect indentation method. The extracted modulus is around 174Gpa which is closer to the literature value. It is also noticed that with increasing film thickness, the titanium layer effect decreased.

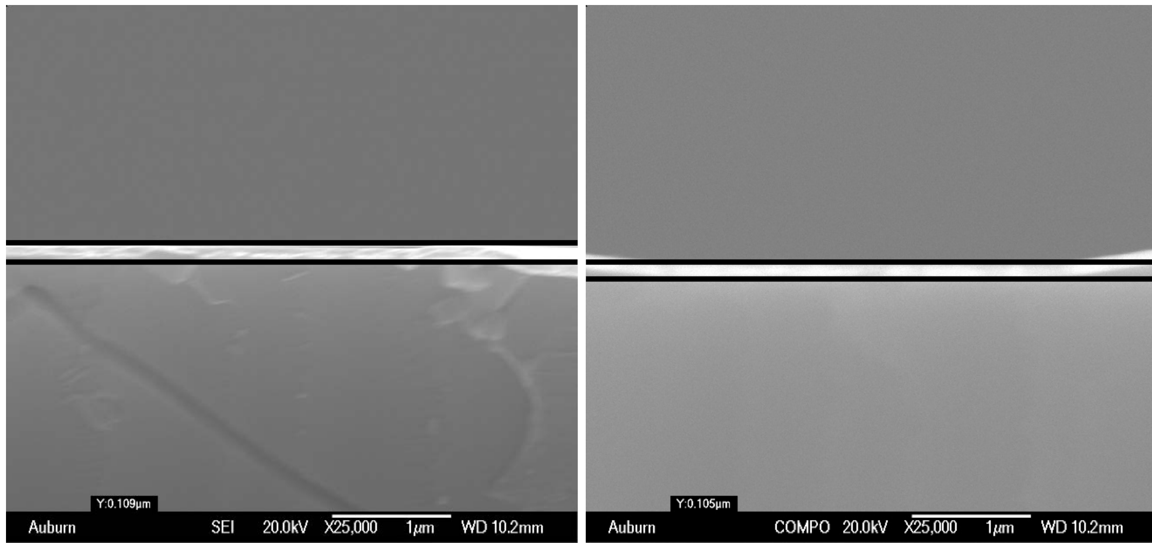

Figure 34 107nm deposition thickness without Ti measurement under SEI and COMPO mode

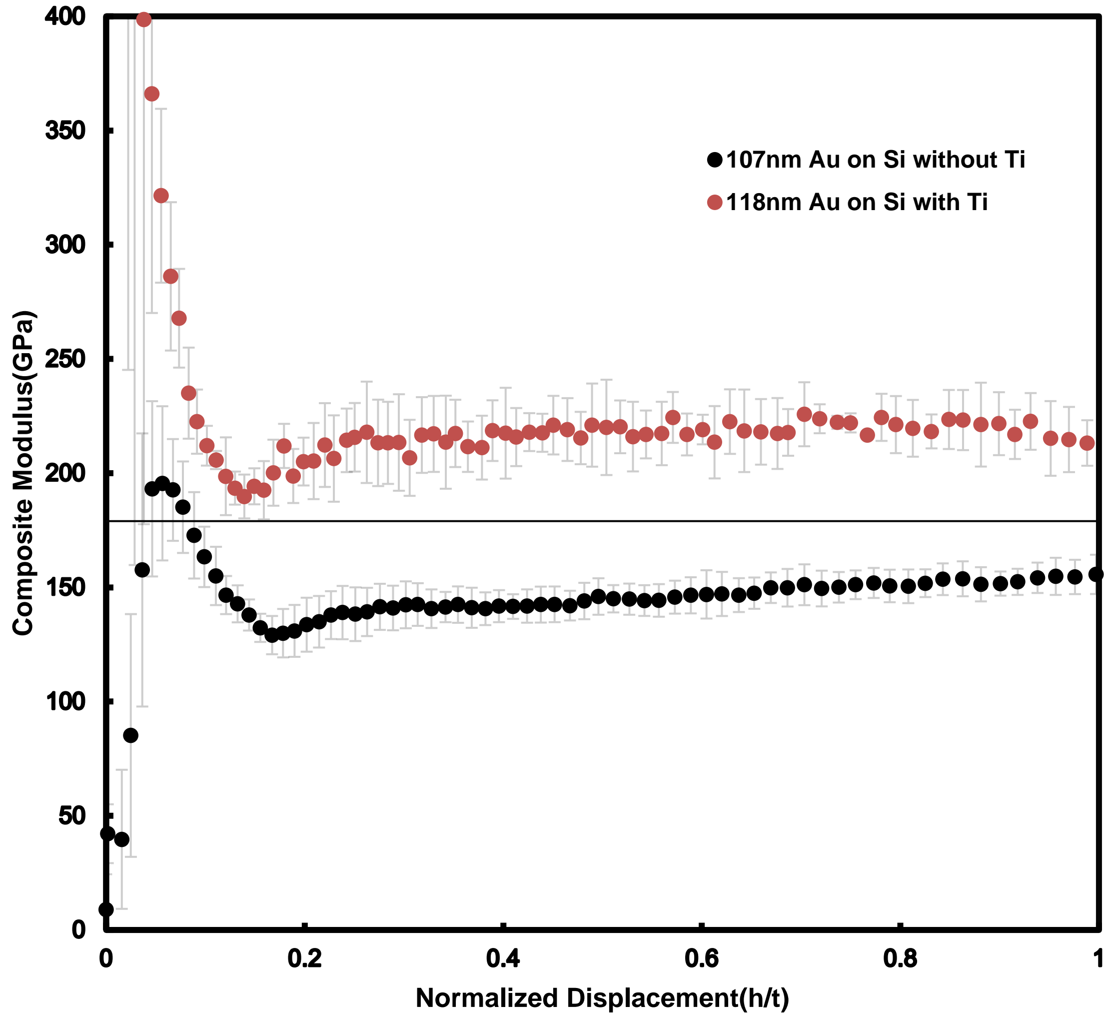

Figure 35 Composite modulus of 107nm Au on silicon without Ti and 118nm Au on silicon with Ti

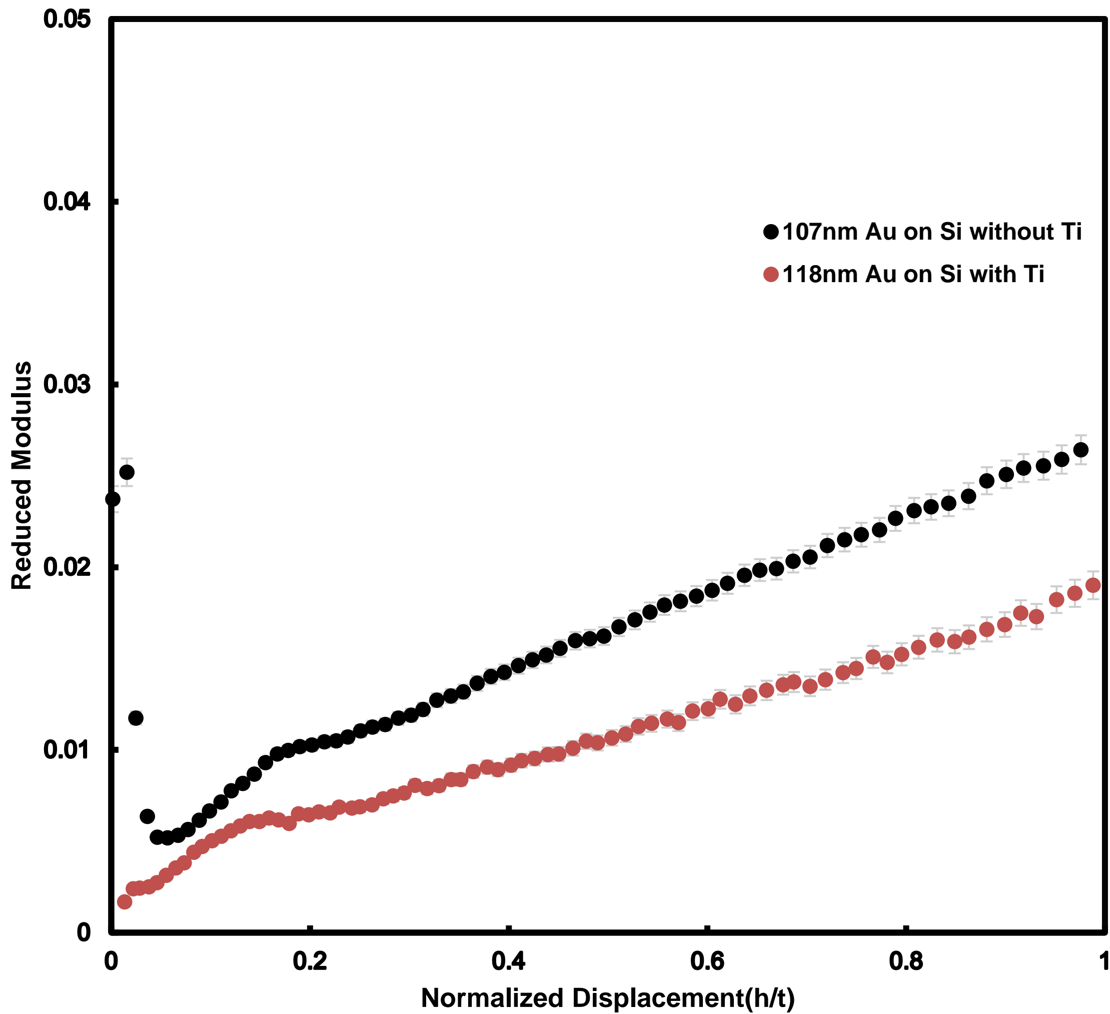

Figure 36 Reduced modulus of 107nm Au on silicon without Ti and 118nm Au on silicon with Ti

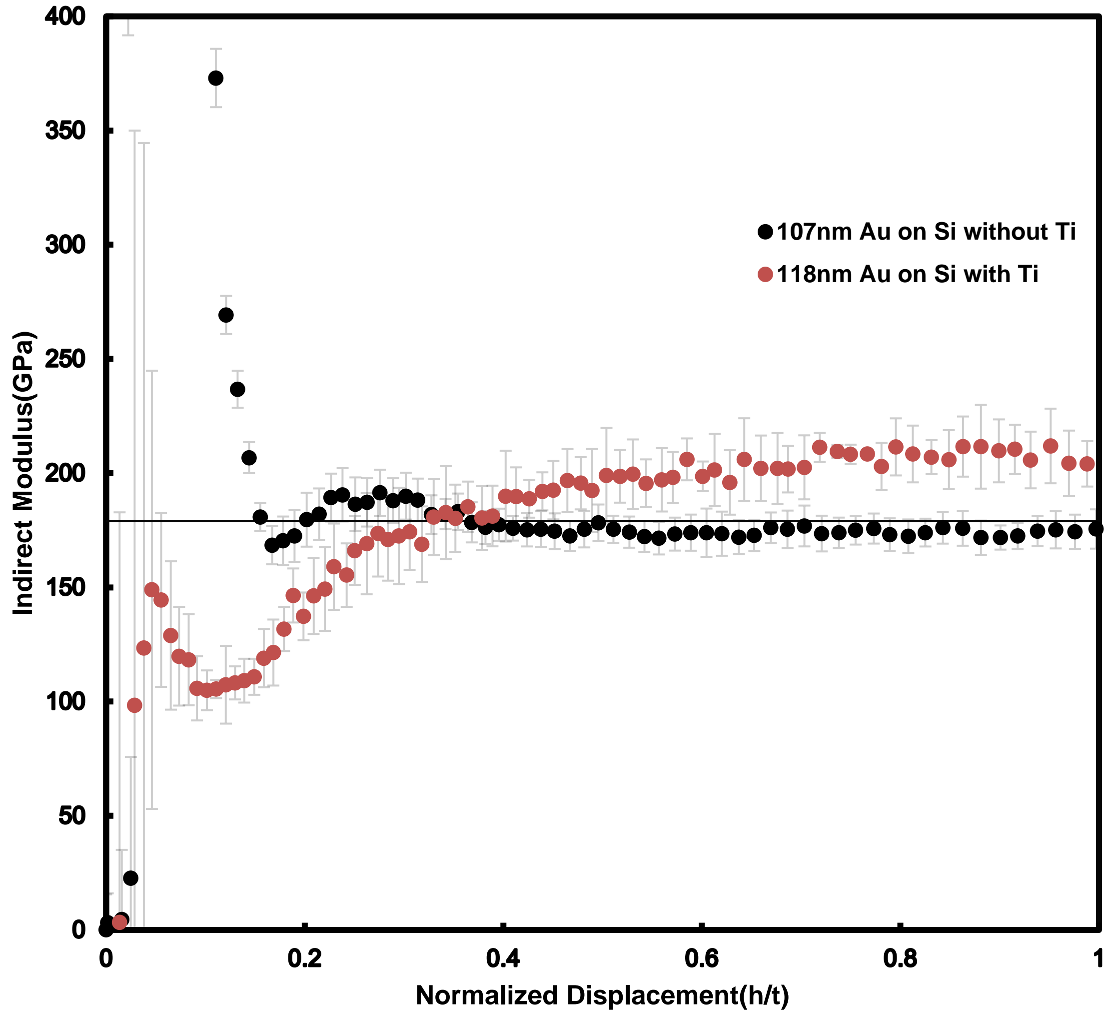

Figure 37 Indirect modulus of 107nm Au on silicon without Ti and 118nm Au on silicon with Ti

However, there are some limitations for Denton Sputter system. The geometry of Denton sputter system is not suitable for ultra-thin film deposition since cathode is 60 degree towards the sample which causes uneven film surface. High energy power might heat up the thin film which changes the microstructure of film. Finally, Denton sputter system normally takes three hours to finish sputtering process including pumping and it is not cost effective for ultra-thin film within one hundred nanometers.

It is really important to find an alternate method to substitute the Denton sputter system in ultra-thin coating range. Pelco sputter coater is a cheaper and faster option compared with Denton sputter coater. Additionally, it is accessible to most of labs since it coats the samples with thin conductive

gold layer for imaging without any strict requirement. The deposition time normally takes within minutes.

Next, simple sputter method was discussed and compared with Denton sputter system.

5.2 Investigate Simple Gold Coater for Widespread Use of the Indirect Indentation Method

The Pelco SC-6 sputter coater is generally used for sputtering 10nm to 100 nm gold on the sample surface to help get better SEM images since some samples are insulators that will lead to electrons pile up on the top of the sample surface and get abnormal bright blurred images. The control parameters for sputtering are current(mA), working distance (WD), deposition time(T) and pressure(mbar). The coating film thickness in this research is based on these parameters as Table 5 shows.

Table 8 Gold Thickness and deposition time by Pelco

Pelco Sputter System	Thickness(nm)	Deposition Time(sec)
	27	110
	48	216
	76	280
	85	430
	96	465
	154	650
	297	1090

Table 8 gives several different thickness gold depositing on silicon substrates and these groups were analyzed later in this chapter.

5.2.1 Fitting the Indirect Indentation Method on Pelco Sputtered Gold film on Silicon

The 76nm gold film which was confirmed in Figure 38 was first deposited on silicon substrate. The parameters are in Table 8. It seems that the composite modulus in Figure 39 keeps straight line as the extracted modulus. However, based on the previous analysis, this might be a coincidence because each composite modulus is calculated from nano indenter directly and it has some variations in ultra-thin range. The slope of reduced modulus was 0.0198. When applied the indirect indentation method which is based on the calculation of the instantaneous slope from Figure 40, the substrate data could be extracted accurately as Figure 41 shows. The straight black line represents the literature value of Silicon modulus. From indentation depth >20nm, the indirect indentation modulus clearly straight out with less deviation compared with direct indent on the raw silicon substrates. The indirect indentation method extracted the silicon substrate modulus precisely.

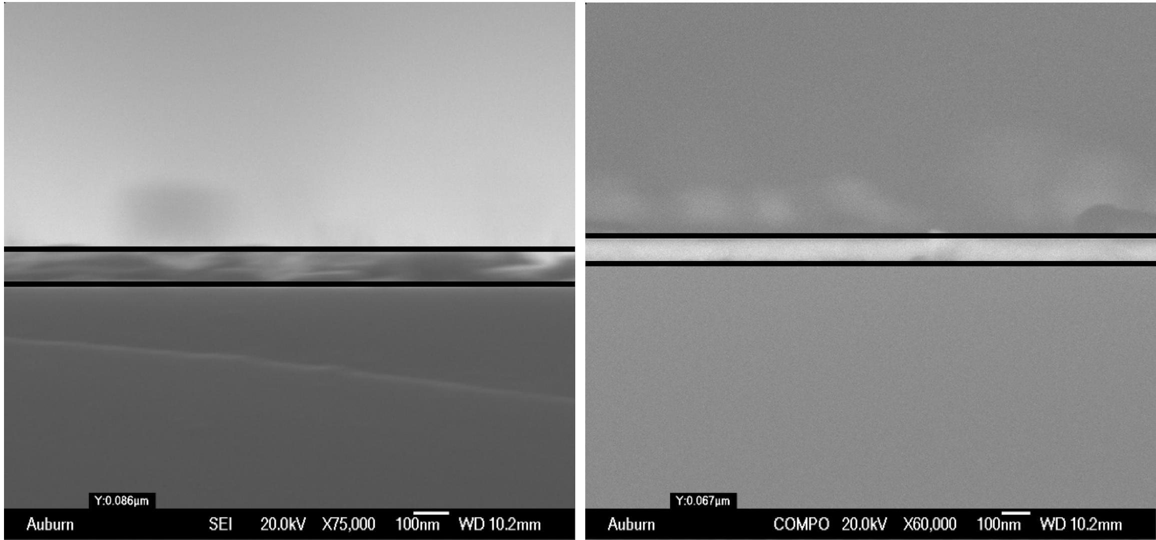

Figure 38 Deposition thickness measurement under SEI and COMPO mode

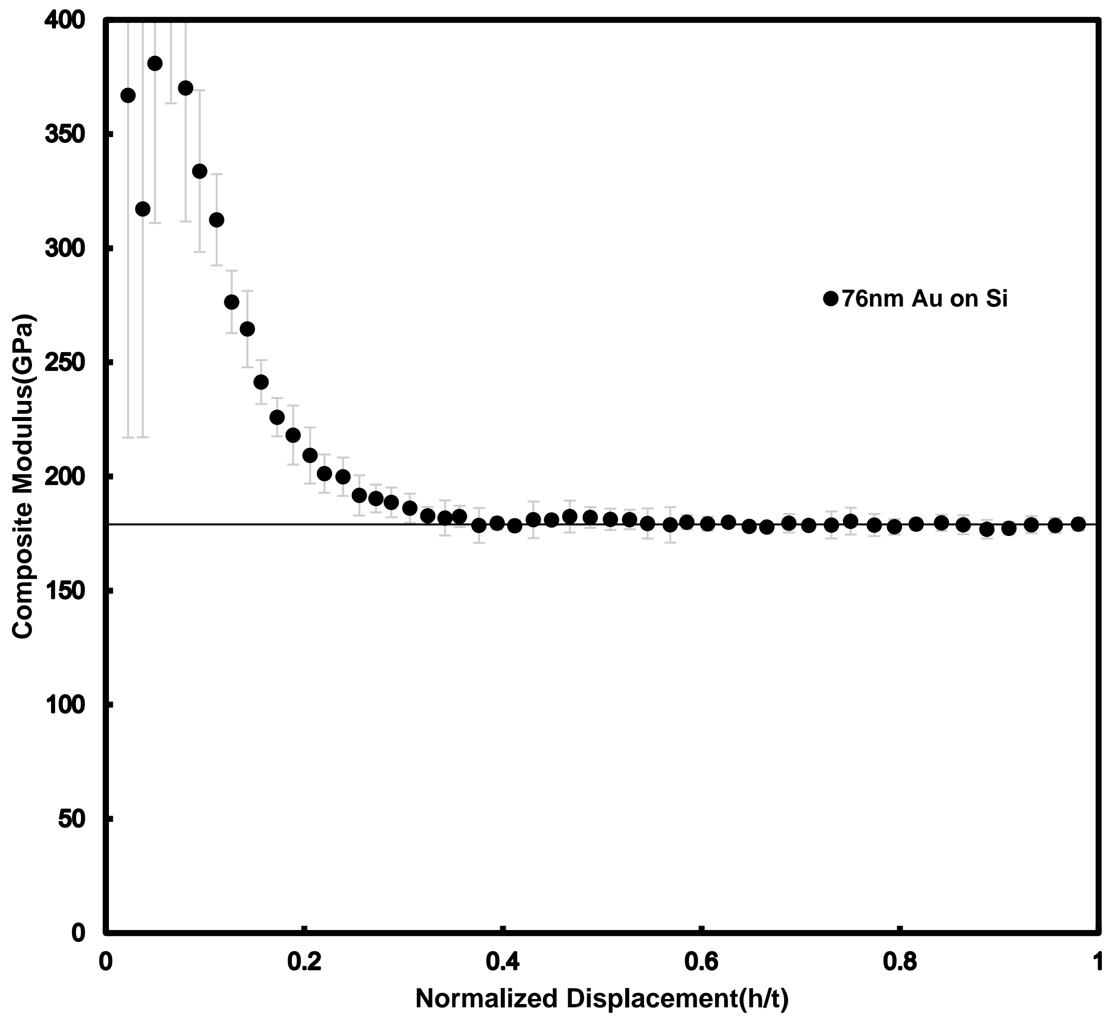

Figure 39 Composite modulus of 76nm gold on silicon

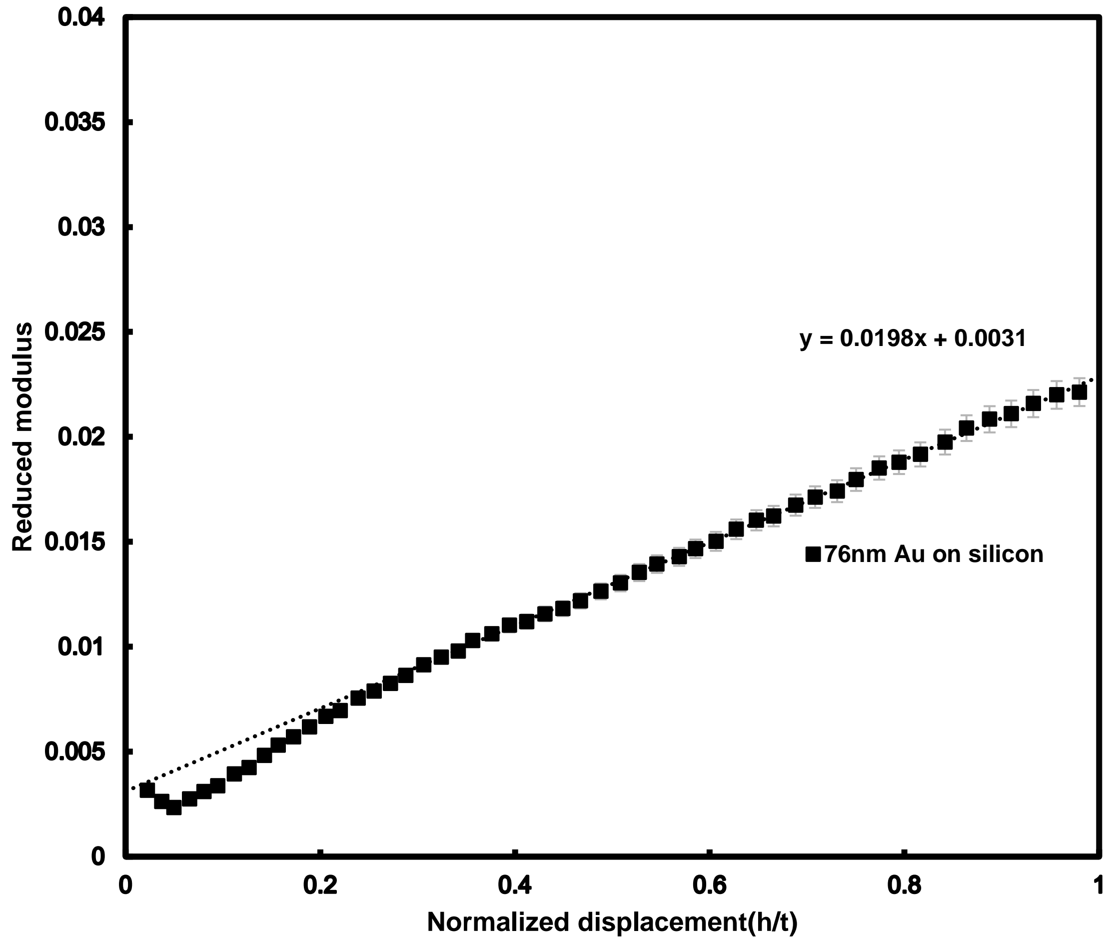

Figure 40 Reduced modulus of 76nm gold on silicon

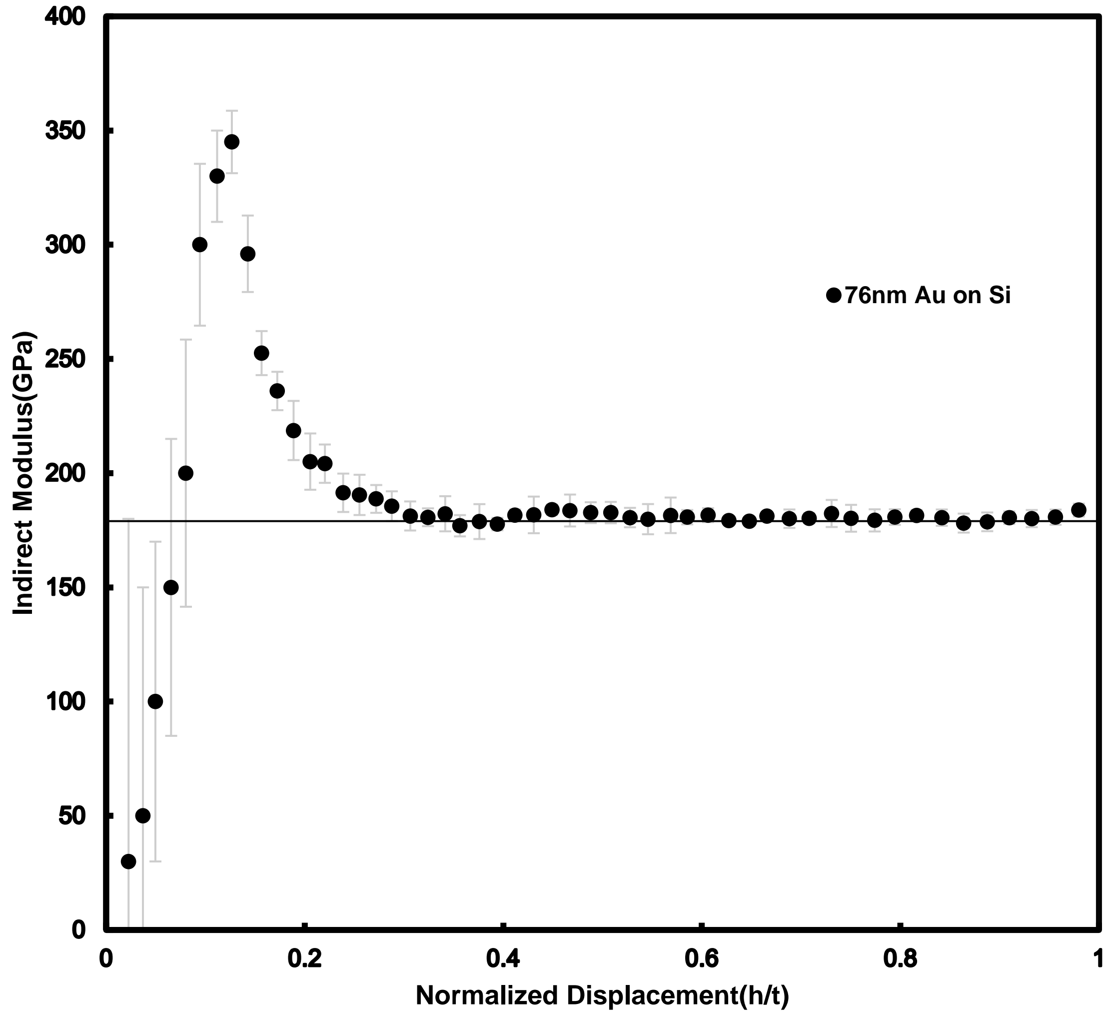

Figure 41 Indirect modulus by applying the indirect indentation (solid markers) of gold film of 76nm thicknesses on silicon with literature value (solid line)

In Table 9, the extracted silicon modulus from average data point is 179GPa within standard deviation range. The direct indentation data from average data point is 208GPa which is 15% more than literature value as Figure 42 shows.

Table 9 Average Indentation Modulus from direct and indirect indentation

Thickness(nm)	Direct Indentation Modulus (GPa)	Indirect Indentation Modulus (GPa)
76	**208**±5.4	**179**±4.6

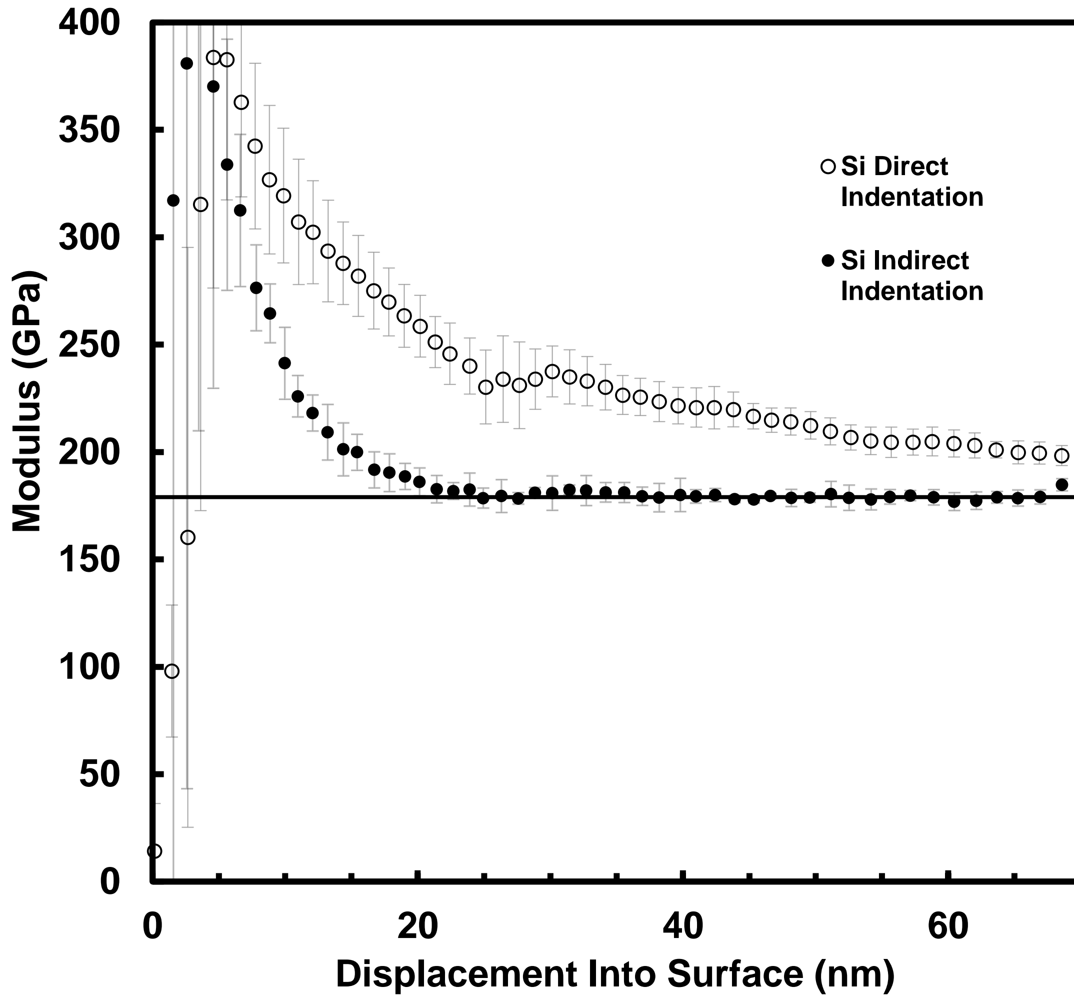

Figure 42 Indirect modulus by applying the indirect indentation (solid markers) on 70nm thicknesses gold on silicon and direct indentation modulus on silicon substrate (void markers)

It is hard to get the real material modulus from the direct indentation. In the early stage of indentation, it seems that the indentation result is even higher than the literature value. This is

because the indenter tip is not fully contacted with film and it is hard to get a SEM image under shallow depth. However, with the indenter tip punching through the film, cracks were generated which cause the stored elastic energy lost to generated to new surfaces. As Figure 42 shows, the direct indention modulus decreased continuously with deeper indentation depth. It is difficult to acquire Silicon elastic modulus according to the transition.

Even though the indentation depth increases, the Chen-Prorok model still predicts silicon substrate modulus consistently.

5.2.2 Results Comparisons between Denton Sputtered Films and Pelco Sputtered Films

In order to confirm the consistency of indirect indentation method (Chen-Prorok model), six different film thickness (27nm,48nm ,85nm,96nm,154nm,297nm) of gold were coated on silicon substrates with Pelco sputter coater compared with Denton sputter coated film. The composite modulus from Figure 43 demonstrates each group varies according to different thickness. Some of them are over 200 GPa and others are even lower than 150 GPa. The silicon's elastic modulus is 179GPa as the black solid line showed in the figure. The variation of composite modulus from different group makes it difficult to extract silicon modulus. Then the reduced modulus of all groups was extracted in Figure 44. Though the composite modulus were different, the linear approximation slope line of reduced modulus was almost parallel to each other.

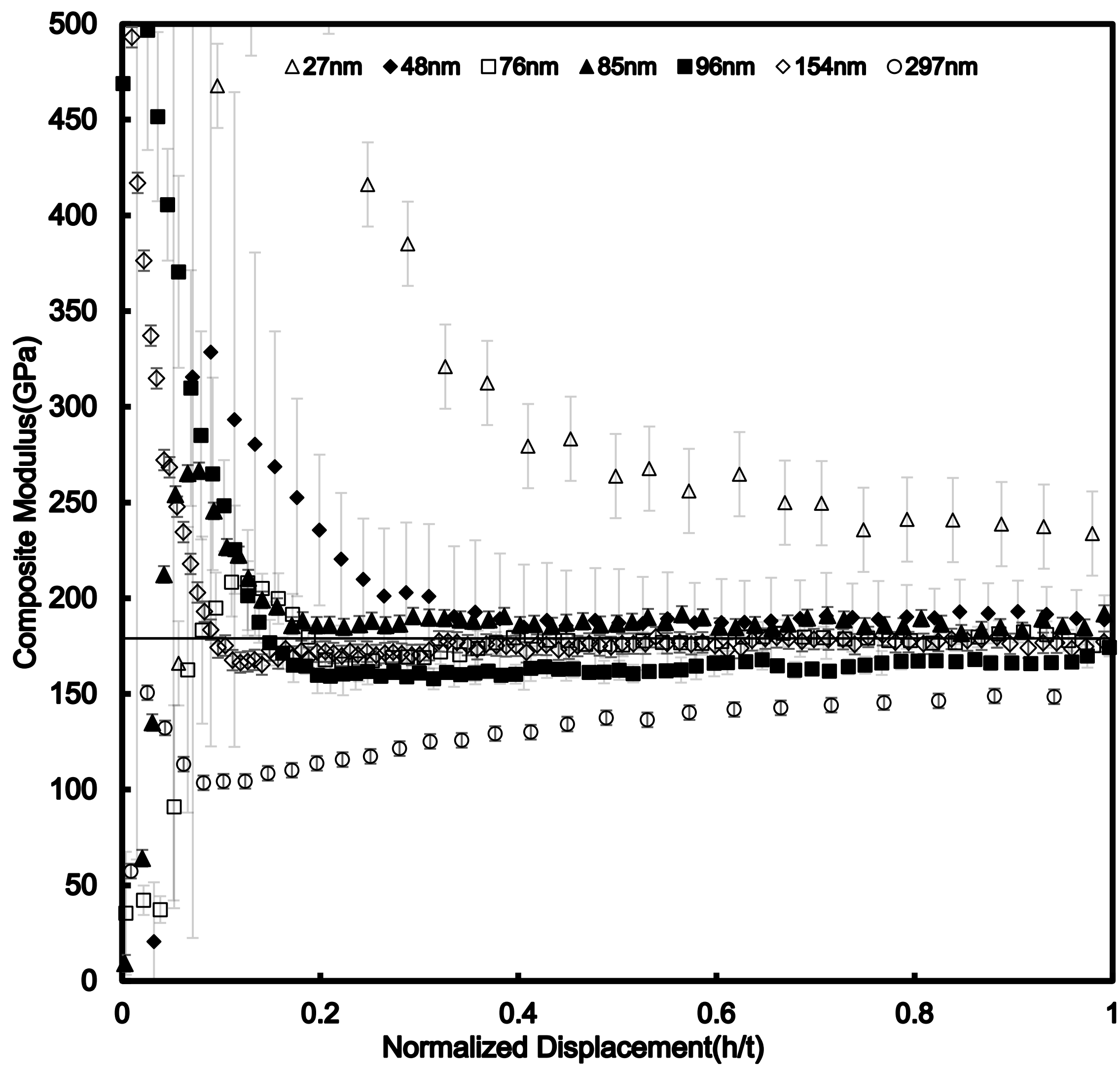

Figure 43 Experimental modulus for all thicknesses of gold film on silicon substrate

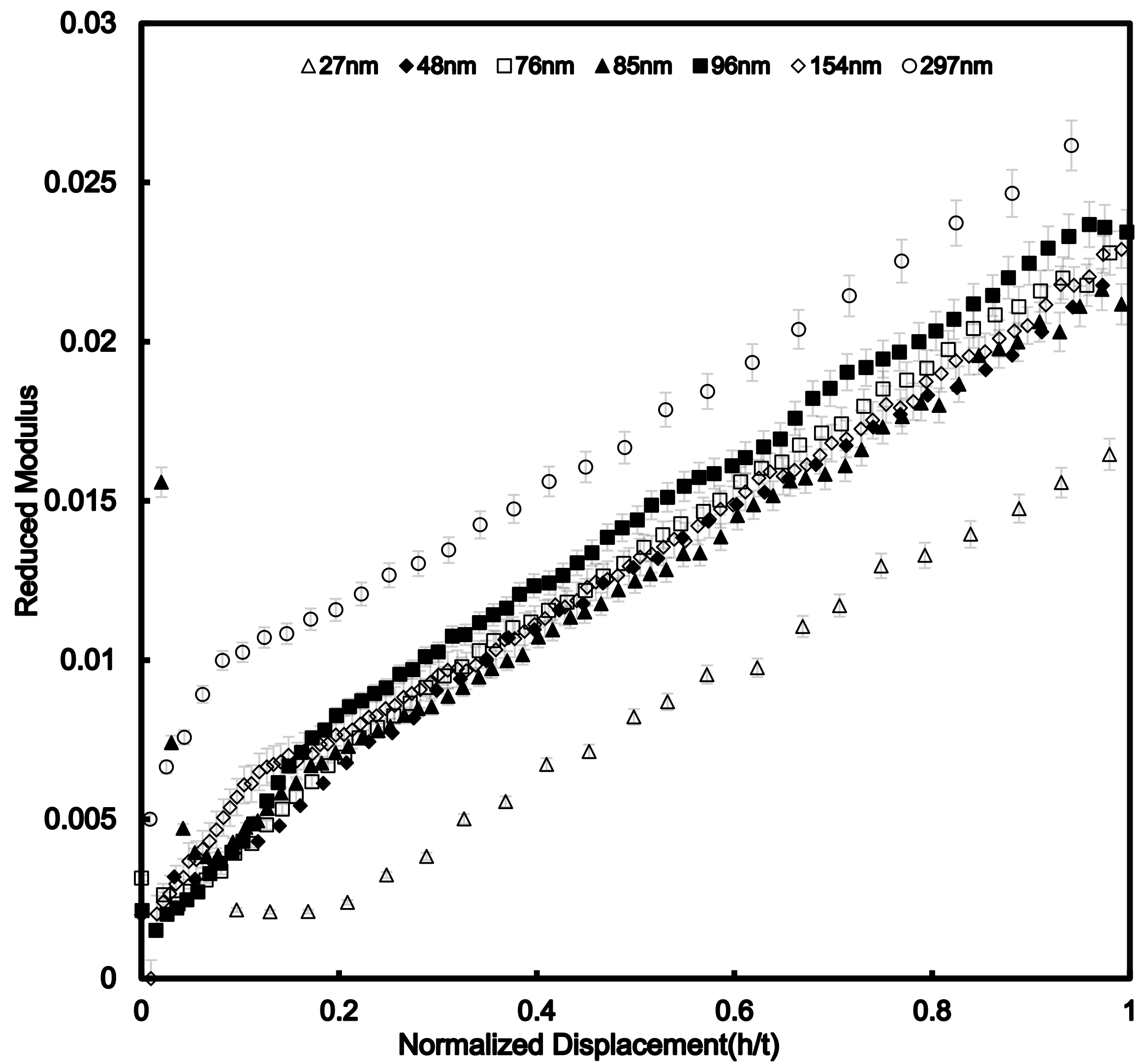

Figure 44 Reduced modulus for all thicknesses of gold film on silicon substrate

Table 10 Slopes and indirect modulus with different thickness

Thickness(nm)	**Slope**	**Indirect Modulus (GPa)**
27	0.0172	207±4.7
48	0.0179	200±5.4
76	0.0198	179±4.6
85	0.0189	188±4.4
96	0.0195	180±4.8
154	0.0204	175±4.6
297	0.0202	178±5.3

Figure 45 shows the indentation result from Pelco sputter. There is a clear trend that after film thickness is thicker than 50nm, the numerical results are more consistent compared with 27nm and 50nm. These two set seem to have a large deviation on experiment modulus based on previous research results. Then the method (Chen-Prorok model) was applied to all the numerical results as Figure 46 shows. The indirect indentation method (Chen-Prorok model) confirmed that as the film thickness of gold is over 50nm, the extracted silicon modulus is within literature value range(179Gpa). While the film thickness is lower than 50nm, the extracted modulus is relatively higher than literature value which is around 200Gpa. It is interesting to compare with Denton sputter film. The same result was got compared with Pelco sputter film on substrate and was even higher which is 220Gpa from Chen-Prorok model.

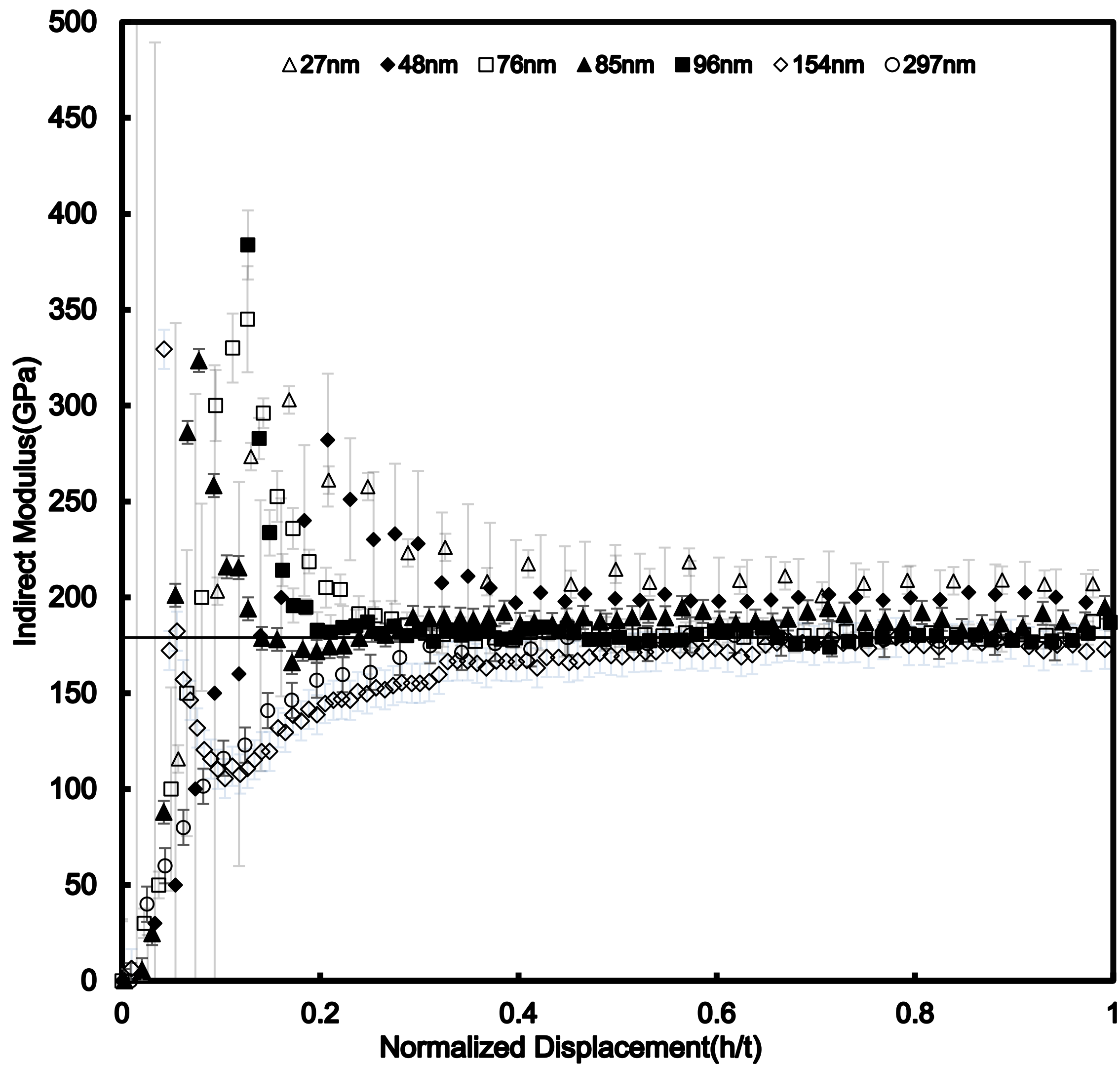

Figure 45 Indirect modulus for all thicknesses of gold film on silicon substrate

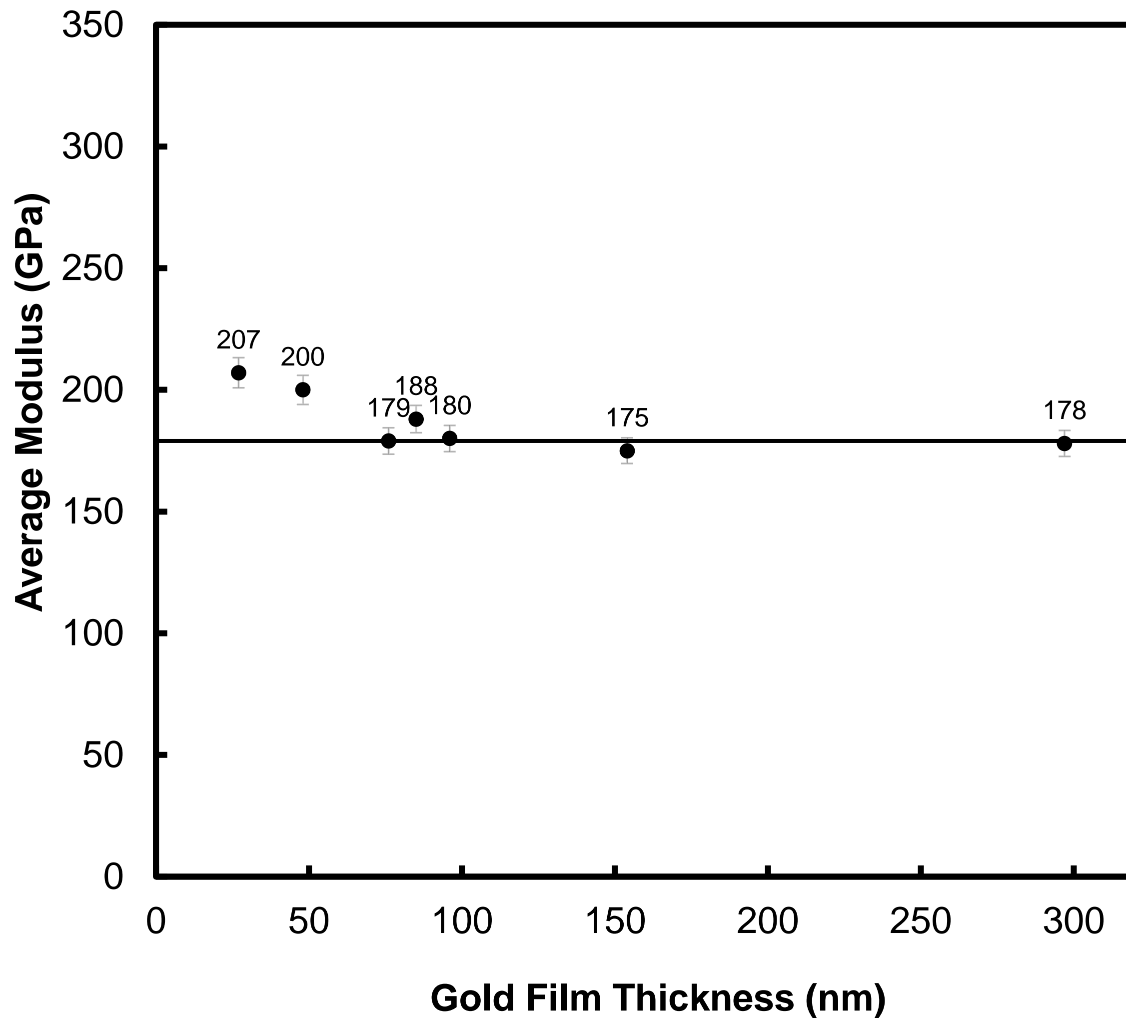

Figure 46 Average indentation results from Chen-Prorok model with different thickness gold on silicon substrates deposited by Pelco sputter coater

The first possible reason is that ceramic material always has bad wettability compared with other materials. Without adhesion or seeding layers, it is difficult for gold particles to form the continuous film at ultra-thin thickness range which is mainly driven by low surface adhesion of the metal. As the metal thickness increases, the three-dimensional individual gold islands grow in size and range. Gradually, they contact with each other and coalesce to form electrically isolated fractal clusters which means the voids are filled up and become structurally continuous. The continuous gold film' material properties has dramatically different compared with discontinuous

one. Indirect indentation method is based on the assumption that the gold film is continuous. If the film was discontinuous, the model would not work. The results of SEM images taken by JEOL 7000F under 20kV and 10mm working distance support the explanation. From Figure 47, gold was deposited on silicon substrate without any surface treatment. Gold forms smaller and more densely islands which is around 10nm. There are many gaps between each cluster which appeal the silicon substrate. It shows that it is a discontinuous film. It is even more obvious that the gold film had been annealed under 200 C for 1h. The gold clusters rearrange and combine which even leave more voids and gap as Figure 48 shows. This confirmed that there is not enough gold particle to cover the whole silicon surface area. However, with film thickness increasing, gold clusters grow, diffuse and finally coalesce each other to get a continuous layer of gold film as Figure 48 shows. It is found that gold film needs at least 50 nm thick to form a continuous layer which fits the numerical data and Chen-Prorok model.

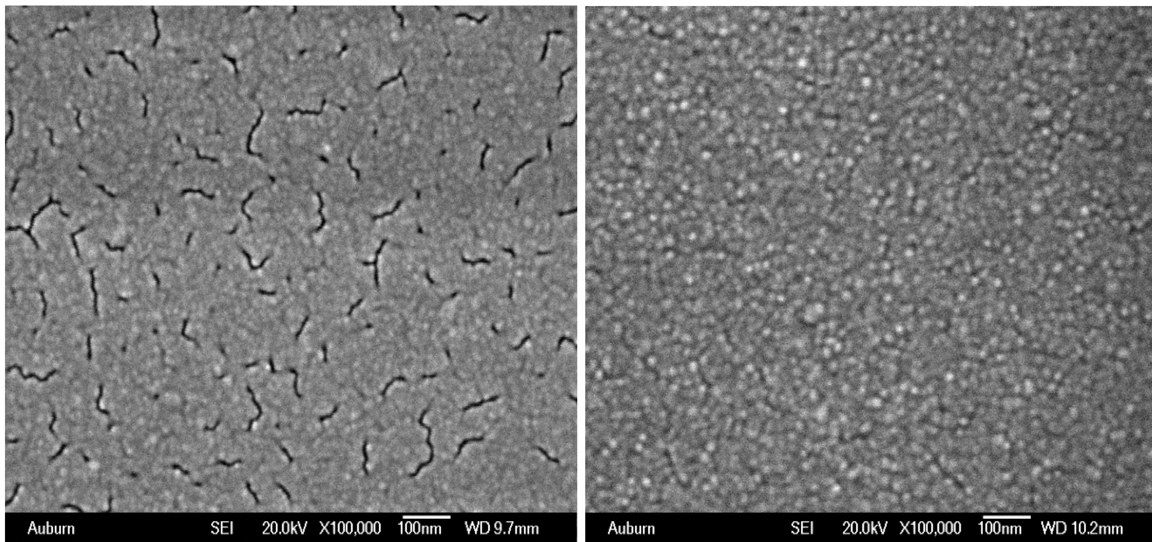

Figure 47 27nm Gold film surface (left) and 76nm Gold film surface (right)

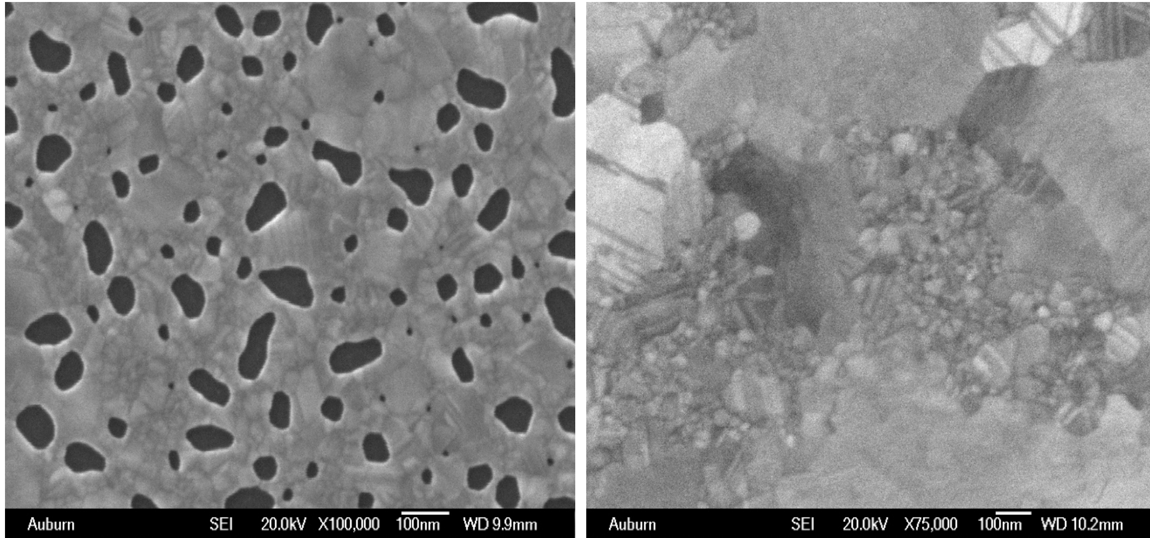

Figure 48 27nm (left) and 76nm gold film surface with heat treatment(right)

The contact area equation is no longer suitable for this situation so this causes inaccuracy calculation of contact area which leads to higher results at first 50nm indentation depth range. Both Denton and Pelco sputter deposited film show the similar results.

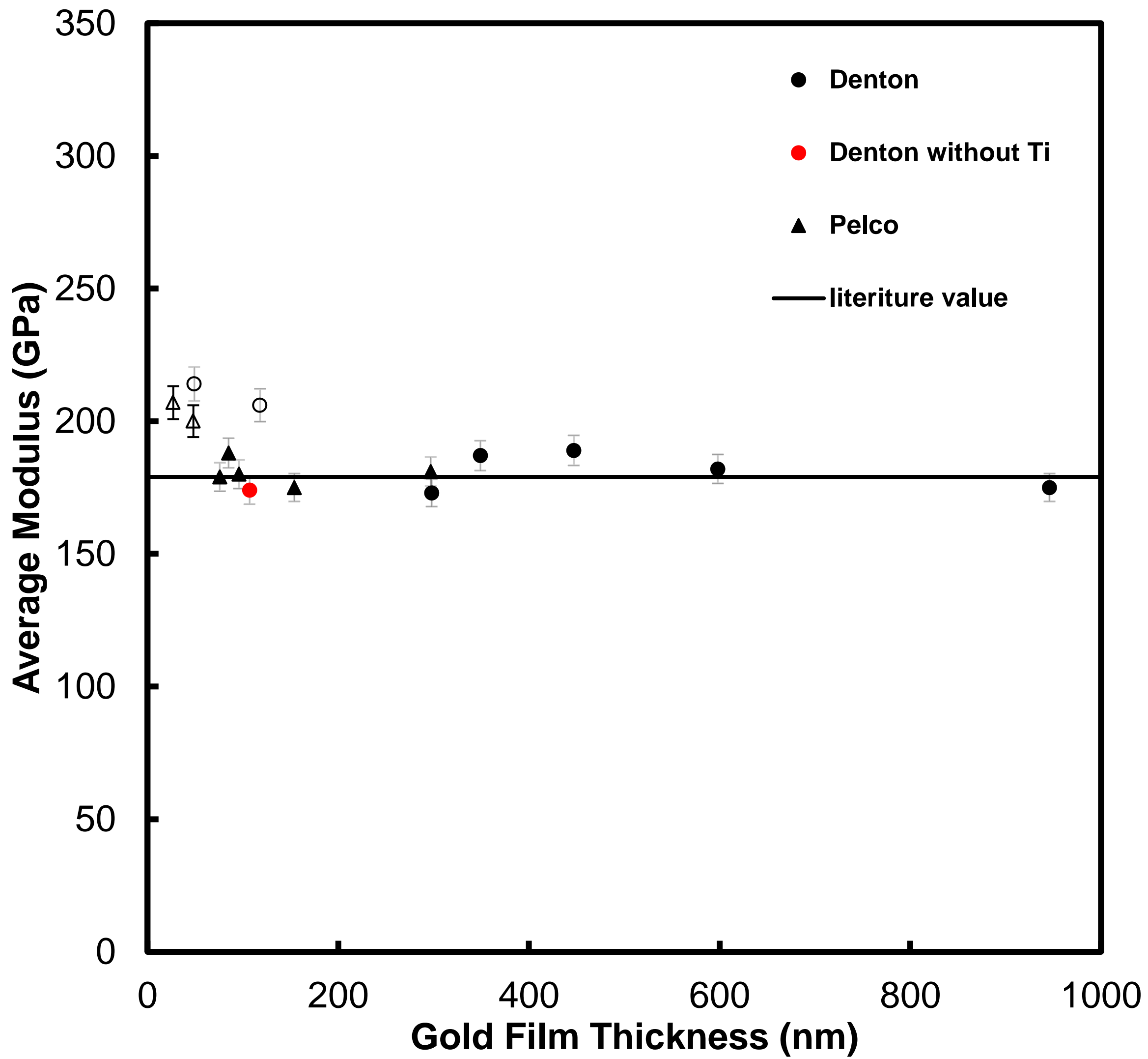

Figure 49 Comparisons between Denton and Pelco sputter film

The reason that the maximum thickness of Pelco sputter gold films went to 300nm instead of 800nm is normally about 1 hour and half for depositing 300nm gold on substrates as Figure 49 shows. If the thickness went up to 800nm, it might take more than four hours. Due to the limitation of Pelco sputter system, the deposition process has to be cooled down 5-10 minutes and repeated for each time which deposits around 30nm. It is not practical to deposit film manually. Instead, Denton has automatic sputter system which could deposit from several nanometer thick to several micron meter thick. Based on the demand, it is convenient for researcher to choose.

As a comparison between Pelco and Denton sputtered gold film on silicon, Pelco sputter coater is prior to Denton sputter coater within 300nm range. If further thicker film is needed for applications like electronic device, Denton sputter coater is a good choice.

5.2.3 Different Substrates' Effects

The substrates were chosen carefully to prevent any plastic deformation, and were all sputtered at the same time to ensure uniform thickness by Pelco sputter coater [51-54]. Even though the material properties are different, the model still accurately predicts the experimental composite modulus. Figure 52 demonstrates that the indirect modulus from the indirect indentation method based on Figure 51, (solid symbol marks) matches the literature value from every single ceramic material. The film was 76nm thick, and the indirect modulus started to become stable line from 0.4 to 1. An array of 25 indents was completed, and averages with standard deviation are shown with the error bars. The slope from reduced modulus of each substrate was in Table 11. These substrates will be discussed in the following section individually.

In the Table 12, indirect modulus is closer to literature values. It is interesting to notice when the normalized displacement has reached over 0.8, the indirect modulus seems to be off the literature values a lot. This is an indication that the MgO substrate is likely fracturing at this penetration depth [54-60]. The harmonic displacement of this particular testing cannot sustain enough value after 80% of the film thickness, this can be attributed to the high stiffness and low hardness of this composite, and can cause experimental error [61-65].

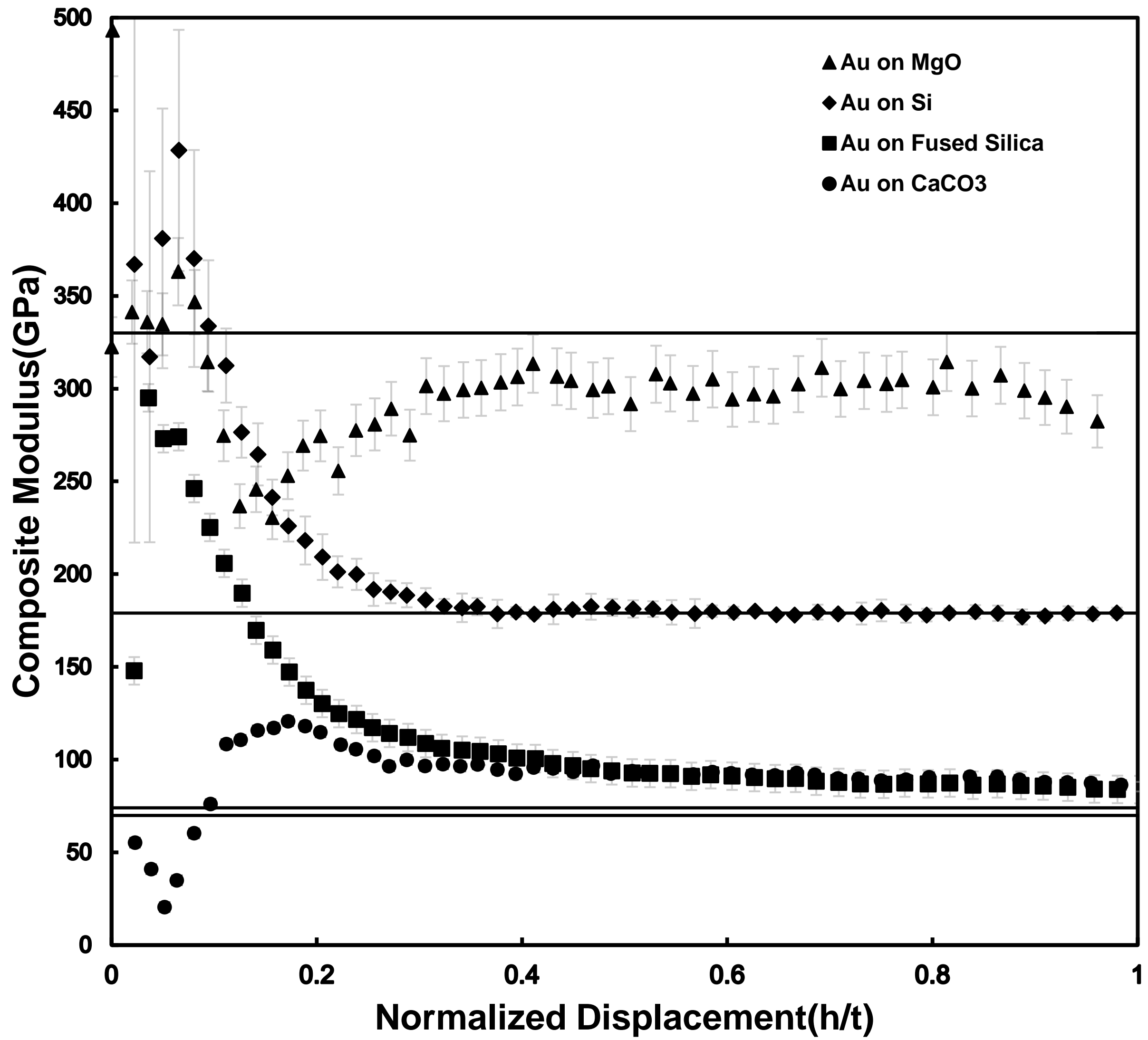

Figure 50 Composite modulus of 76nm gold on ceramic substrates

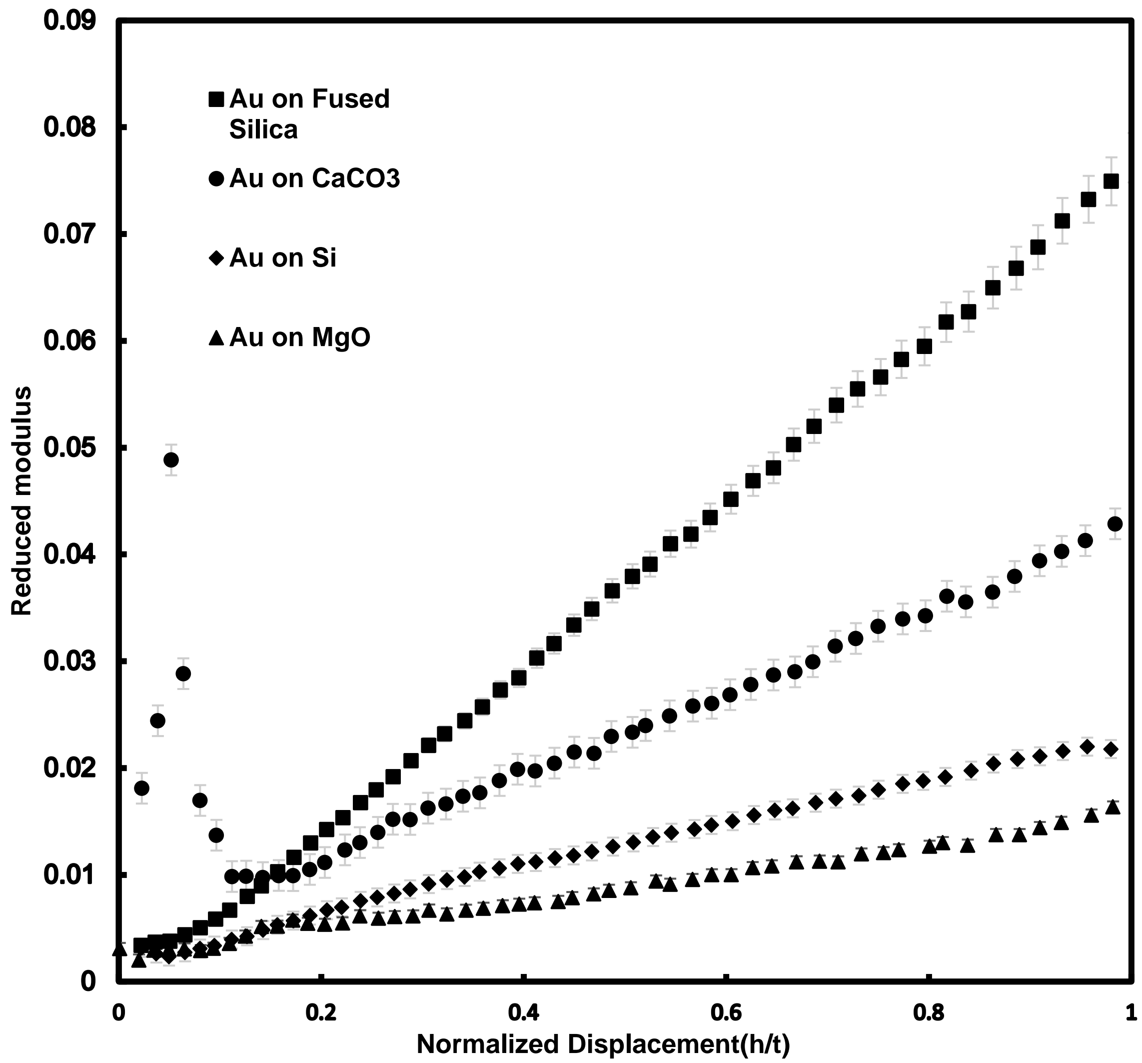

Figure 51 Reduced modulus of 76nm gold on ceramic substrates

Table 11 Slopes and indirect modulus with 76nm gold on different substrates

Substrates	Slope	Indirect Modulus (GPa)
Si	0.02000	179±4.6
Fused Silica	0.00788	75±2.2
MgO	0.01300	320±10.4
CaCO3	0.04210	77±3.3

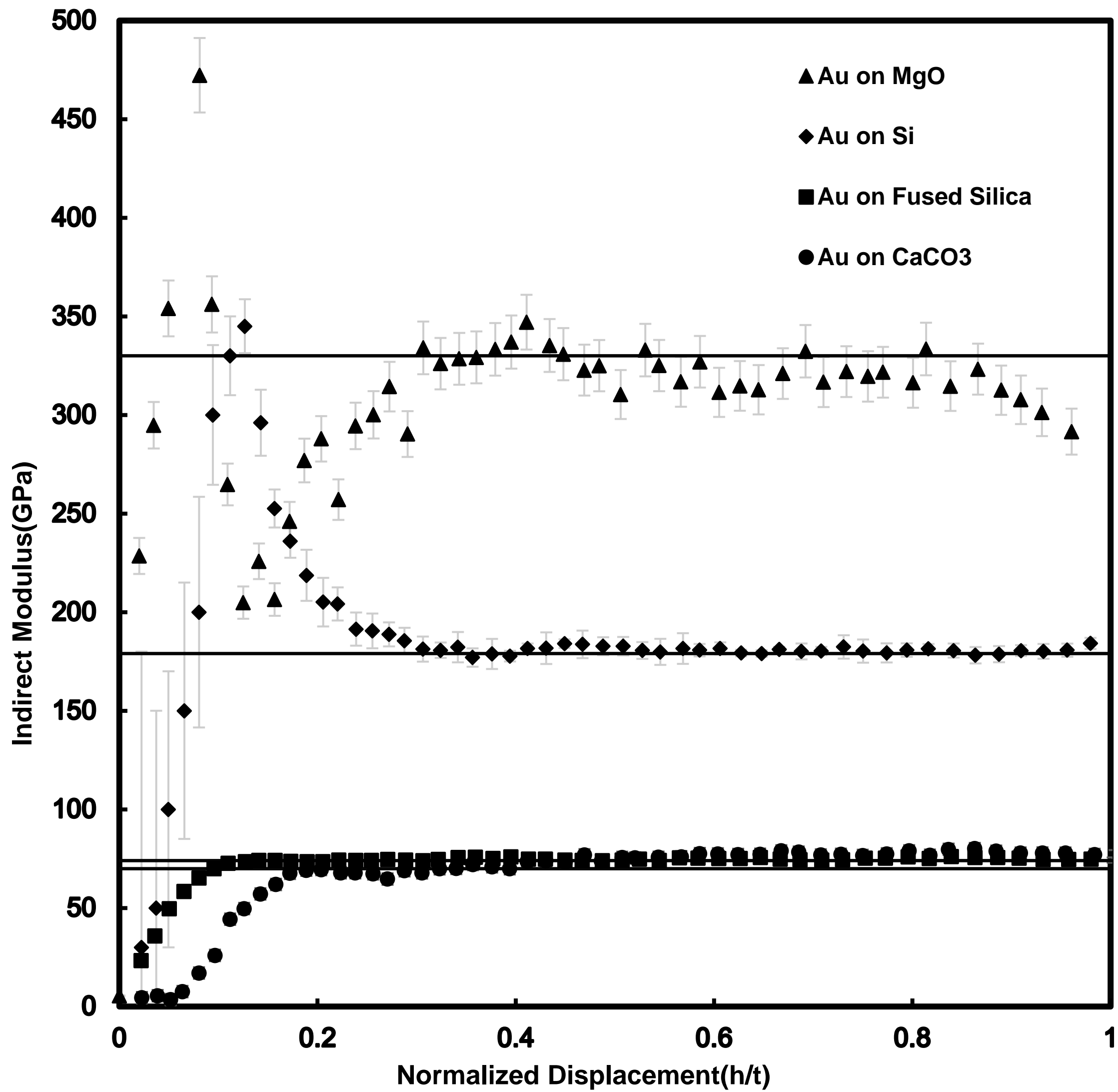

Figure 52 Indirect modulus of 76nm gold on ceramic substrates

Table 12 Comparison between direct modulus and indirect of gold film on different substrates

Material	Elastic modulus (literature value)	Poisson's ratio	Elastic modulus From indirect Indentation (GPa)	Elastic modulus from direct indentation (GPa)
MgO (100)	330	0.24	320±10.4	235±15.4
$CaCO_3$(100) <001>	70	0.31	77±3.3	89±5.2
Si (100)	179	0.27	179±4.6	208±7.6
Fused Silica	74	0.17	75±2.2	94±4.9

5.2.4 Various Substrates with Different Gold Film Thickness

The data is even more interesting when comparing across different film thicknesses on different substrates. All the substrates were deposited with three different thickness gold by Pelco sputter system which are 76nm, 96nm and 154nm for comparison.

First, the composite modulus of gold on fused silica were plotted in Figure 53. For 76nm gold on fused silica, the composite modulus (black solid mark) decreased with increasing indent depth. Till the end of indentation, the composite modulus was still above the literature value as solid straight line showed. For 96nm and 154nm gold on fused silica, the indentation results dropped below the literature value at the end. Among all the data, the real substrate elastic modulus is difficult to get. To extract the fused silica modulus, the indirect indentation method was applied to all the three group. The reduced modulus was plotted first in Figure 54. The slopes of these group were almost same to each other in Table 13. With values of the slope, the indirect modulus was extracted 75GPa,71GPa and 70 GPa compared with literature value(72GPa). The calculated results became stable as a straight line after h'>0.4 which the indirect method got the fused silica modulus precisely within small deviation in Figure 55.

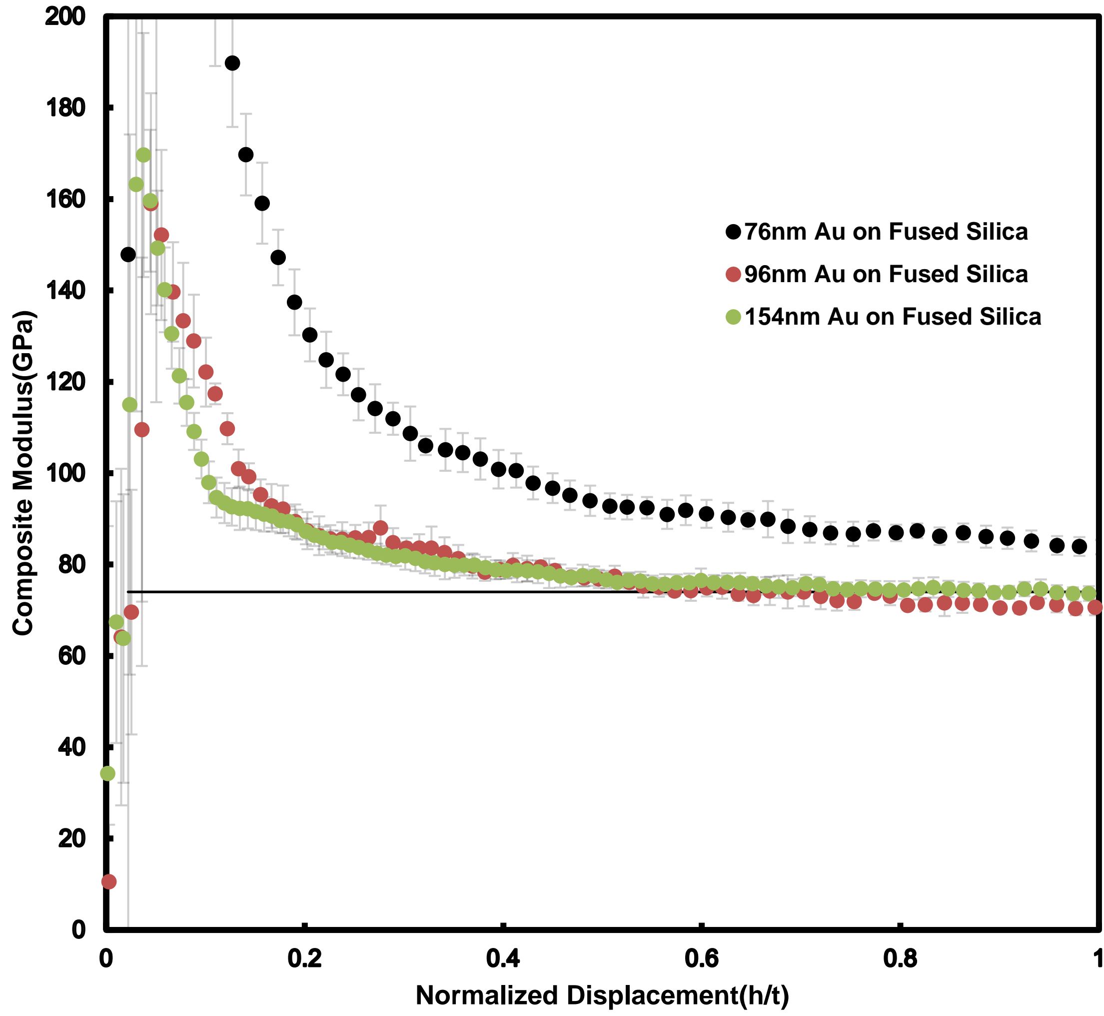

Figure 53 Composite modulus of 76nm,96nm,154nm gold on fused silica

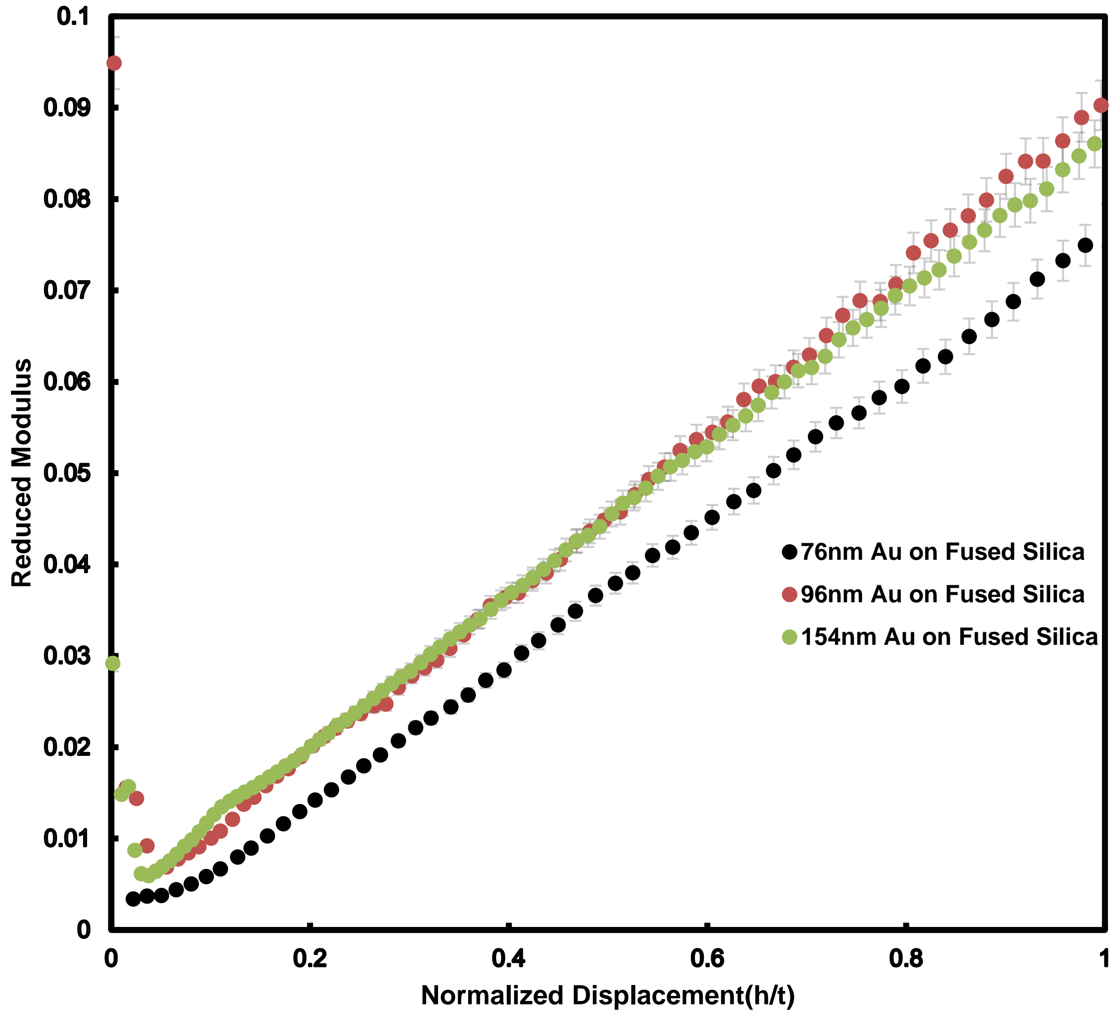

Figure 54 Reduced modulus of 76nm,96nm,154nm gold on fused silica

Thickness(nm)	Slope	Indirect Modulus (GPa)
76	0.00788	75±2.2
96	0.0084	71±1.9
154	0.00836	70±2.3

Table 13 Slopes and indirect modulus with 76nm,96nm,154nm gold on fused silica

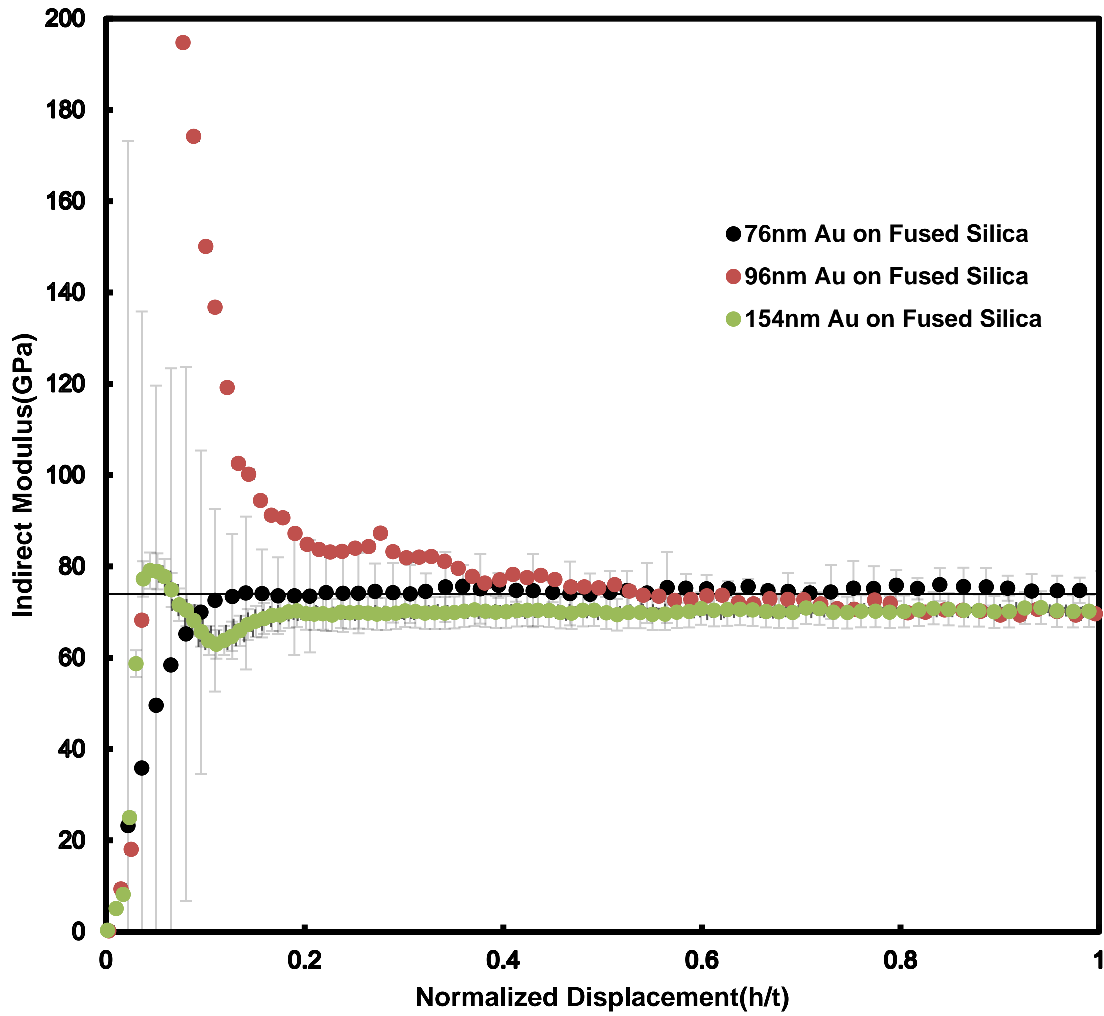

Figure 55 Indirect modulus of 76nm,96nm,154nm gold on fused silica

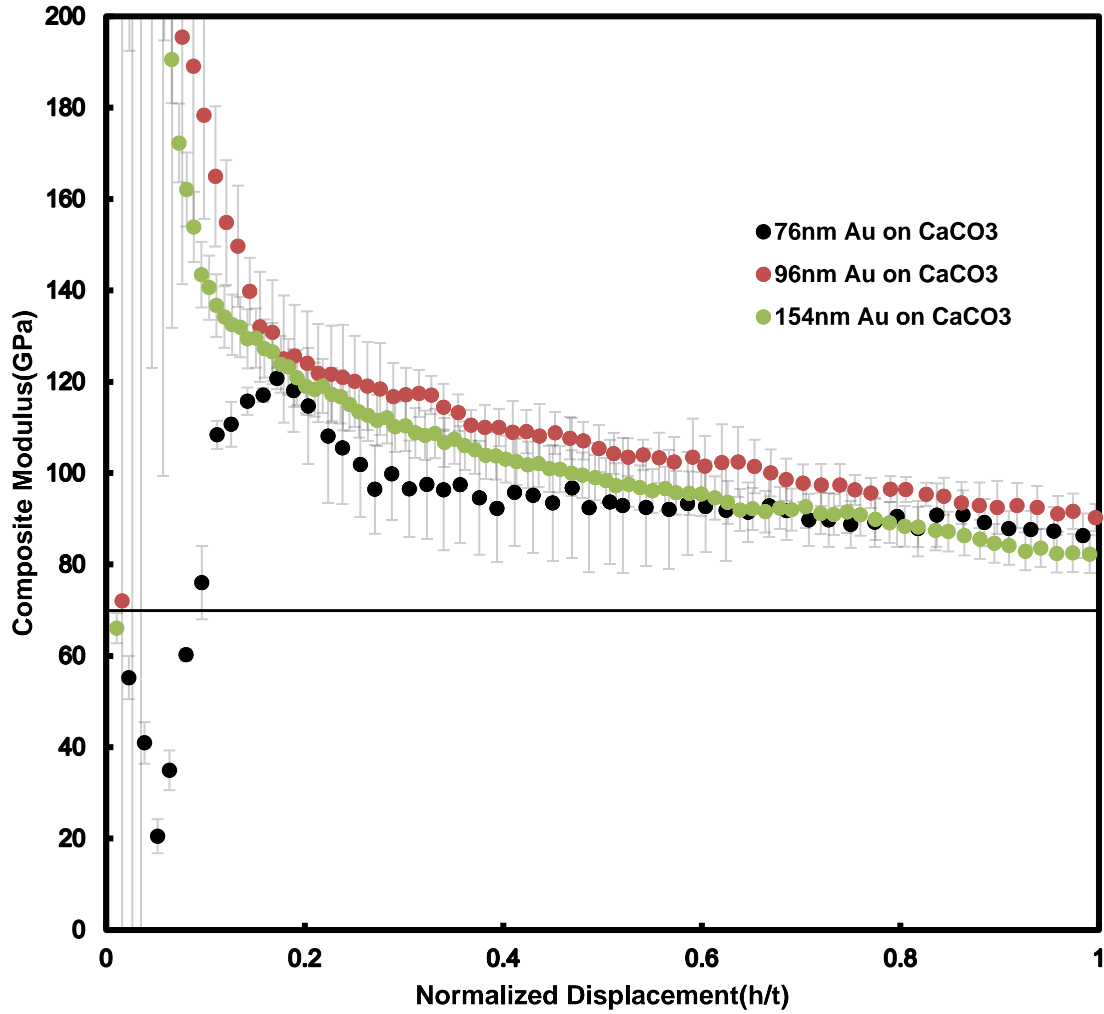

Figure 56 Composite modulus of 76nm,96nm,154nm gold on CaCO3

Next, it is even obvious that three groups of gold on CaCO3's composite modulus decreased continuously with tip punching through in Figure 56. The solid line is the literature value of CaCO3's modulus(69.9GPa). The composite modulus was far from the literature value. Then the indirect modulus was calculated based on composite modulus in Figure 57. From the indentation results in Figure 58, all these three lines met the literature line after h'>0.6. The average result of gold on CaCO3 were 77GPa, 72GPa and 71 GPa which were closer to the real modulus compared with direct indentation result.

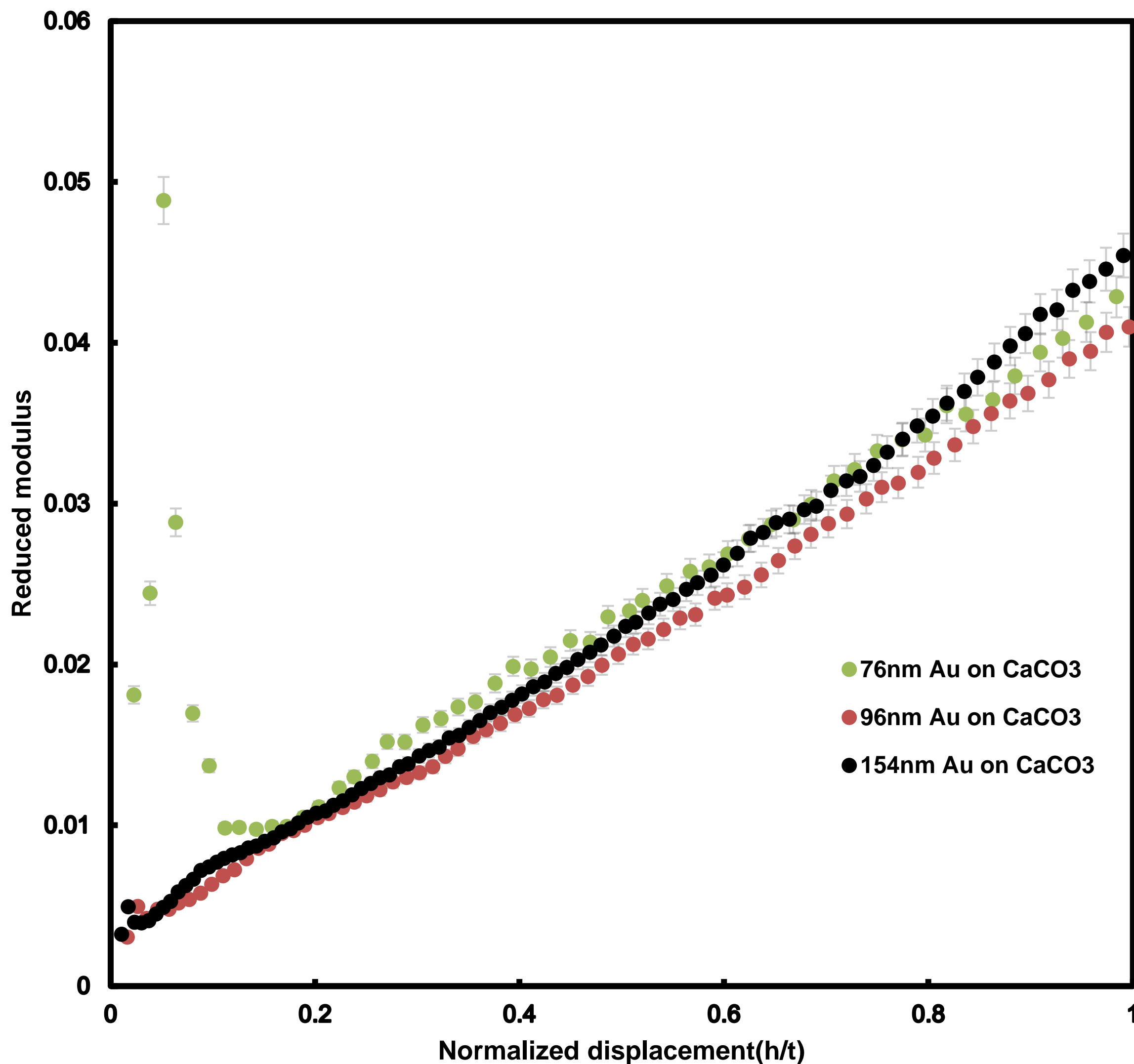

Figure 57 Reduced modulus of 76nm,96nm,154nm gold on CaCO3

Thickness(nm)	**Slope**	**Indirect Modulus (GPa)**
76	0.0421	77±3.3
96	0.0439	72±2.9
154	0.0467	71±3.1

Table 14 Slopes and indirect modulus with 76nm,96nm,154nm gold on CaCO3

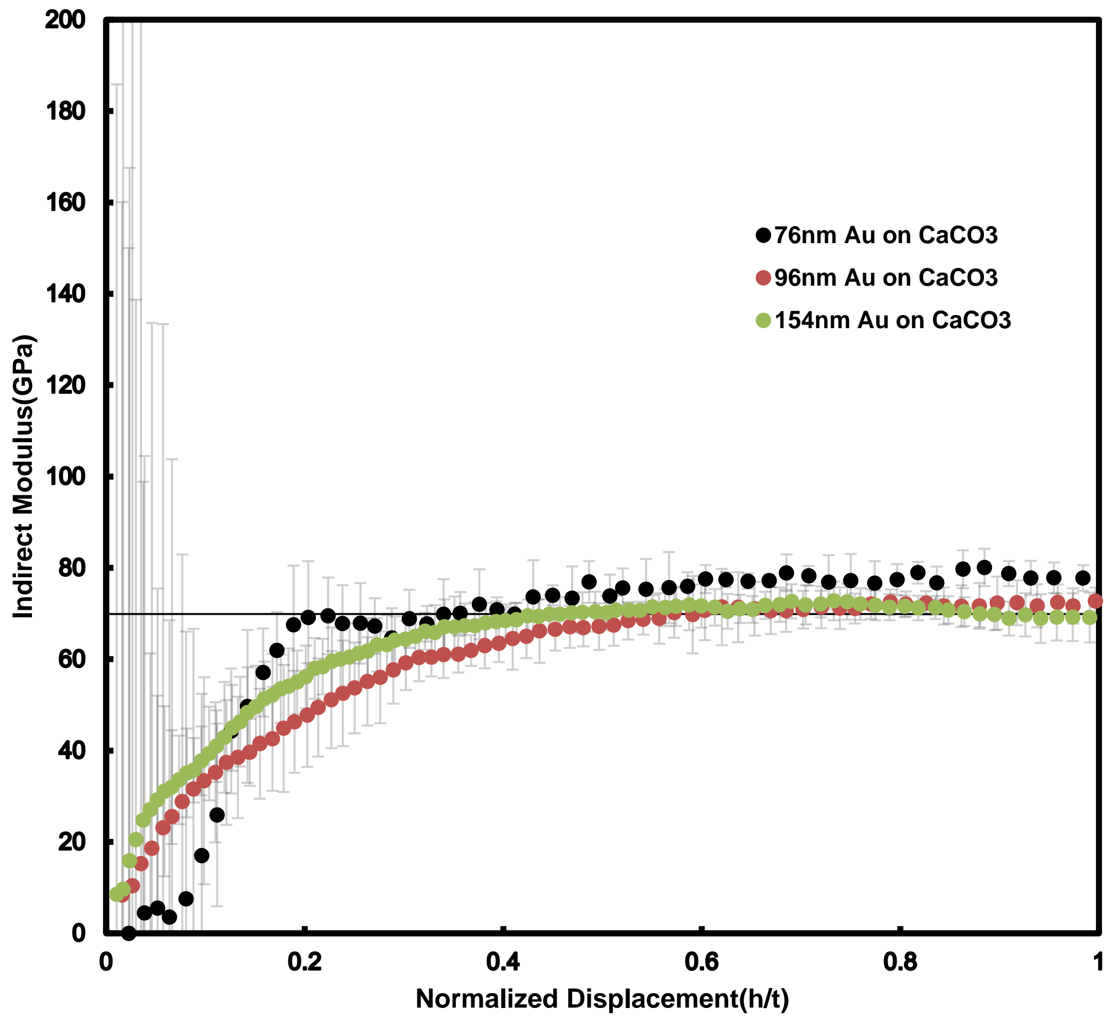

Figure 58 Indirect modulus of 76nm,96nm,154nm gold on CaCO3

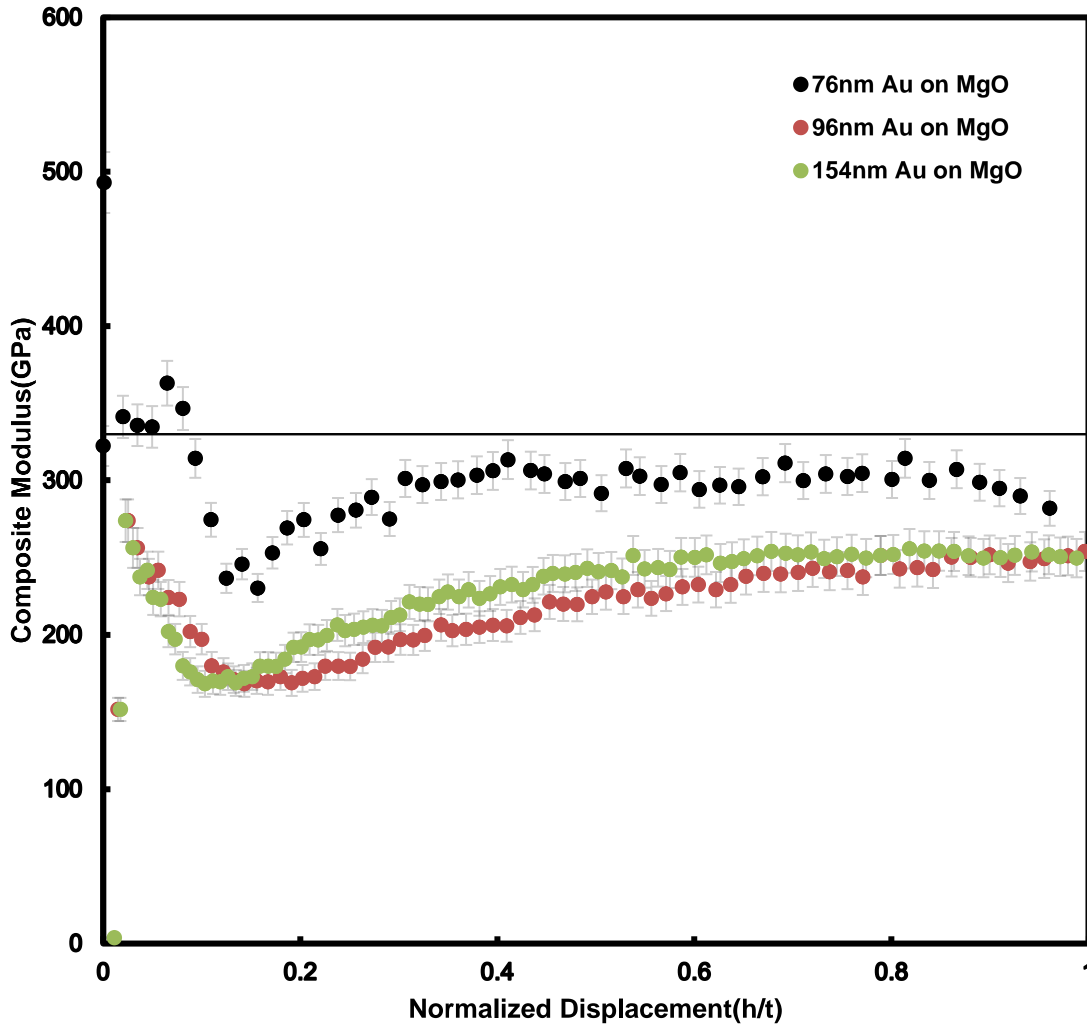

Figure 59 Composite modulus of 76nm,96nm,154nm gold on MgO

Finally, the MgO group was chosen. The reason is MgO has very high stiffness and low hardness. The silicon modulus is in mid-range of ceramic material and fused silica is a standard of nanoindentation test for calibration. CaCO3 has low modulus. The variety of chosen material can deliver more information based on indirect indentation method. The composite modulus from h'>0.1 dropped below the literature value because the gold modulus is relatively low compared with MgO as Figure 59 shows. Even till film thickness depth, the composite modulus was still under literature value. MgO's reduced modulus was plotted in Figure 60 and the slopes were obtained in Table 15. After h'>0.8 as discussed above, the indirect modulus became much lower because of instrument limitation. However, averaging the indentation results from h'=0.6 to 0.8

can still get a comparable result. The Figure 61 shows the indirect modulus of MgO of three different thickness and these three groups of data got similar trend.

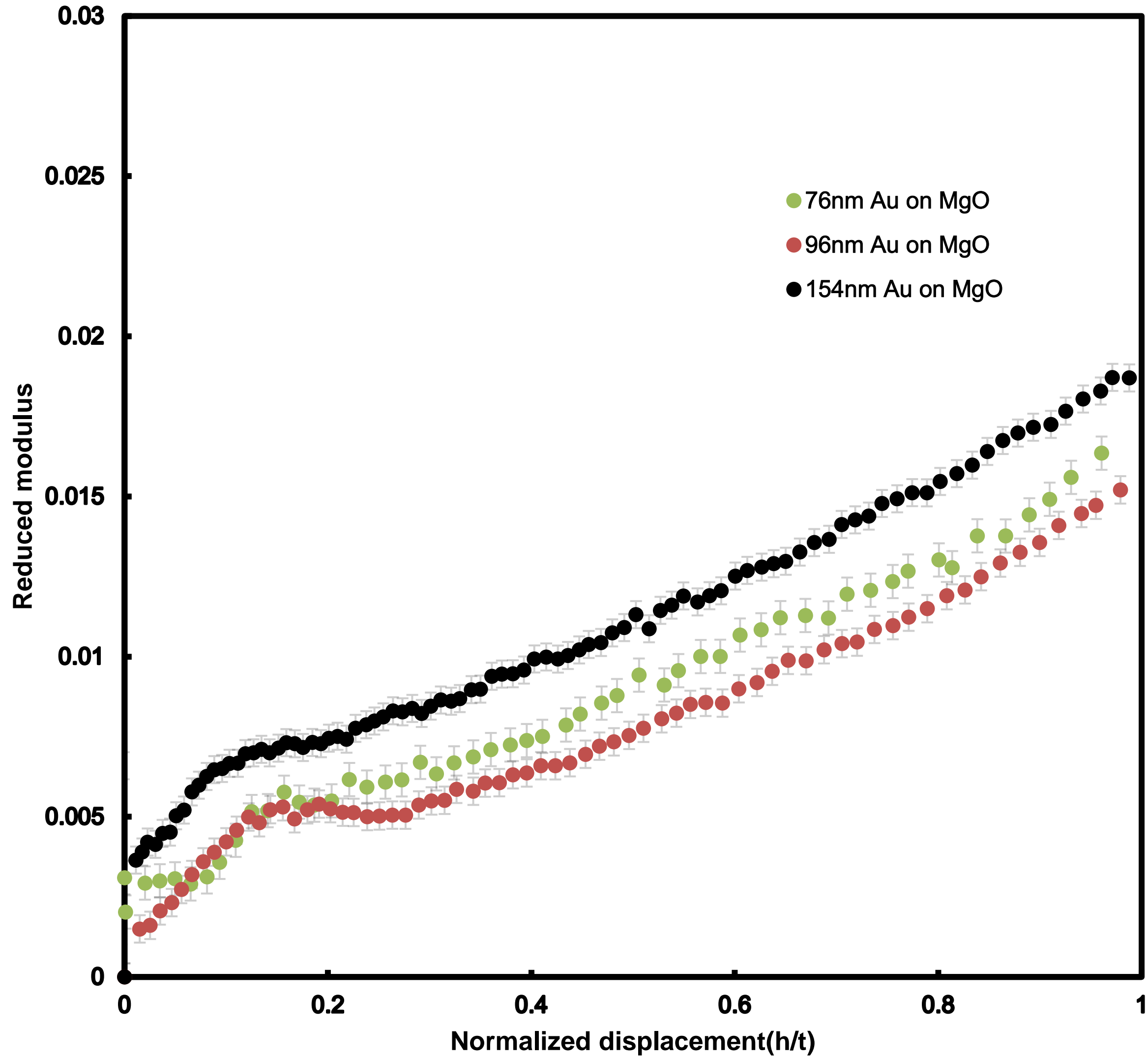

Figure 60 Reduced modulus of 76nm,96nm,154nm gold on MgO

Thickness(nm)	Slope	Indirect Modulus (GPa)
76	0.013	320±10.4
96	0.0129	322±9.6
154	0.0151	300±10.8

Table 15 Slopes and indirect modulus with 76nm,96nm,154nm gold on MgO

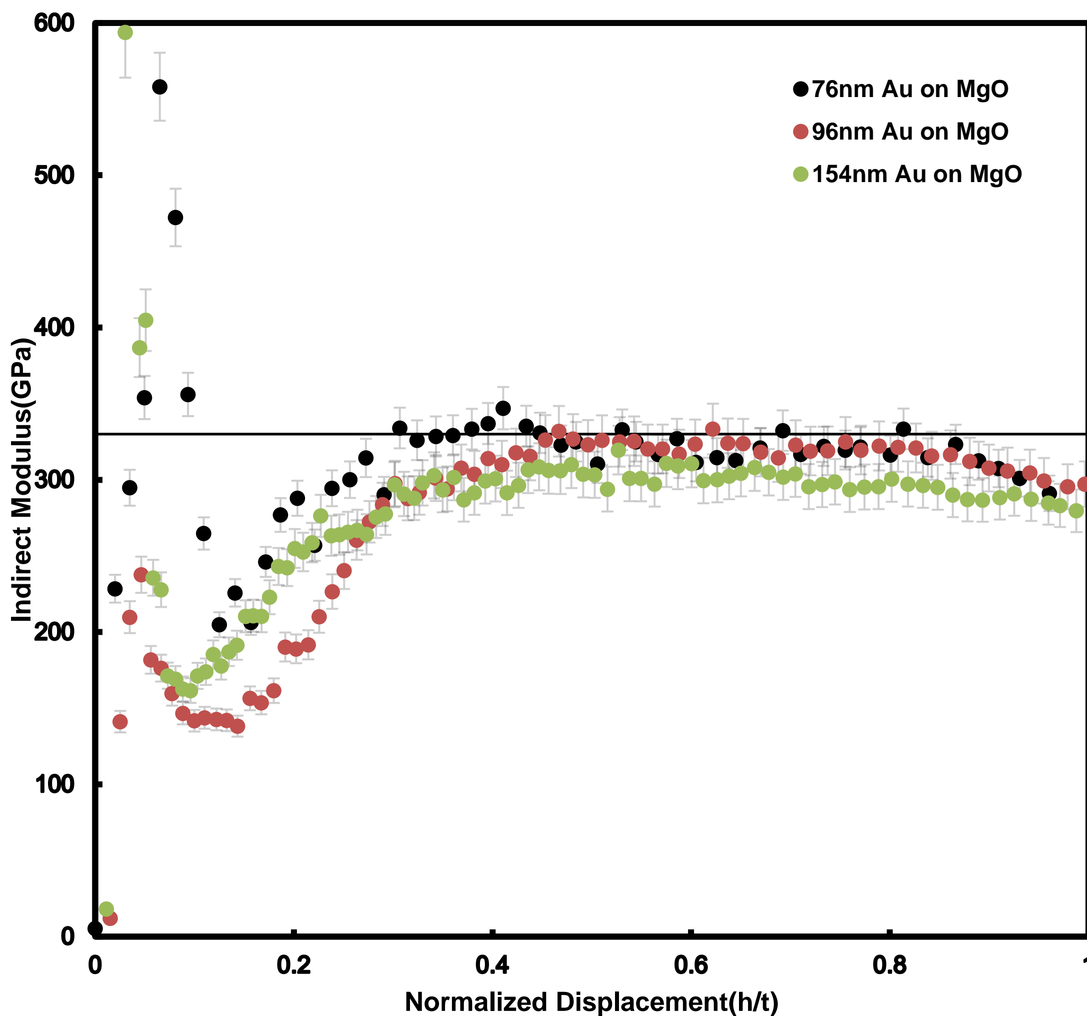

Figure 61 Indirect modulus of 76nm,96nm,154nm gold on MgO

Neither the substrate nor the film thickness is affecting the indirect indentation method (Chen-Prorok model) to extract substrates' modulus. This shows that the Chen-Prorok model might account for different ceramic material's effect; instead, different thickness and ceramic material are not affecting the elastic measurement at all.

5.3 Approach to Analyze Parameters that may Affect the Indirect Indentation Method

There are few important parameters in indirect indentation method (Chen-Prorok model) which are film Poisson's ratio, film thickness, substrate Poisson's ratio and experiment modulus from indenter. Experimental modulus is determined by the nano indenter. Poisson's ratio is basically based on literature value and estimated from experience for example ceramic material's Poisson's ratio is 0.17~0.31[46-50]. Film thickness is mainly controlled by deposition time, voltage, current, vacuum pressure and others. It is curious to analyze these parameters in Chen-Prorok model that how they affect each other and improve substrate modulus extraction.

Within this chapter, each individual parameter will be discussed and analyzed in details. It is very important to understand the indirect indentation method (Chen-Prorok model) and optimize its advantage to learn elastic behaviors during the indentation process.

5.3.1 Different Thickness's Effects

Although there are some deviations from standard value, either due to bad film or shallow depth lead to lack of tip contact with film itself, most of results from the indirect indentation method are reliable and predictable.

These effects are non-relation with the model itself. It is interesting to find whether thickness as one of parameters in the model plays a role in the modulus extraction or not. 107nm gold on silicon was used as an example to find the relation between thickness and final result.107nm real thickness was altered to 53.5nm,75nm,91nm,128nm,144nm,161nm to find out how affects the model.

It is an increasing trend from lower modified thickness to higher modified thickness as Figure 62 shows. The black solid line represents the literature value of silicon. The black dots are extracted modulus from indirect indentation method (Chen-Prorok) with altered thickness. Changing thickness will change normalized displacement(h'=h/t) which leads to the slope change. While slope changes, the final extracted modulus deviates. That is the reason why the modulus varies. The original reduced modulus of 107nm gold film on silicon is in Figure 36. In order to show directly, these groups reduced modus were plotted on Figure 63.

$$\frac{1}{E_t}\frac{1}{\left(1-\exp\left(-\frac{\nu_s}{h'}\right)\right)} \sim \frac{1}{E'_f} + \frac{1}{E_s}\left(\frac{\nu_s-\nu_f}{\nu_s} - 0.5 + \frac{h'}{\nu_s}\right)$$

(8)

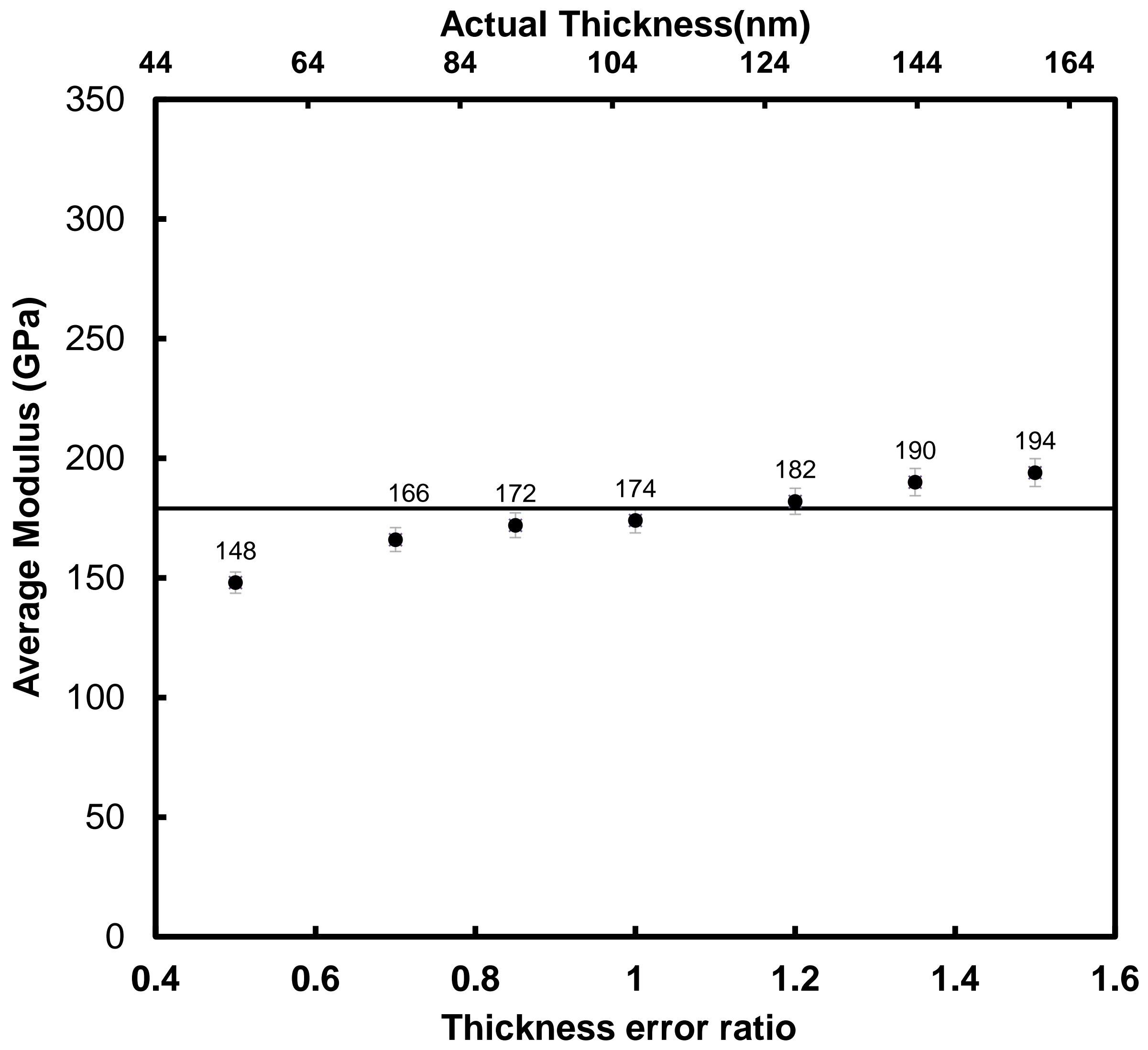

Figure 62 Average modulus versus thickness error ratio

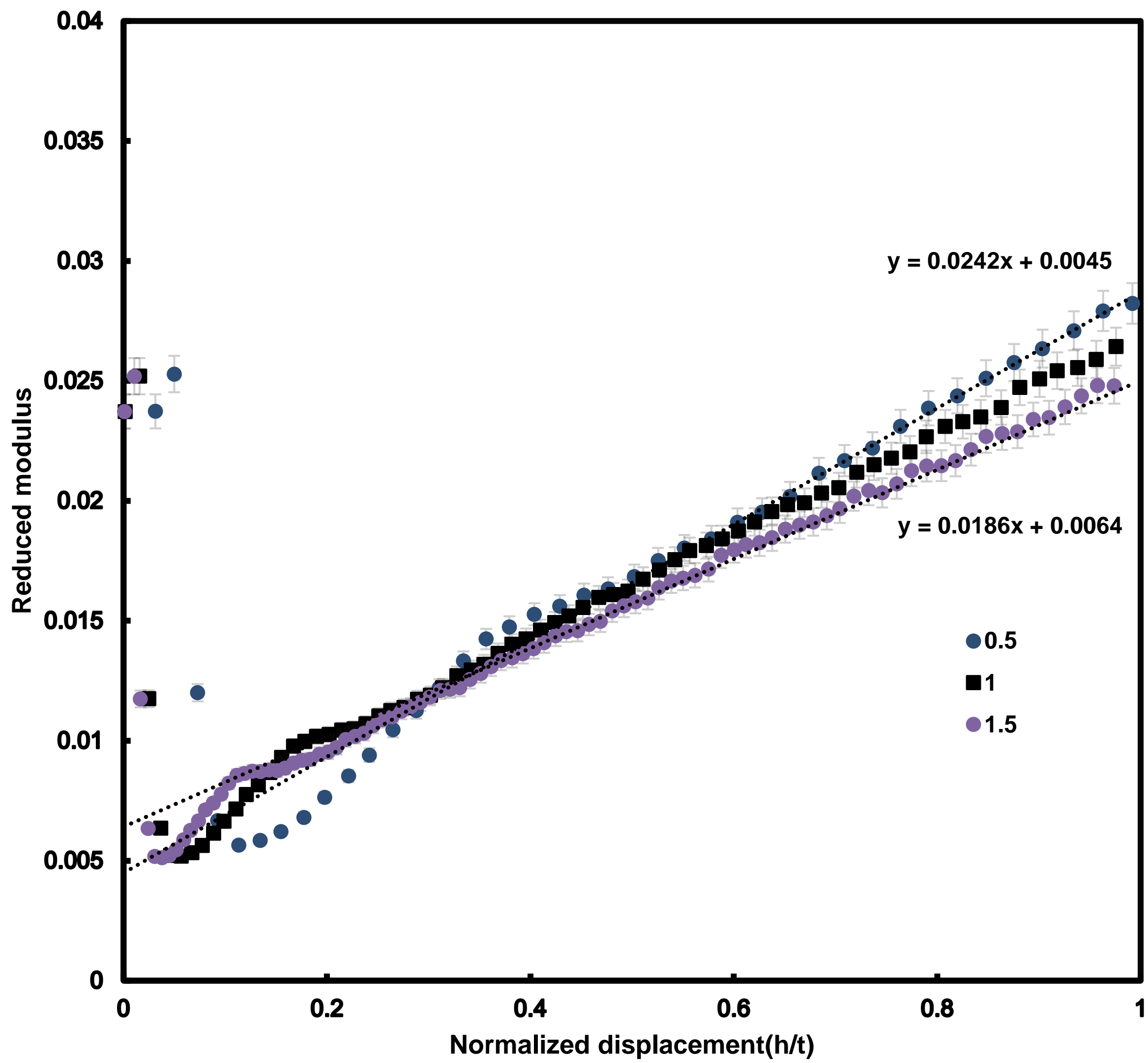

Figure 63 Reduced modulus of 107nm gold on silicon with changed thickness

Table 16 Slopes and indirect modulus with different thickness

Thickness(nm)	Slope	Indirect Modulus (GPa)
53.5	0.0243	148±4.5
75	0.0215	166±4.8
91	0.0208	172±5.1
107	0.0206	174±5.2
128	0.0196	182±5.4
144	0.0187	190±5.8
161	0.0186	194±5.4

Another reason why the data was off when the thickness lower than 50% is that continuous film requires at least 50nm thickness and the slope from reduced modulus had been changed heavily as figure 63 illustrates. The indentation depth isn't a reasonable range for our assumption within 50nm range. For universal use for the method, each material has different wettability and it is safe to deposit a gold film which the thickness is over 50nm.

However, within 20% thickness deviation from the original, the extracted substrate modulus is still predictable and reliable. It requires high standard for researchers to measure the exact thickness of film in nano range. From the analysis above, the model allows to get roughly estimate thickness up to 20% deviation from the original thickness to extract the substrate modulus. This observation confirms that thickness is not affecting the indirect indentation method (Chen-Prorok model) in a reasonable range.

The next step is to see if Poisson's ratio affects or not. More data analysis and experiment will be done to test the hypothesis.

5.3.2 Different Poisson's ratios' Effects

The Poisson's ratio is a very important parameter for elastic modulus. In the indirect indentation method, Poisson's ratio is used to counter the effect from experimental data. As equation 8 shows above, there are substrate's Poisson's ratio and film's Poisson's ratio. Film's Poisson ratio plays a role in Zhou-Prorok model because the model is determined by a combination of film and substrate

effects. However, Chen-Prorok's model is a revised version of Zhou-Prorok model by using a hyperbolic function to substitute and simplify certain parameters, the final result is only related to substrate's Poisson's ratio since the slope is calculated from $\frac{1}{E_t}\frac{1}{\left(1-\exp\left(-\frac{\nu_s}{h'}\right)\right)}$ and the extracted modulus is the slope divided by substrate Poisson's ratio.

It is curious to find if the substrate Poisson's ratio is modified, the extracted modulus changes 100nm gold on silicon was used as sample to get uniform result. Silicon's Poisson's ratio is 0.28 and was modified to 0.1,0.21,0.23,0.25,0.29,0.31 and 0.4 as Figure 64 shows.

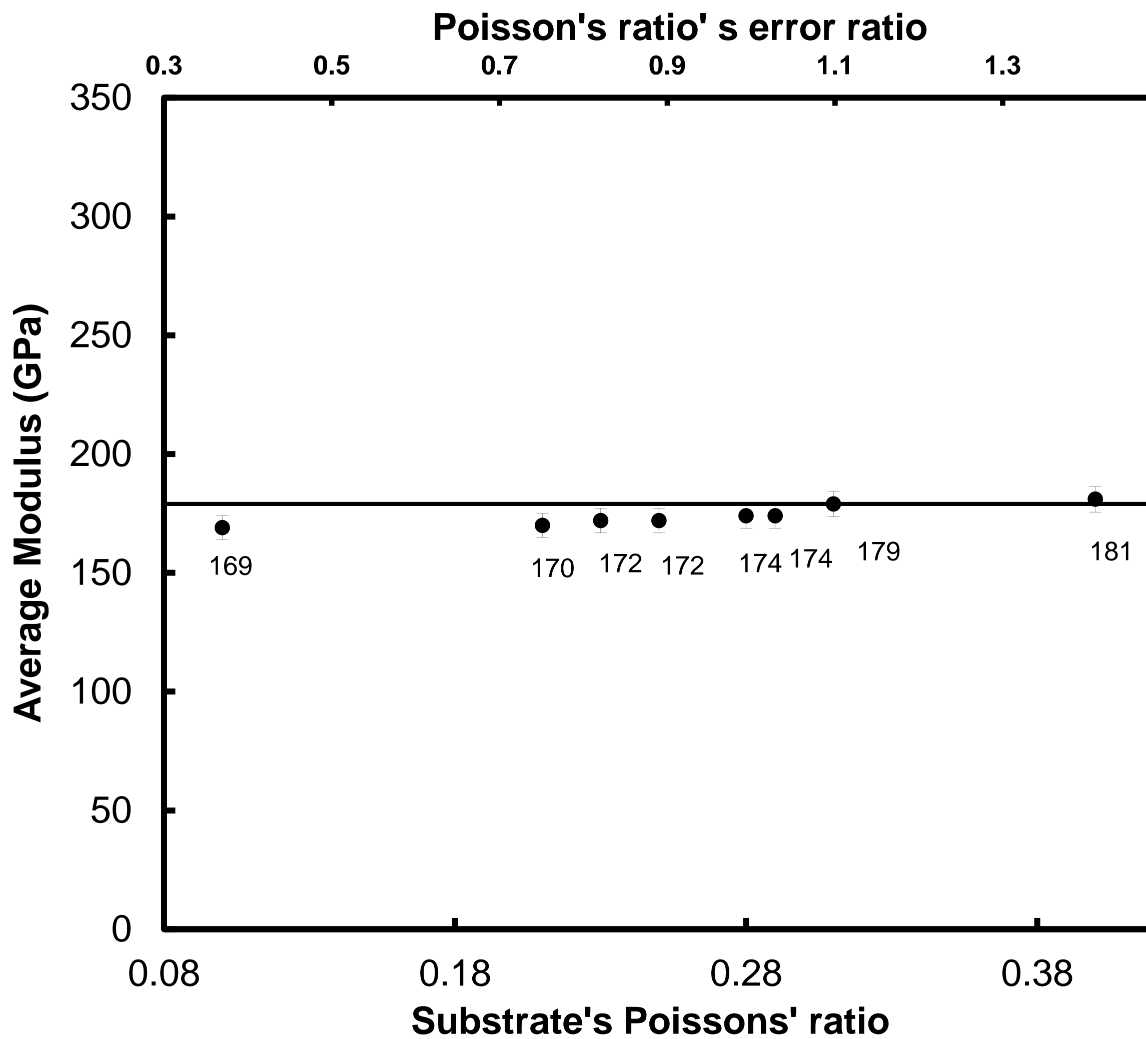

Figure 64 Average modulus versus different Poisson's ratio

Reduced modulus was shown in the Figure 65, it seems that the reduced modulus with different Poisson's ratio changes a lot. However, the indirect modulus only varies around 9GPa.

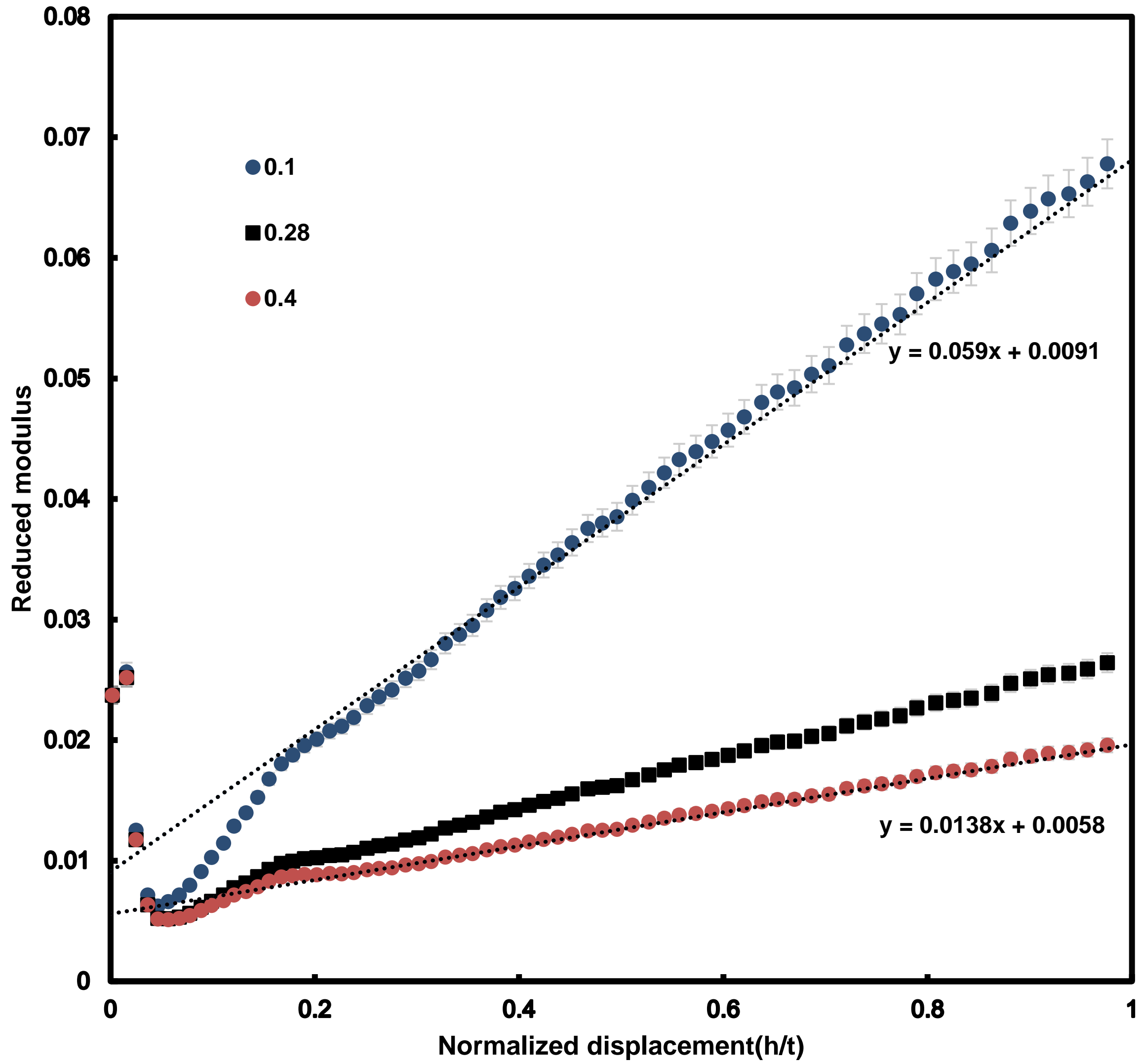

Figure 65 Reduced modulus of 107nm gold on silicon with changed Poisson's ratio

Poisson’s ratio	Slope	Indirect Modulus (GPa)
0.1	0.059	169±4.7
0.21	0.028	170±5.1
0.23	0.0252	172±5.2
0.25	0.0232	172±5.2
0.28	0.0206	174±5.4
0.29	0.0198	174±5.3
0.31	0.0181	179±5.4
0.4	0.0138	181±5.4

Table 17 Slopes and indirect modulus with different Poisson’s ratio

As discussed above, indirect modulus is from the slope of reduced modulus. Although the slope has been changed in Table 17, the Poisson’s ratio of substrate has been modified as well to manipulate the slope difference. The slope of reduced modulus is $\frac{1}{E_s \nu_s}$. Indirect modulus is one versus substrate Poisson’s ratio multiply slope. While Poisson’s ratio decreased, the slope of reduced modulus increased and vice versa. This makes the final result barely change.

Poisson’s ratio changed to 0.1 and 0.4 as two extremes. One is relatively stiff material which barely deforms and another is closed to gold’s Poisson’s ratio which spread the load out easily. Even these two cases changed the reduced modulus slope a lot and the final result are within 5% compared with its literature value.

In the range Poisson’s ratio of ceramic material, indirect modulus isn’t affected. Most of researchers need to get an exact Poisson’s ratio to estimate the ceramic modulus due to unique structures and properties [43-48,62-65]. However, with the indirect indentation method, Poisson’s ratio is not a big concern, and the model predicts the substrate’s modulus precisely with minor deviation.

The next step is to examine film thickness of different substrates. Besides the model itself, it is peculiar to find whether varying different substrates, the model could still predict ceramic substrates' modulus without punching into.

6.0 Conclusions

Nanoindentation is an essential tool in recent years. We want to give more suggestions in this area and help other get accurate and reliable data from our equations and methods. Until now, we have improved the way to deposit the films and were able to predict modulus on most ceramic substrates.

First, it was found that Pelco sputter coater works well with the indirect indentation method (Chen-Prorok model). Film quality is not an important factor to extract substrates' modulus. This new method makes sputter easier compared with Denton sputter unit. The required vacuum pressure could be achieved without very high vacuum state and the sputter parameters are well maintained to control the thickness of film. Within this finding, sputter process is improved. In few hundred nanometers, Pelco sputter method is suggested.

Next, film thickness, Poisson's ratio and different type of substrates are independent factors of the indirect indentation method (Chen-Prorok model). Based on analytic parameters and experiment results, as long as the film thickness is thick enough to form a continuous layer and well pass the radius of indentation tip radius, film thickness plays no role in the model which could be roughly estimated according to sputter current and vacuum pressure. Although Poisson' s ratio is a vital factor to materials' elastic properties, it was confirmed that barely affects elastic modulus subtraction because there is not clear variation with changing Poisson's ratio. Each ceramic material has unique microstructure and property. However, these effects are either compensated or explained by Chen-Prorok model. This helps Chen-Prorok model to deal with various substrates with minimum material effects.

Within this research, these findings show the relationship between substrates and films and how they affect each other. The effect of film has been minimized in order to peel off the real substrate's modulus. These studies could help better understand elastic behaviors during the indentation process and give some useful suggestions about testing films on substrates combinations in the future.

7.0 Future Work

There are many directions for this research to continue. More films and substrates combinations of indentation results analysis will quantify and confirm the superiority of Chen-Prorok model. With abundant data, extracting ceramic elastic properties by nanoindentation will no longer suffer from failures or inaccuracy. Additionally, the film material chosen could be optimized to reduce the sputtering cost and increase the handling convenience since gold is kind of noble material. Chromium film is a good alternative choice for its good wettability with ceramic compared with gold film. Chromium was also a decent material to apply for measuring elastic properties of brittle materials because of its low Poisson's ratio. It could directly transfer more the applied load to the substrate at lower indent depths compared with gold film. The substrate doesn't need to be coated with adhesion layer. Some work has been done with depositing and indenting six different thickness chromium film on silicon substrates by using Denton sputter coater. The indirect modulus results are exhibited in Figure 66. Table 18 gives the literature values. In Figure 67, the solid straight line represents silicon literature value and the solid marks are the average results of extracted modulus from h'=0.6 to h=1.0. All six extracted modulus are within 10% deviation of standard silicon modulus. However, some data points need to be further explored and analyzed like 300nm chromium on silicon and 1050nm chromium on silicon in the future.

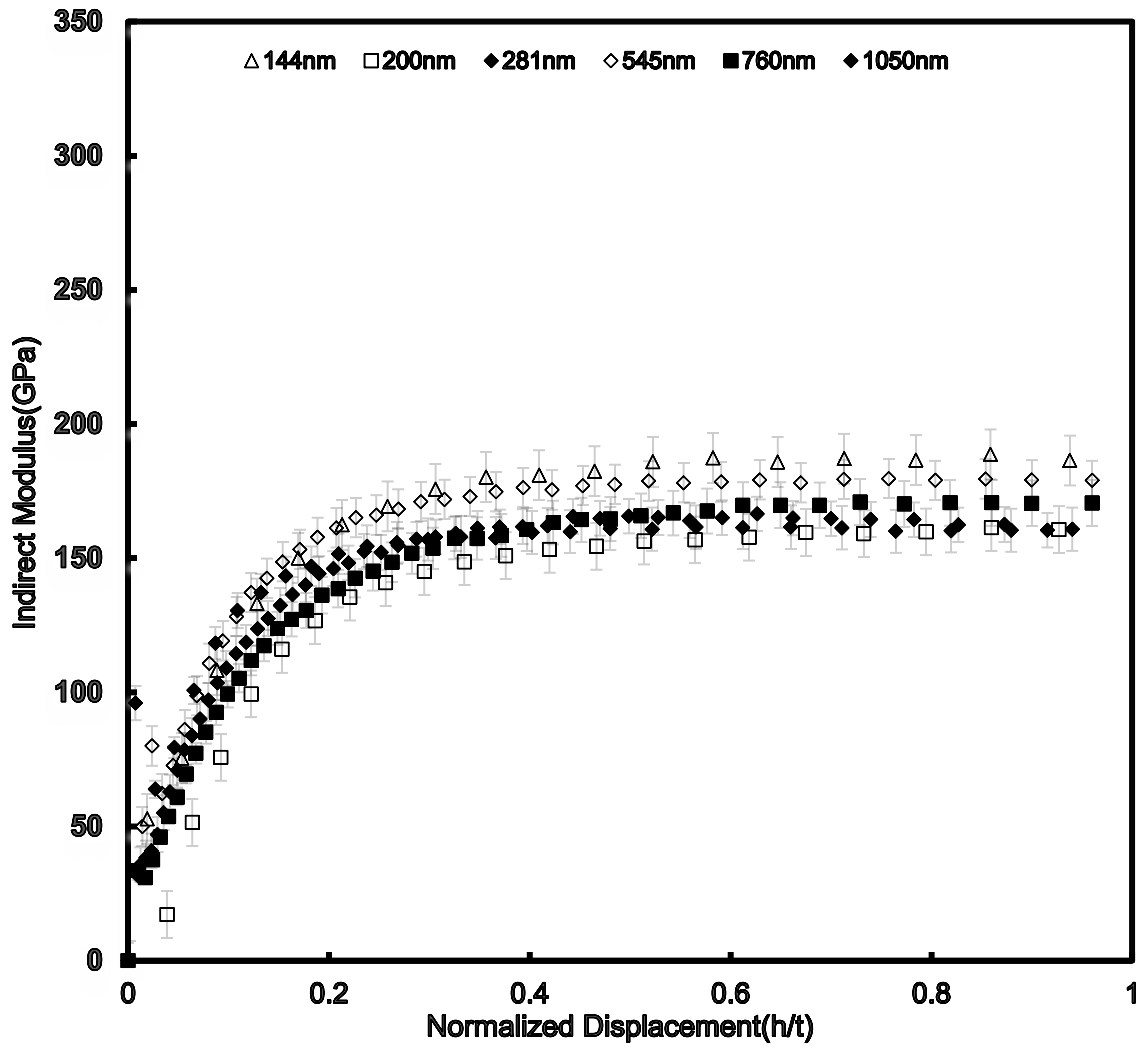

Figure 66 Indirect modulus for all thicknesses of chromium film on silicon substrate by applying Chen-Prorok model

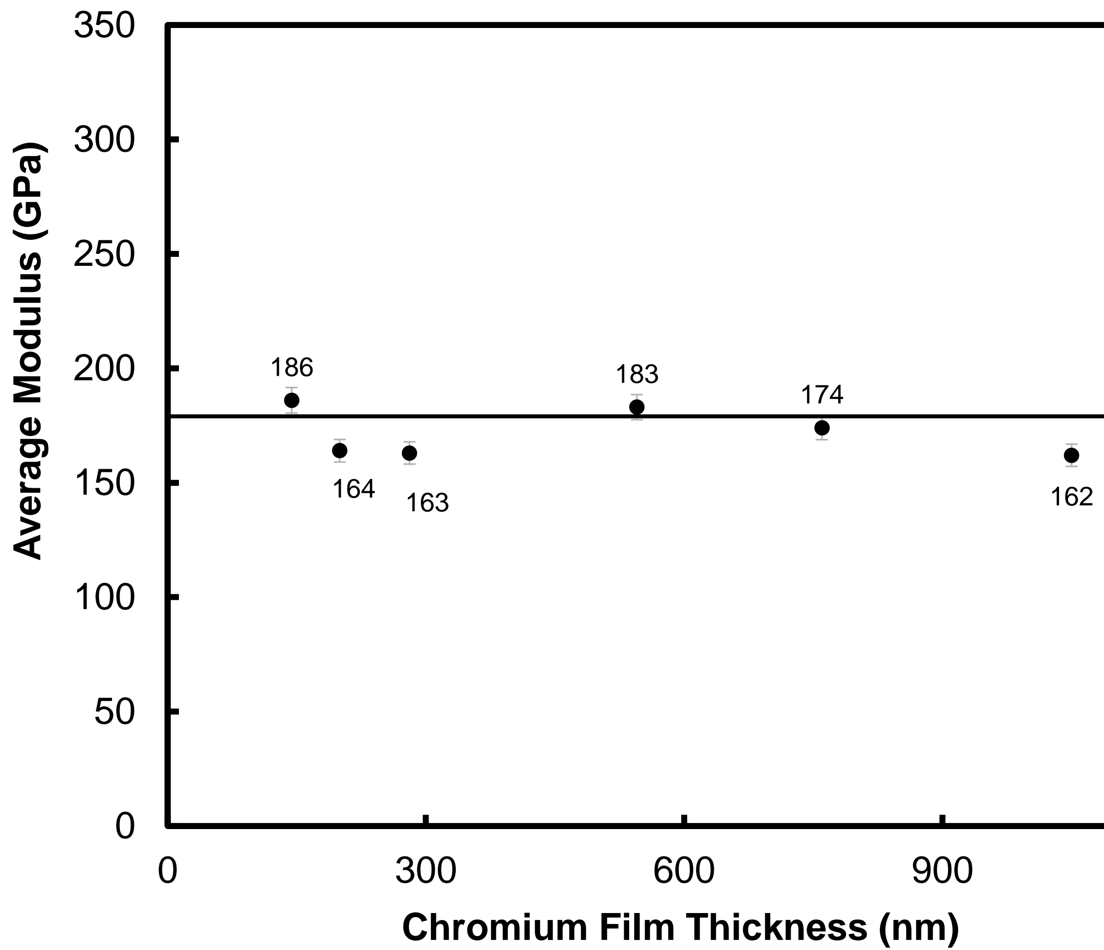

Figure 67 Average indirect indentation results from Chen-Prorok model with different thickness chromium on silicon substrates

Table 18 literature values of film and substrates

Es (GPa)	Ef (GPa)	vs	vf
179	279	0.28	0.21

Another direction is that Pelco sputter coater has three main parameters (vacuum pressure, working distance, current) to determine the gold film thickness. To examine these parameters for other targets like chromium is good for applying different film material on different substrates based on specific requirement but was out of scope of this work. Also, improving deposition steps might help get better film quality under certain settings.

Finally, based on the analysis of nanoindentation data, Chen-Prorok model works very well in the elastic parts. It is extremely curious to push the equations forward into the plastic portion for example hardness.

Chen-Prorok's model is a revised version of Zhou-Prorok model by using a hyperbolic function to substitute and simplify certain parameters. In Equation 3, we know that hardness is acquired from the load by area. Since we have film and substrate combinations, the hardness is a composite. Then we use rules of mixture first to get the Equation 9.

$$H_C = aH_f + bH_S \tag{9}$$

where Hc is the composite hardness of film and substrates, a is a weighting factor for film hardness; Hf is film hardness, b is weighting factor for substrate hardness, and Hs is substrate hardness.

From Equation 9, to use weighting factor from parameter fitting model to substitute a and b to get Equation 10. The reason we do this is because hardness is a mix of elastic and plastic material properties. Our weighting factor works for elastic parts well, so it might be a good beginning for learning the plastic part.

$$H_C = H_f \left(1 - exp\left(-\frac{\nu_s}{h'}\right)\right) + H_S\, exp\left(-\frac{\nu_f}{h'}\right) \tag{10}$$

where h' is indentation depth(h) versus thickness(t), ν_s is Poisson's ratio of the substrate, ν_f is Poisson's ratio of the film.

As similar way Similar to Yan, we used a linear approximation to substitute the hyperbolic function of weighting factors' and got Equation 11

$$\frac{H_C}{\left(1-exp\left(-\frac{\nu_s}{h'}\right)\right)} \sim H_f \; + H_S\left(\frac{\nu_s - \nu_f}{\nu_s} - 0.5 + \frac{h'}{\nu_s}\right) \tag{11}$$

From equation 11, the same method could be used to extract the substrate hardness as elastic modulus. The substrate hardness is only related to the slope of left portion and Poisson's ratio of the substrate.

Based on the Chen-Prorok model, it is not yet known if we mathematically revised the elastic equation into a new plastic equation that could precisely predict the properties. Some important parameters such as grain size and yield stress have not been estimated in the model. The relationship between these parameters is crucial to add these in the equation since hardness is a combination of elastic and plastic behaviors. These parameters will be explained in details to help researchers to better understand. No previous research has been done before.

8.0 Reference

[1] Pharr, G. M., and W. C. Oliver. "Measurement of thin film mechanical properties using nanoindentation." Mrs. Bulletin17.7 (1992): 28-33.

[2] Urena, A., et al. "Characterization of interfacial mechanical properties in carbon fiber/ aluminum matrix composites by the nanoindentation technique." Composites science and technology 65.13 (2005): 2025-2038.

[3] Oliver, W. C., & Pharr, G. M. (1992). An improved technique for determining hardness and elastic modulus using load and displacement sensing indentation experiments. Journal of materials research, 7(06), 1564-1583.

[4] Sullivan, Marianne, and Barton C. Prorok. "Evaluating indent pile-up with metallic films on ceramic-like substrates." Journal of Materials Research 30.13 (2015): 2046-2054.

[5] K. P. Sanosh, A. Balakrishnan, L. Francis, and T. N. Kim, "Vickers and Knoop Micro-hardness Behavior of Coarse-and Ultrafine-grained Titanium," Journal of Materials Science & Technology, vol. 26, pp. 904-907, 2010.

[6] M. F. Doerner and W. D. Nix, "A method for interpreting the data from depth-sensing indentation instruments," Journal of Materials Research, vol. 1, pp. 601-309, 1986.

[7] Saha, Ranjana, and William D. Nix. "Effects of the substrate on the determination of thin film mechanical properties by nanoindentation." Acta materialia 50.1 (2002): 23-38.

[8] I. N. Sneddon, "The relation between load and penetration in the axisymmetric Boussinesq problem for a punch of arbitrary profile," International Journal of Engineering Science, vol. 3, pp. 47-57, 1965.

[9] Zhou, B., and B. C. Prorok. "A discontinuous elastic interface transfer model of thin film nanoindentation." Experimental Mechanics 50.6 (2010): 793-801.

[10] B. Zhou and B. C. Prorok, "A new paradigm in thin film nanoindentation," J. Mater. Res., vol. 25, pp. 1671-1678, 2010..

[11] Sullivan, MariAnne, and Bart Prorok. "Evaluating pile-up and sink-in during nanoindentation of thin films." MEMS and Nanotechnology, Volume 5. Springer, Cham, 2016. 45-50.

[12] Chen, Yan, et al. "A new method to extract elastic modulus of brittle materials from Berkovich indentation." Journal of the European Ceramic Society 38.1 (2018): 349-353.

[13] G. M. Pharr, "Measurement of mechanical properties by ultra-low load indentation," Materials Science and Engineering: A, vol. 253, pp. 151-159, 1998.

[14] Qian, Linmao, et al. "Comparison of nano-indentation hardness to microhardness." Surface and Coatings Technology 195.2-3 (2005): 264-271.

[15] Fang, Te-Hua, Win-Jin Chang, and Cheng-I. Weng. "Nanoindentation and nanomachining characteristics of gold and platinum thin films." Materials Science and Engineering: A 430.1-2 (2006): 332-340.

[16] Fang, Te-Hua, Sheng-Rui Jian, and Der-San Chuu. "Nanomechanical properties of TiC, TiN and TiCN thin films using scanning probe microscopy and nanoindentation." Applied Surface Science 228.1-4 (2004): 365-372.

[17] Petrov, I., et al. "Microstructural evolution during film growth." Journal of Vacuum Science & Technology A: Vacuum, Surfaces, and Films 21.5 (2003): S117-S128.

[18] J. William D. Callister and D. G. Rethwisch, Fundamentals of Materials Science and Engineering: An Integrated Approach vol. 3: John Wiley & Sons, 2008..

[19] R. Saha and W. D. Nix, "Effects of the substrate on the determination of thin film mechanical properties by nanoindentation," Acta Materialia, vol. 50, pp. 23-38, 2002.

[20] R. Saha and W. D. Nix, "Soft films on hard substrates — nanoindentation of tungsten films on sapphire substrates," Materials Science and Engineering: A, vol. 319–321, pp. 898-901, 2001.

[21] L. Wang and B. C. Prorok, "The Influence of Deposition Technique on the Strain Rate Dependence Behavior of Nanocrystalline Gold Films," in Proceedings of the 2009 SEM Annual Conference and Exposition on Experimental and Applied Mechanics, Session 35 ed. Albuquerque, NM, 2009.

[22] Wang, Liwei, and Bart Prorok. "Investigation of the influence of grain size, texture and orientation on the mechanical behavior of freestanding polycrystalline gold films." MRS Online Proceedings Library Archive 924 (2006).

[23] Chen, Yan. "Measurement of Reliable Indentation Elastic Modulus in Brittle Materials from Berkovich Nano Indentation." (2016).

[24] R. Saha and W. D. Nix, "Soft films on hard substrates — nanoindentation of tungsten films on sapphire substrates," Materials Science and Engineering: A, vol. 319–321, pp. 898-901, 2001.

[25] K. W. McElhaney, J. J. Vlassak, and W. D. Nix, "Determination of indenter tip geometry and indentation contact area for depth-sensing indentation experiments," J. Mater. Res., vol. 13, pp. 1300-1306, 1998.

[26] Chicot, D., Y. Benarioua, and J. Lesage. "Hardness measurements of Ti and TiC multilayers: a model." Thin Solid Films 359.2 (2000): 228-235.

[27] A. Bolshakov, W. C. Oliver, and G. M. Pharr, "Influences of stress on the measurement of mechanical properties using nanoindentation: Part II. Finite element simulations," Journal of Materials Research, vol. 11, pp. 760-768, 1996.

[28] W. C. Oliver and G. M. Pharr, "Measurement of hardness and elastic modulus by instrumented indentation: Advances in understanding and refinements to methodology," J. Mater. Res., vol. 19, pp. 3-20, 2004.

[29] K. O. Kese, Z. C. Li, and B. Bergman, "Method to account for true contact area in soda-lime glass during nanoindentation with the Berkovich tip," Materials Science and Engineering: A, vol. 404, pp. 1-8, 2005.

[30] J. William D. Callister and D. G. Rethwisch, Fundamentals of Materials Science and Engineering: An Integrated Approach vol. 3: John Wiley & Sons, 2008.

[31] P. Boch, J. C. Glandus, J. Jarrige, J. P. Lecompte, and J. Mexmain, "Sintering, oxidation and mechanical properties of hot pressed aluminum nitride," Ceram. Int., vol. 8, 1982.

[32] R. R. Gupta and M. D. Lechner, Landolt-Bonstein-Group III Condensed Matter. New York: Springer, 2005.

[33] Jönsson, B., and S. Hogmark. "Hardness measurements of thin films." Thin solid films 114.3 (1984): 257-269.

[34] G. M. Pharr, J. H. Strader, and W. C. Oliver, "Critical issues in making small-depth mechanical property measurements by nanoindentation with continuous stiffness measurement," Journal of Materials Research, vol. 24, pp. 653-666, 2009.

[35] L. Wang, C. Liang, and B. C. Prorok, "A comparison of testing methods in assessing the elastic properties of sputter-deposited gold films," Thin Solid Films, vol. 515, p. 7911, 2007.

[36] Doron-Mor, Ilanit, et al. "Ultrathin gold island films on silanized glass. Morphology and optical properties." Chemistry of Materials 16.18 (2004): 3476-3483.

[37] Fujiwara, Hiroyuki. Spectroscopic ellipsometry: principles and applications. John Wiley & Sons, 2007.

[38] Laref, Slimane, et al. "Size-dependent permittivity and intrinsic optical anisotropy of nanometric gold thin films: a density functional theory study." Optics express 21.10 (2013): 11827-11838.

[39] Page, Trevor F., Warren C. Oliver, and Carl J. McHargue. "The deformation behavior of ceramic crystals subjected to very low load (nano) indentations." Journal of Materials Research 7.2 (1992): 450-473.

[40] Chen, Weiqiang, et al. "Ultra-thin ultra-smooth and low-loss silver films on a germanium wetting layer." Optics express 18.5 (2010): 5124-5134.

[41] Perriot, Antoine, and Etienne Barthel. "Elastic contact to a coated half-space: Effective elastic modulus and real penetration." Journal of Materials Research 19.2 (2004): 600-608.

[42] Tsui, T. Y., and G. M. Pharr. "Substrate effects on nanoindentation mechanical property measurement of soft films on hard substrates." Journal of Materials Research 14.1 (1999): 292-301.

[43] Yoder, K. B., et al. "Elastic rebound between an indenter and a layered specimen: Part II. Using contact stiffness to help ensure reliability of nanoindentation measurements." Journal of materials research 13 (1998): 3214-3220.

[44] Wortman, J. J., and R. A. Evans. "Young's modulus, shear modulus, and Poisson's ratio in silicon and germanium." Journal of applied physics 36.1 (1965): 153-156.

[45] Chen, Chien-Chih, et al. "Elasticity of single-crystal calcite and rhodochrosite by Brillouin spectroscopy." American Mineralogist 86.11-12 (2001): 1525-1529.

[46] Malynych, Serhiy Z., and George Chumanov. "Vacuum deposition of silver island films on chemically modified surfaces." Journal of Vacuum Science & Technology A: Vacuum, Surfaces, and Films 21.3 (2003): 723-727.

[47] Olmon, Robert L., et al. "Optical dielectric function of gold." Physical Review B 86.23 (2012): 235147.

[48] Pavaskar, Prathamesh, et al. "A microscopic study of strongly plasmonic Au and Ag island thin films." Journal of Applied Physics 113.3 (2013): 034302.

[49] Hövel, Martin, Bruno Gompf, and Martin Dressel. "Dielectric properties of ultrathin metal films around the percolation threshold." Physical Review B 81.3 (2010): 035402.

[50] Hugall, James T., et al. "Solvent-resistant ultraflat gold using liquid glass." Langmuir 28.2 (2011): 1347-1350.

[51] Riboh, Jonathan C., et al. "A nanoscale optical biosensor: real-time immunoassay in physiological buffer enabled by improved nanoparticle adhesion." The Journal of Physical Chemistry B 107.8 (2003): 1772-1780.

[52] Gaillard, Y., C. Tromas, and J. Woirgard. "Quantitative analysis of dislocation pile-ups nucleated during nanoindentation in MgO." Acta Materialia 54.5 (2006): 1409-1417.

[53] Tromas, C., et al. "Pop-in phenomenon during nanoindentation in MgO." The European Physical Journal-Applied Physics 8.2 (1999): 123-128.

[54] Kurosaki, Ken, et al. "Nanoindentation tests for TiO2, MgO, and YSZ single crystals." Journal of alloys and compounds 386.1-2 (2005): 261-264.

[55] Tromas, C., et al. "Study of the low stress plasticity in single-crystal MgO by nanoindentation and atomic force microscopy." Journal of materials science 34.21 (1999): 5337-5342.

[56] Huang, Y., et al. "A model of size effects in nano-indentation." Journal of the Mechanics and Physics of Solids 54.8 (2006): 1668-1686.

[57] Cáceres, D., et al. "Hardness and elastic modulus from nanoindentations in nominally pure and doped MgO single crystals." Philosophical Magazine A 82.6 (2002): 1159-1171.

[58] Sangwal, K., P. Gorostiza, and F. Sanz. "In situ study of the recovery of nanoindentation deformation of the (100) face of MgO crystals by atomic force microscopy." Surface science 442.2 (1999): 161-178.

[59] Dong, Zhigang, Han Huang, and Renke Kang. "An investigation of the onset of elastoplastic deformation during nanoindentation in MgO single crystal (0 0 1) and (1 1 0) planes." Materials Science and Engineering: A 527.16-17 (2010): 4177-4184.

[60] Plassard, Cédric, et al. "Intrinsic elastic properties of Calcium Silicate Hydrates by nanoindentation." 2007.

[61] Das, Oisik, and Debes Bhattacharyya. "Development of polymeric biocomposites: particulate incorporation, interphase generation and evaluation by nanoindentation." Interface/Interphase in Polymer Nanocomposites; Netravali, AN, Mittal, KL, Eds (2016): 333-374.

[62] Zeng, Fanlin, et al. "Nanoindentation, nanoscratch, and nanotensile testing of poly (vinylidene fluoride) ‐ polyhedral oligomeric silsesquioxane nanocomposites." Journal of Polymer Science Part B: Polymer Physics 50.23 (2012): 1597-1611.

[63] Shchennikov, Vladimir V., and Sergey V. Ovsyannikov. "Phase transitions from mechanical contraction: direct observation of phase-transition-related volumetric effects in ZnO, GaAs, CaCO3, and CeNi under compression up to 25 GPa." High Pressure Research 29.4 (2009): 514-519.

[64] Gadelrab, K. R., F. A. Bonilla, and M. Chiesa. "Densification modeling of fused silica under nanoindentation." Journal of Non-Crystalline Solids 358.2 (2012): 392-398.

[65] Woirgard, J., and J. C. Dargenton. "An alternative method for penetration depth determination in nanoindentation measurements." Journal of materials research 12.9 (1997): 2455-2458.

[66] Kurkjian, Charles R., Gunther W. Kammlott, and M. Munawar Chaudhri. "Indentation behavior of soda - lime silica glass, fused silica, and single - crystal quartz at liquid nitrogen temperature." Journal of the American Ceramic Society 78.3 (1995): 737-744.

[67] Dey, Arjun, and Anoop Kumar Mukhopadhyay. Nanoindentation of brittle solids. CRC Press, 2014.

[68] Zhu, T. T., A. J. Bushby, and D. J. Dunstan. "Size effect in the initiation of plasticity for ceramics in nanoindentation." Journal of the Mechanics and Physics of Solids 56.4 (2008): 1170-1185.

[69] Woirgard, J., et al. "Study of the mechanical properties of ceramic materials by the nanoindentation technique." Journal of the European Ceramic Society 18.15 (1998): 2297-2305.

[70] Singh, D. R. P., Nikhilesh Chawla, and Y-L. Shen. "Focused Ion Beam (FIB) tomography of nanoindentation damage in nanoscale metal/ceramic multilayers." Materials Characterization 61.4 (2010): 481-488.

[71] Page, Trevor F., Warren C. Oliver, and Carl J. McHargue. "The deformation behavior of ceramic crystals subjected to very low load (nano) indentations." Journal of Materials Research 7.2 (1992): 450-473.

[72] Leggoe, J. W. "Determination of the elastic modulus of microscale ceramic particles via nanoindentation." Journal of materials research 19.8 (2004): 2437-2447.

[73] Zeng, Kaiyang, and David Rowcliffe. "Analysis of penetration curves produced by sharp indentations on ceramic materials." Philosophical magazine A 74.5 (1996): 1107-1116.